INAUGURAL - DISSERTATION
zur
Erlangung der Doktorwürde
der
Naturwissenschaftlich - Mathematischen Gesamtfakultät
der
Ruprecht - Karls - Universität Heidelberg

vorgelegt von
Dipl.-Chem. Jens Ulmer
aus Mutlangen
Tag der mündlichen Prüfung: 11. Juli 2005

Quantitative Measurements of Force Distribution in Single and Multi Cellular Systems

Gutachter: Prof. Dr. Joachim P. Spatz
Prof. Dr. Benjamin Geiger

für meine Eltern
Juana und Erich

Contents

Summary

Tissue formation and organ development in animals is a complex, lifelong process. The building blocks of tissue are living cells surrounded by secretion products, mostly proteins and polysaccharides. Aggregates of these proteins have different structural geometries and functionalities depending on localization and task *in vivo*. They form the extracellular matrix (ECM). The detailed quantitative evaluation of tissue construction and tissue-cell interaction is essential for a detailed understanding of organ development and its associated malfunctions which lead to different diseases. However, quantitative studies of cellular events in vivo are restricted since high resolution techniques characterizing cell functions are not suitable for living organism (eg. fluorescence microscopy, local force probing or different blotting techniques).

In vitro models of the ECM represent an approximation of *in vivo* conditions. They offer unique possibilities to investigate cell-ECM interaction with the highest precision, applying quantitative optical, force and chemical techniques. In respect to tissue culture techniques, introduction of artefacts in mammalian cells cultured on flat, rigid and non-natural two dimensional surfaces is apparent. Such surfaces do not possess three dimensionality and variation of compliance on the micrometer scale as observed in the ECM. To circumvent this drawback new materials and techniques are needed, where surface compliance, structural geometry and chemical composition of ECM models can be adjusted independently. In addition, local force and compliance measurements should produce new insights in cell-ECM interaction and tissue development.

The first two parts of this thesis describe a novel micro-engineered mechanical device which serves as a platform for constructing ECM models and as force sensor array. We developed a transparent elastic surface with arrays of micrometer scaled posts. The development process is based on standard photolithographic techniques. Typical structural dimensions of posts are a diameter of 2.5 μm a height of 15 μm. Physical properties of post arrays such as local and macroscopic substrate elasticity were investigated quantitatively. These posts were shown to be able to serve as a quantitative device measuring local forces down to the nanonewton range implied by the calibration analysis. The micro-array offers a template for constructing the ECM *in vitro* with different chemical and mechanical constitutions of the ECM as well as different geometries. The tops of posts were selectively functionalized with either a peptide sequences (arginine-glycine-aspartate, cRGD) or an amorphous matrix protein resulting in well defined surfaces suitable for quantitative force measurements of living cells. By exploring the impact of surface tension of air-water interfaces from protein solution in close contact with a micro-array, the force dependence of fibronectin fibre formation was shown.

Part III describes the application of force sensor arrays for measuring an adherent cell's spatial distribution of local forces along its membrane. Therefore rat embryonic fibroblasts with GFP fusion proteins to paxilin and β_3 integrin were used to localize the focal adhesions with fluorescence microscopy under physiological conditions. Correlation of patch size to generated force revealed local stress values from 0.1 ± 1.5 up to 115 ± 15.1 $nN/\mu m^2$ as a function of cell-state. Using surfaces with different pliabilities by variation of post height and chemical functionality, it was possible to investigate different morphological states of adhesion sites in human foreskin fibroblasts (HFF). The molecular composition of focal contacts strongly depends not only on local substrate stiffness but also on the global compliance of the surface. In the case of fibronectin coated microarrays development of focal contacts was strongly dependent on stiffness of the underlying support. However post arrays with different compliance and coated with cRGD demonstrated that local mechanosensing capabilities of focal contacts is also assisted by different mechanisms which sense global mechanical properties of cell's environment.

The mechanical interplay in a multicellular system was investigated in the last part of this work. During organ development cells aggregate and form multicellular compartments in a very precise manner. In order to maintain regular organ function it is important that cell can communicate during organogenesis. The communication pathways based on biochemical signalling have been extensively investigated over the past twenty years. But less is known about mechanical signalling between cells in multicellular aggregates. Madin-Darby Canine Kidney (MDCK) cells form functional cellular aggregates, termed cysts under special conditions in vitro. The conditions were adapted to induce cyst growth on force sensor arrays allowing precise force mapping during cyst development. In collaboration with Ruth Kroschewski, ETH Zuerich, these data were analysed to verify a computational model calculating of surface-forces generated by MDCK cysts inside a 3 dimensional cell culture system. Switching to a mechanical anisotropic environment meant that MDCK cysts no longer grew as round spheres. Instead cell aggregates generated tubular shapes. So far, tubulogenesis *in vitro* was only inducible by adding growth factors to the culture medium.

Zusammenfassung

Der Aufbau von Gewebe in Säugetieren ist ein komplexer Prozess, der nicht nur während der embryonalen Phase stattfindet, sondern das ganze Leben hindurch anhält. Das Gewebe besteht grundsätzlich aus vielen komplexen Bausteinen, wie beispielsweise aus lebenden Zellen, welche in eine Faserproteinenmatrix eingebettet sind. Die Architektur der Fasermatrix weist dabei unterschiedliche Gestalt und Funktion auf. Die Architektur hängt wiederum von der Aufgabe und der Lokalisierung im Organismus ab. Für die quantitative Untersuchung von zellulären Funktionen *in vivo* sind die heutzutage vorhandenen Untersuchungsmethoden, wie z.B. die Fluoreszenz- bzw. die Kraftmikroskopie oder verschiedene Blotting Techniken, völlig unzureichend. Dieser Umstand macht die Entwicklung von *in vitro* Modellen der extrazellulären Matrix (EZM) notwendig. Diese können jedoch nur eine Annährung an die Bedingungen *in vivo* darstellen. In Bezug auf die allgemeine Zellkultur Techniken, bei denen Säugetierzellen auf flachen, festen zwei dimensionalen Oberflächen kultiviert werden, sind Artefakte bezüglich des Verhaltens von Zellen im Verglich mit dem Verhalten in vivo klar erkennbar. Diese Oberflächen ermöglichen keine dreidimensionale zelluläre Umgebung und zeigen auf der Mikrometerskala keine Veränderung der Oberflächenfestigkeit, wie sie in vivo für die EZM charakteristisch sind. Die Einschränkung dieses scheinbaren Nachteils macht die Entwicklung neuer Techniken notwendig, bei der Festigkeit, Strukturumgebung und chemische Eigenschaften individuell und unabhängig voneinander angepasst werden können.

Die ersten beiden Teile dieser Arbeit befassen sich mit der Beschreibung einer neuartigen mikromechanischen Systemtechnik. Diese besteht aus einer transparenten Oberfläche, dekoriert mit einem Säulenmuster im Mikrometermaßstab. Diese wurden mittels photolithographischer Techniken hergestellt. Typische Strukturgrößen der Säulen betrugen 2,5 μm im Durch messer und 15 μm in der Höhe. Die physikalischen Eigenschaften der Säulenmuster, wie Oberflächen steifigkeit und Benetzbarkeit mit einer Flüssigkeit, wurden quantitativ untersucht. Diese Säulen dienen als quantitative Messsonden um lokale Kräfte im Nanonewtonbereich zu messen. Dies schließt eine Kalibrierung und die Analyse von videomikroskopischen Aufnahmen mit ein. Zudem dient das vorgestellte mikroskopische Säulenfeld als Matrize zum Nachbau der EZM in vitro mit unterschiedlicher chemischer Zusammensetzung, Architektur und Strukturgröße. Hierzu wurden zum einen die Köpfe der Säulen selektiv mit einer Peptidsequenz (Arginine-Glycine-Aspartate, cRGD) oder zum anderen mit einem amorphen Matrixprotein beschichtet, um so definierte Oberflächen für die quantitative Kraftmessung an lebenden Zellen zu erhalten. Es wurde der Einfluss der Oberflächenspannung an der Luft-Wasser Grenzfläche von Proteinlösungen, die in Kontakt mit den Spitzen der Säulenstrukturen

standen, untersucht. Dies ermöglichte die quantitative Erfassung der Kraftabhängigkeit der Fibronektinpolymerisation.

Im dritten Teil der Arbeit wird die Anwendung der Kraftsensoren für die Messung lokaler Kräfte adhärenter Zellen beschrieben. Hierfür wurden embryonale Fibroblasten von Ratten, welche entweder ein GFP-Paxilin oder ein GFP-β_3 Fusionsprotein exprimieren, eingesetzt, um die Fokaladhäsion an lebenden Zellen mittels Fluoreszenzmikroskopie sichtbar zu machen. Die Korrelation zwischen der Größe von fokalen Adhäsionsflächen und der erzeugten Kraft ergab eine Spannung von 0.1 ± 1.5 bis 115 ± 15.1 $nN/\mu m^2$ als Funktion des Zustandes der Zelle. Die Verwendung von Oberflächen unterschiedlicher Festigkeit - welche durch unterschiedliche Säulengeometrien eingestellt wurden - und der chemischen Funktionalität, war es möglich, verschiedene morphologische Zustände der Adhäsionspunkte in humanen Fibroblasten zu unterscheiden. Die molekulare Zusammensetzung des Proteinclusters der fokalen Adhäsion ist nicht nur abhängig von lokal an die Zellmembran angreifende Kraft sondern auch von der makroskopischen Festigkeit des Substrats. Im Falle von mit Fibronektin beschichteten Säulensubstraten war die Entwicklung der Fokaladhäsion stark von der Steifheit des unterliegenden Materials abhängig. Die Verwendung von RGD beschichteten Säulensubstraten unterschiedlicher Festigkeiten zeigte, dass die lokale mechanosensitiven Eigenschaften der Fokaladhäsion durch einen unabhängigen Mechanismus, welcher die globalen mechanischen Eigenschaften der Zellumgebung bestimmt, unterstützt wird.

Die mechanische Wechselwirkung eines multizellulären Systems wurde im letzten Teil der Arbeit untersucht. Während der Organentwicklung lagern sich Zellen zu Gruppen zusammen und bilden multizelluläre Einheiten in einer strukturell sehr definierten Art und Weise. Die Gewährleistung einer geregelten Organfunktion erfordert die Kommunikation der Zellen untereinander und mit dem einschließenden Gewebe. Die Kommunikationswege basieren auf biochemischen Signalen, welche in den letzten zwanzig Jahren intensiv erforscht wurden. Aber nur wenig ist über den mechanischen Signalweg zwischen Zellen in multizellulären Aggregaten bekannt. Insbesondere wird die chemomechanische Kopplung von Signalwegen immer intensiver erforscht. Madin-Darby Canine Kidney (MDCK) Zellen bilden unter bestimmten Bedingungen in vitro funktionale Aggregate, so genannte Zysten. Die Kulturbedingungen wurden soweit angeglichen, um das Zystenwachstum auf Kraftsensoren zu ermöglichen. Damit wurde die auftretende Kraftverteilung während der Zystenentwicklung präzise dargestellt. In Zusammenarbeit mit Ruth Kroschewski von der ETH Zürich wurden die so erhaltenen Daten verwendet, um ein computergeneriertes Model der Kraftverteilung an MDCK-Zysten innerhalb eines drei-dimensionalen Zellkultur-Systems zu verifizieren. Zudem konnte gezeigt werden, dass unter Verwendung einer strukturell und mechanisch nicht isotropen Umgebung das Zystenwachstum nachhaltig beeinflusst wird. Die normalerweise rund wachsenden Zysten zeigten auf anisotropen Säulensubstraten eine schlauchartige Geometrie, welche bis dahin nur unter Verwendung von Wachstumsfaktoren induziert werden konnte.

Part I

Actual state of knowledge

Chapter 1

General view

Cells are the fundamental units of life. Their behavior such as migration, proliferation, differentiation and gene expression is predominantly dictated by the readout inside the cell but also by the surrounding environment. In vivo, the local tissue structure defines the cellular environment, constraining how cells interact with the surrounding extracellular matrix (ECM), neighboring cells, soluble growth factors, and physical forces. These 'microenvironmental' cues do not only cooperate to regulate the behavior of individual cells - including cell proliferation, differentiation, and gene expression - but also govern emergent properties of the multicellular community. Although understanding these interactions between cells and their surroundings is a fundamental aspect of both, biology and tissue engineering, only a few experimental models exist to control these interactions at the cellular length scale, making it difficult to study the structure-function relationships of cells and tissues. Unlike cells growing in a soft environment, cells cultured on tissue culture dishes or glass coverslips are attached (often via adsorbed ECM proteins) to essentially rigid materials. Therefore, the question arises: Do cells perceive and respond to the rigidity of these conventional materials in ways that contrast with their behavior in much more compliant materials such as tissues, gels, or sublayers of cells? The answer to this question appears important in its impact not just on standard cell culture but also, perhaps, for understanding disease processes, morphogenesis, and tissue-repair strategies.

1.1 Physical state of cellular environment determines cells' fate

Almost 80 years ago, Paul Weiss showed that fibroblasts cultured in a blood plasma clot varied in shape from stellate to bipolar depending upon the orientation of the fibrous network of the clot, and he used this observation to emphasize the dynamic interaction between cells and their physical environment [198]. Around the same time, Warren Lewis observed mesenchymal cells on glass coverslips and reported 'tension striae' or stress fibers in the flattened cells [115]. Ironically, given the ease of culturing and observing mammalian cells on glass and, later 'tissue culture' plastic substrata, 2D cell cultures became standard for most research purposes.

The recent reintroduction of soft materials (either 2D or 3D) as a cell culture substrate emphasized how sensitive cells respond to changes in the physical properties of the cell culture

support. Epithelial cells and fibroblasts were the first cells reported to detect and respond distinctly to soft versus stiff substrates[150] . They have a higher motility on soft surfaces as compared to glass. The adhesion sites were smaller and more dynamic, allowing the cells to migrate faster over the surface. Moreover, fibroblasts showed capabilities to sense stiffness gradients moving always from soft to hard materials, referred to as durotaxis. Although the molecular pathways in the mechanical regulation during cell's life are still only partially known, some evidence exists that a feedback loop, activating different signalling proteins needed to assemble actin, is disabled in cells growing on or inside soft materials (see also part III).

Despite the differences in morphology according to substrate compliance, cells growing in soft gels show also distinguished proliferation patterns and changes in the formation of cell substrate adhesions. In fibroblasts, when growing in floating 3D reconstituted gels of collagen, the typical pattern of actin stress fibers are inexistent compared to the same cells cultured on flat two-dimensional rigid surfaces with the same chemical input. Furthermore, cells in mechanically unloaded gels are quiescent in terms of reduced cell division, however, they still can reorganize collagen fibrils through migration which densify the gel. After reaching a certain threshold of matrix stiffness and ligand density, further contraction of the cell-matrix agglomerate is mediated via an intracellular process called acto-myosin contractility.

Taking into account that fibroblasts in vivo are building up new matrices after wounding and reorganize existing tissue, these individual phenomenas can be summarized to a general view: In normal tissue fibroblasts experience a relatively low amount of tension owing to stress-shielding by the surrounding collagen matrix, so that the organization of a contractile cytoskeleton is not stimulated. This stage correlates to cells growing in soft unloaded collagen gels in vitro. After wounding different grow factors are released from the blood clot and stress fields inside the tissue change suddenly. Under these new conditions fibroblasts differentiate to proto-myofibroblasts and start to migrate towards the stiffer blood clot filling the wound with newly synthesized fibronectin and collagens. The stage of proto-myofibroblasts is comparable to fibroblasts cultured on rigid 2D substrates. Apart from changes in the chemical environment inside the wound, the cells respond to higher stiffness with further differentiation. Myofibroblasts expressing alpha smooth muscle actin in the presence of TGF beta and fibronectin, containing ED-A in the spliced region, generate tension via actin stress fiber formation causing the wound to contract. Therefore, the different phases in the life-cycle of dermal fibroblasts can be simulated with different cell culture systems[53].

Differentiation of cells according to substrate compliance was also found to be improtant after heart attacks or parapleiga. Both are irreversible malfunctions of tissue but stem cell therapy tries to revert these results in new approaches of regenerative medicine. The stiffening of infarct zones for example is mainly caused by replacing the dead muscle cells by fibrotic connective tissue. Restoring the affected area back to a fully function heart tissue by injecting mesenchymal stem cells leads to cellular expression of myocyte markers, but differentiation clearly stops short of myofibril assembly. The reason is unclear, but physical aspects of the microenvironment, especially mechanical compliance of matrix and perhaps adjacent cells, are becoming increasingly linked to gene expression and protein organization. Engler et al. showed in an in vitro approach that substrate compliance similar to muscle tissue is necessary for myotube differentiation into functional subunits of a muscle [61].

Furthermore it is also important to regulate ligand density together with substrate rigidity in order to create the proper environmental conditions for cell proliferation and differentiations. Ligand cues can have different dimensions and even nanometric scaled distances of single recognition sites for cell adhesion can affect cellular response in a dramatic way by switching from stationary to motile cells by only varying dimensions about 20 nm[29].

Furthermore, tissue stiffness may also contribute to cancer development since tumor diagnosis is based on differences in tissue rigidity sensible by palpation, and pathologists have long known that cancer involves distinct changes in the extracellular matrix (ECM) which normally holds cells together within distinct tissue patterns. Alterations of mechanical properties can, in fact, influence tumor development as illustrated by experiments that show how rigidification of ECM shifts the cell to malignacy [147]. Once more, integrin activation followed by enhanced contractility and tension inside the cells alters the cellular force balance that can impact cell proliferation via the mitogenic EGFR/Erk and mechanotransducing Rho/ROCK pathways. Generalized, a physical cue lacking chemical signature inside the tissue may therefore switch cells, even between normal and cancerous states, perhaps by initiating a cascade of multiple switches that simultaneously trigger the leap from one self-stabilizing attractor state to another within the genome-wide cell regulatory network [93]. This mechanism may also explain why continued culturing of normal cells for many passages on rigid plastic dishes often leads to spontaneous transformation in vitro.

The majority of the present thesis is dedicated to the importance of reconsidering physics for cell and developmental biology. First the basic physical aspects of how ECM molecules are assembled into complex three-dimensional networks including surface interaction of proteins at air water-interfaces and shear-stress mediated protein-elongation and -aggregation will be presented. The interaction of living cells with these artificially generated tissue model systems was further analyzed with physical and biochemical methods to shed light on the complex interplay of biological and physical aspects in cellular viability.

1.2 Environmental geometry controls cellular growth

Besides tissue compliance, geometrical arrangement, as well as the density of tissue components has a dramatic impact to cellular control mechanisms. The various 3D forms that tissues exhibit (e.g. tubular, branched, lobular, acinar, etc.) often result from establishment of localized differentials in cell growth during embryogenesis [92]. During angiogenesis, for example, cells at the tips of sprouting blood vessel proliferate more rapidly than cells located only some micrometers away in the clefts of the same vessel leading to regional tissue expansion. Local cell proliferation over time and space leads to the fractal patterns characteristic of all epithelial and endothelial tissues. Positional information responsible for spatially constrained cell growth patterns during organ development is commonly thought to be due to gradients of soluble morphogens or local production of growth factors [124, 202]. However, cell and tissue distortion are observed before growth is initiated in some developing tissues , and it is difficult to explain how soluble gradients of mitogens can produce discrete growth boundaries over the length scale of a single cell, especially in microenvironments saturated with

multiple mitogens [138]. Recent investigations clarified that these local growth differentials may have a mechanical basis. The form of any structure inside a living organism is somehow determined through a dynamic equilibrium of physical forces and can be characterized by its own distinct pattern of internal forces. Thus, the internal mechanical stresses characteristic of a tissue's 3D conformation may convey a physical form of positional information that feeds back to spatially constrain cell proliferation and thereby drive tissue morphogenesis [184].

For example by culturing cells on differently shaped ECM islands, Nelson and co-workers were able to demonstrate that the geometry of the entire tissue dictates the growth pattern: accumulations of proliferating cells were consistently positioned in discrete regions of the cellular monolayer, including along the short edges of rectangles and outer periphery of circles and annular rings, where mechanical stresses were most highly concentrated [137]. This work is based on previous findings, where spatial geometry of cell adhesion can distinguish between proliferating and apoptotic cells. Critical values of adhesion area and ligand density can be attributed either to cell death, when cells are grown on isolated 20 μm islands of fibronectin, or cell growth if cultured on smaller but narrower islands keeping the overall projected ECM area constant [31]. In fact, the establishment of local differentials in cell growth and viability drives pattern formation due to the capability that a living cell can filter the same set of chemical inputs (activation of integrin and growth factor receptor signaling) to produce different functional outputs (growth versus apoptosis) as a result of local mechanical deformation of the cell or nucleus.

Furthermore, pattern formation during embryogenesis is not only dictated by switching between a cell's life and death, the cellular orientation during mitosis contributes also to the shaping of organs during development. Thiery et al. found that the determination of spindle orientation in cultured cells is largely dependent on the spatial distribution of the ECM. Spindle orientation may be influenced by the cell shape anisotropy during cell rounding but its final orientation is defined by the cortical marks that become associated with the retraction fibers. After respreading, these fibers are used to guide the two daughter cells to their destination inside the tissue.

In vivo it was found that epithelial cells always keep spindle orientation restricted during mitosis, so that daughter cells cannot escape from the epithelial sheet. Part of the mechanism may be controlled by "chemical patterning" inside the cell but also cellular geometry has a great input to mitosis. Some results in the last part pointed out that anisotropy in the extracellular environment of a multicellular system can affect the direction of growth during cystogenesis.

Summarizing the body of acquired knowledge, physical methods can contribute to a better understanding of the cellular complexity and the interaction between intra- and extra-cellular processes, yet their applications in molecular cell biology is still in an initial stage.

Part II

Development of force sensors

Chapter 2

Introduction

The use of physical methods in living systems is a relatively new and emerging field in biology. Especially in the last decade, physical methods like AFM or optical tweezers were adopted for the characterization of biological systems. Other approaches used functional substrates, where force measurements are no longer spatially restricted to a single spot. Aside from these passive force measurements some methods were developed that allow active manipulation of the living specimen and change environmental conditions, which again affects the behaviour of the investigated sample. This chapter gives a brief overview of some now common techniques used in cell biology and describes the development of a new force sensor array build up of vertically aligned PDMS posts. Ten years ago Rovensky et al. used for the first time surfaces decorated with silicon spikes in order to create a discontinued surface to investigate the lamellae formation in between filopodias [167]. Turner et al. used micro-fabricated pillars in astroglial cell culture which preferentially attached to the microstructured surface [191]. Unfortunately during the course of this thesis Tan et al. picked up the idea and introduced in 2003 a elastomeric based force sensor array to measure forces generated from single mammalian cells [188].

Chapter 3

Theory

3.1 Force measurement in biological systems

The structure and function of many living cells depend directly on their global and local mechanical environment. The importance of mechanical stimuli can be appreciated at the tissue level through well-known examples such as muscle atrophy and bone resorption in the absence of skeletal loading, and has been implicated at the cellular level in terms of processes inducing adhesion, motility and differentiation. Fundamental understanding of these basic cellular mechanisms and of the pathological response of the cell will be facilitated greatly by developments in the fields of cell and molecular biomechanics [193]. To understand the interactions caused by biochemical and mechanical stimuli, it is necessary to separate these issues by different model systems. In particular, application of external mechanical stimuli can induce biochemical reactions, including the synthesis of new bio-molecules, like collagens or other proteins from the ECM [5][1]. Likewise, changes in chemical stimuli, including pH, temperature, and biomolecular activity, can alter the structure and mechanical integrity of the cell and their environment, even in the absence of mechanical stimuli [73, 16]. Since the development of new physical techniques like scanning probe microscopy or optical/magnetical tweezers, interdisciplinary approaches from different fields contributed significantly to adapt physical and chemical techniques to biology. Thus, it is now possible to probe the interaction forces between individual molecules that comprise the cell and its local environment, as well as the mechanical response of the entire cell down to a resolution in the fN (10^{-15} N) and Å(10^{-10} m) range. Tab.3.1

3.1.1 Techniques used to measure forces in biology

Fig. 3.1 indicates the range of force and displacement covered by these approaches, as compared to the range relevant to representative biological structures/processes. Physical values, like passive (viscoelastic properties of single cells with or without their environment) or active forces (generated by cell movement) are of special concern in biological systems:

- With optical/magnetic tweezers experiments it is possible to quantify passive forces in biophysics [114, 88]. Optical tweezers are based on the controlled displacement of

[1] for detail see Part II

Application	Technique	Abbreviation	Example
Single cell	Substrate composition	SC	Effects of substrate stiffness on cell motility
	Embedded particle tracking	EPT	Measuring cell migration forces
	Force sensor array	FSA	Measuring cell traction forces
	Uniaxial cell puller	UCP	Viscoelastic properties of keratinocytes
Single cell & single molecule	Atomic force microscopy	AFM	Cell stiffness and traction forces
	High resolution force spectroscopy	HRFS	Measure ligand-receptor unbinding forces
	Optical tweezers	OT	Measuring erythrocyte elasticity
	Magnetic tweezers	MT	Viscoelastic deformation of cells and membranes

Table 3.1: Applications of experimental approaches in cell/molecular mechanics and relevant nomenclature. Table adapted from [193]

dielectric objects that are either attached to single molecules or a cell membrane with a laser beam. The applied force can be easily calculated by:

$$F = -kx \tag{3.1}$$

where k is the optical trap stiffness and x is the bead displacement due to momentum conversation, measured via image analysis or optical interference patterns. The value of k can be tailored by varying the trap design and is in the order of 50 $pN/\mu m$ [7]. The maximum force generated with OTs is nowadays 600 pN with 1 pN resolution.

- Uniaxial cell puller: Micoulet et al. used a soft and a rigid glass micro-plate with known spring constants and pulled on a cell which was adhered in between the plates. They showed that biochemical input can alter viscoelastic properties of malignant cell via the rearrangement of keratin, a protein building up the cell cytoskeleton, in the presence of scp. The force resolution is limited to a range of 10 to 50 nN, caused by the minimal optical resolution of 500 nm [16].

- Force sensor arrays: The first experiments using modified surfaces to explore cell generated forces were carried out on soft artificial membranes (PDMS) to detect cell generated wrinkles [85]. Observing the number and the extensions of wrinkles qualitatively, predictions can be made about the direction of cell movements. In 1997 Pelham et al. used surfaces with different compliances to guide cell movement. The fish fibroblasts used by the authors migrate from the soft areas to the stiffer areas but not vice versa indicating that a cell can sense its environment (durotaxis) [150]. More detailed Munevar et al.

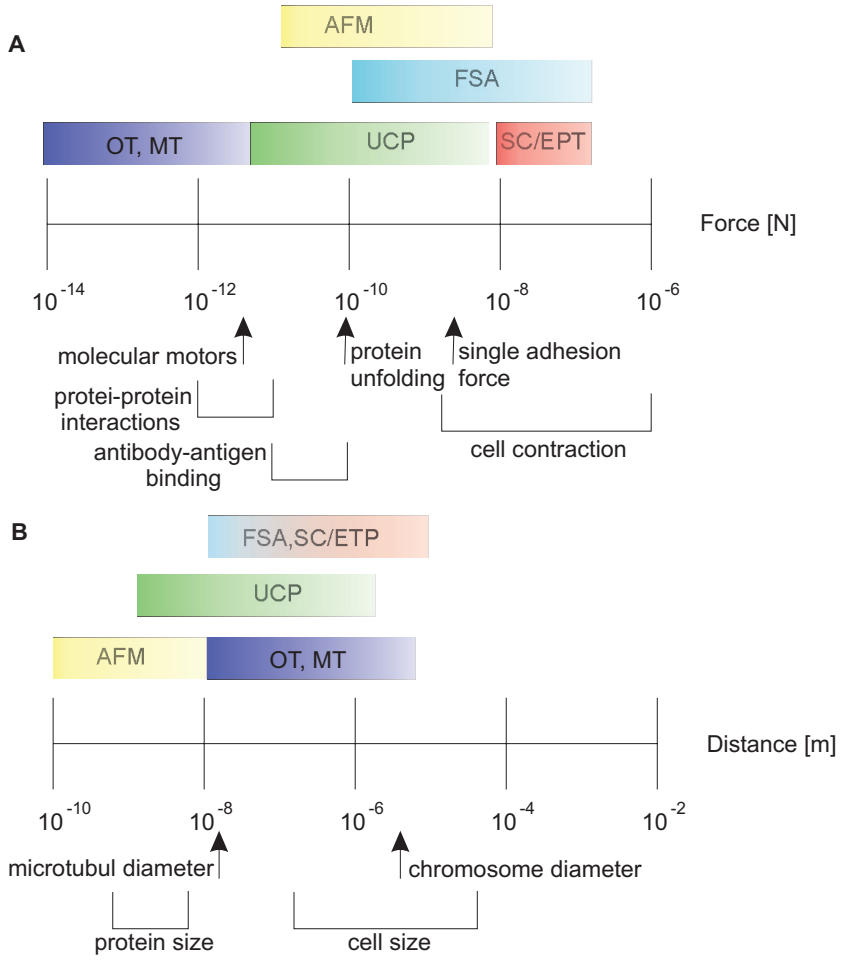

Figure 3.1: A: Force range of experimental techniques and biological events; B: Displacement range of experimental techniques and dimension of biological structures. Abbreviation: AFM: Atomic force microscopy; FSA: Force sensor array; MT/OT: magnetic/optical tweezers; SC/EPT: Substrate composition with embedded particle tracking; UCP: uni-axial cell puller. Adapted from[193]

used soft hydrogels with embedded micro spheres to measure the cell generated force and its directions during cell movement, locally with sub-micron resolution (traction force microscopy) [136]. Micropatterned flexible substrates (PDMS) were used by Balaban et al. to measure local forces exerted by fibroblasts and cardiac myocytes at specific points where the cell is adhering to their environment [8]. For the first time it was possible to correlate exerted force and the area of single focal contacts. They calculated values from cell generated stress at focal contact sites of about $5.5 \pm 2\ nN/\mu m^2$ [2]. Tan et al. published the application of separated elastic post to get individual readable force sensors [3] [188]. They used standard photolithography to create a silicon replica, then cast the elastomer PDMS within that replica to form microstructures. With these point-like force sensors, Tan et al. showed that cells can form focal adhesions to deflect them towards the cell center. The stiffness can be adjusted by changing geometry of the individual

[2] for details of the theory, see [176]

[3] Therefore it is no longer necessary to calculate the force from elasticity theory of soft materials

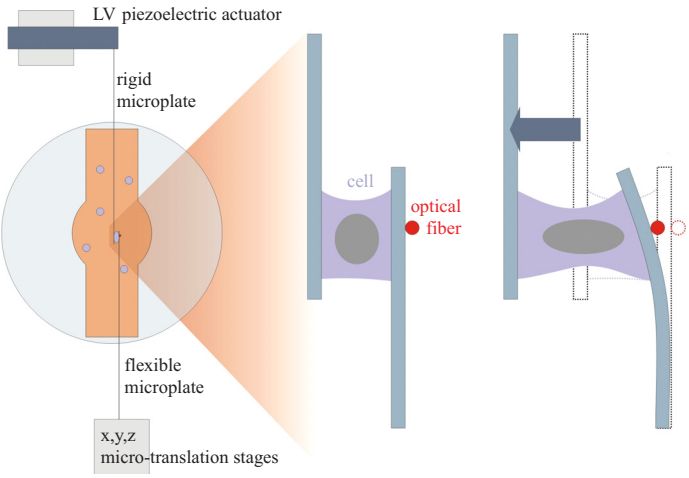

Figure 3.2: Schematic draw of uniaxial cell pulling in between two microplates. While the rigid microplate is deforming the cell the displacement of the soft microplate is monitored with a photosensitive detector system. From the delayed movement one can calculate viscoelastic properties of the cell with and without the influence of biochemical drugs. Drawing from [16]

posts or by varying the Young's modulus of the polymer. Pillar deviation was imaged with high resolution phase contrast or fluorescence microscopy. From image analysis a limited force resolution of 10 nN was calculated. F is given by standard linear elastic beam theory:

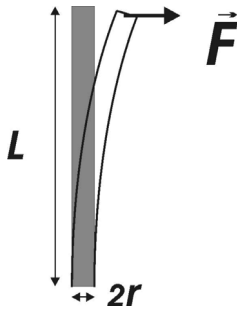

Figure 3.3: From elastic beam theory the spring constant can be calculated using beam length and diameter. Concerning to the theory it is necessary to have pillars with high aspect ratios to increase force resolution.

$$F = -\frac{3}{4} E \frac{r^4}{L^3} x \tag{3.2}$$

There is the need to restrict cell attachment only to the top part of such arrays. The calculated force F strongly depends on where the force is applied to the posts. Therefore several techniques have been developed to functionalize only pillar tops with bio- (fibronectin, FN; collagen type I(CTI)) or biomimetic molecules like the tripetide sequence Arginine, Glycin, Aspartate (short RGD).

- Single molecule interactions: Going from single cell mechanics down to the level of bimolecular interactions it is necessary to change force resolution. The best way to measure

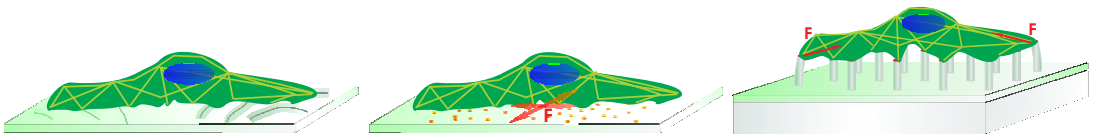

Figure 3.4: Methods to study cell exerted forces to surfaces A: Wrinkles in soft materials are generated by cell contractility[85]. B: Cell migration can be visualised with embedded particles in soft polyacrylamide gels. During cell locomotion, particles are displaced and a force field of surface stress can be computed from elasticity theory [51]C: Principle of force sensor array: While a cell is growing on top of the functionalized arrays the exerted force can be calculated from the pillar displacement.

weak interactions from single cell-cell or cell-substrate contacts is to use high resolution force spectroscopy (HRFS)with an atomic force microscope (AFM). While this technique enables Ångstrom-scale positioning accuracy there is also the ability to image biological features under physiological conditions and manipulate single biological structures with nm and pN resolution. To estimate for example chemomechanical interactions with cell surface proteins (receptors) it is necessary to functionalize the AFM tip with molecules of interest (ligand) to determine the unbinding force between them or to explore the kinetics of molecular interactions as a function of chemical and mechanical environments [15]. With HRFS it is also possible to measure single protein mechanics like unfolding of the FIII domains in fibronectin which plays an important role in fibronectin polymerisation [139].

Chapter 4

Photolithography for FSA formation

4.1 Methods used for standard photolithography

On the basis of the growing field of micro-fabricated devices like small pumps, waveguides for optical networks, sensors and miniaturised magnetic disk drives and to overcome the cost-intensive LIGA[1]-process, IBM introduced at the beginning of the 90s a low molecular weight negative photoresist which form stable cross-linked high aspect-ratio films upon irradiation with the i-line (365 nm) obtained from mercury lamps. The resist is based on the bis-pheno-A novolac Epon SU-8, which is cross-linked by a cationic ring opening polymerization of the epoxy groups with a commercially available triaryl-sulfonium salt as photoinitiator (CYRACURE UVI, Union Carbid, MA, USA) (see Fig. 4.1). The triarylium-sulfonium salt is converted into an acid upon the exposure with uv-light. During the heating process after the light exposure (post exposure bake, PEB) the acid molecules react with the glycidyl-residue by opening the epoxy ring. The acid molecule regenerates and can induce further polymerisation. T_g of unexposed SU-8 is approximately 50°C. Such a low T_g value would have prohibited the use of PEB temperatures any higher than the room temperature in order to keep the linewidth undisturbed by the acid diffusion. The T_g value of the polymer begins to grow rapidly with the increase of the number of cross-links thus dramatically decreasing the acid diffusion rate. For fully crosslinked SU-8 T_g exceeds 200°C (after hard bake). In this way the polymerisation process is constrained in the areas of the resist where the initial acid concentration exceeded a certain threshold value. Therefore, SU-8 resist offers a threshold exposure behaviour, which in other words means a high contrast and probably high resolution. There are several advantages of this system:

- The high content of epoxy groups in the monomer (for SU-8 there are 8) and the aromatic backbone results in a highly cross-linked matrix with remarkable thermal and chemical stability.

- The low molecular weight of around 7000 g/mol makes it soluble in a variety of organic solvents such as propylene glycol methyl ether acetate (PGMEA) or gamma-butyrolacton

[1] Lithographie, Galvanoformung-Abformung

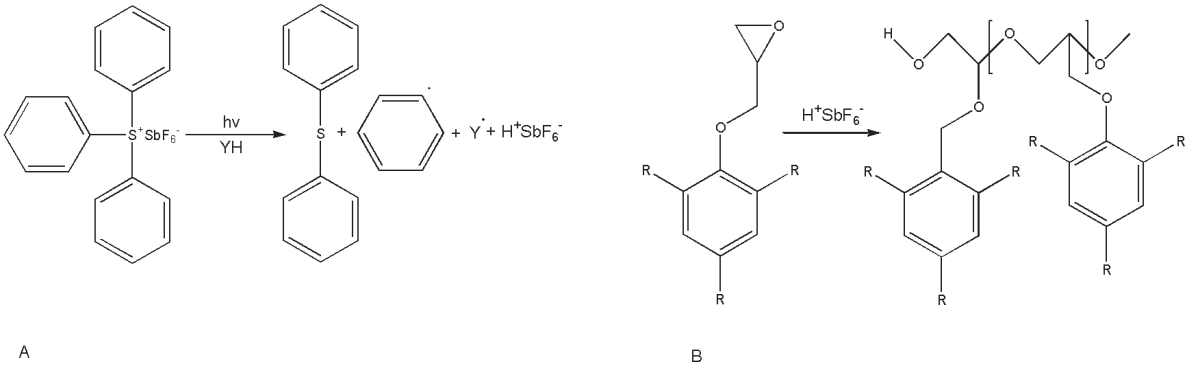

Figure 4.1: Scheme of photo-initiated polymerisation of SU-8: A: The aryl-sulfonium salt is cleaved by light. The generated acid opens the epoxy ring and cross-links the bis-phenol-A novolac to a 3D network.

(GBL), to provide solutions containing up to 85% solids by weight. Therefore thicknesses of 200 μm can be obtained with a single spin-coating step.

- The very low optical absorption of SU-8 in the near UV (from 300 nm to 400 nm provides high aspect structures with ratios up to 14:1).

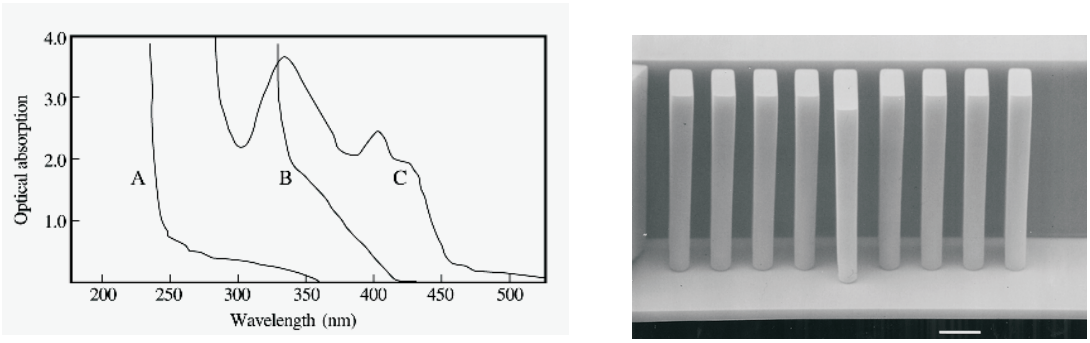

Figure 4.2: Left: Optical absorption of resists thick film processing : A: 25 μ m of SU-8; B: 25 μm of dry-film RISTON T-168 resist; C: 10 μm of positive diazo resist. Right: Hi aspect-ratio structure generate by photolithography in SU-8 resist. Scale bar is 10 μm

4.2 Limitations in photolithography

The aspect-ratio in thick resist methods with optical lithography is basically diffraction limited. To get a detailed view into these limitations the standard lithographic techniques are described in the following.

4.2.1 Shadow printing lithography

The structure is generated by patterning a transparent support, mask (normally fused silica glass) with chromium by optical (low resolution structures) or e-beam lithographic (high

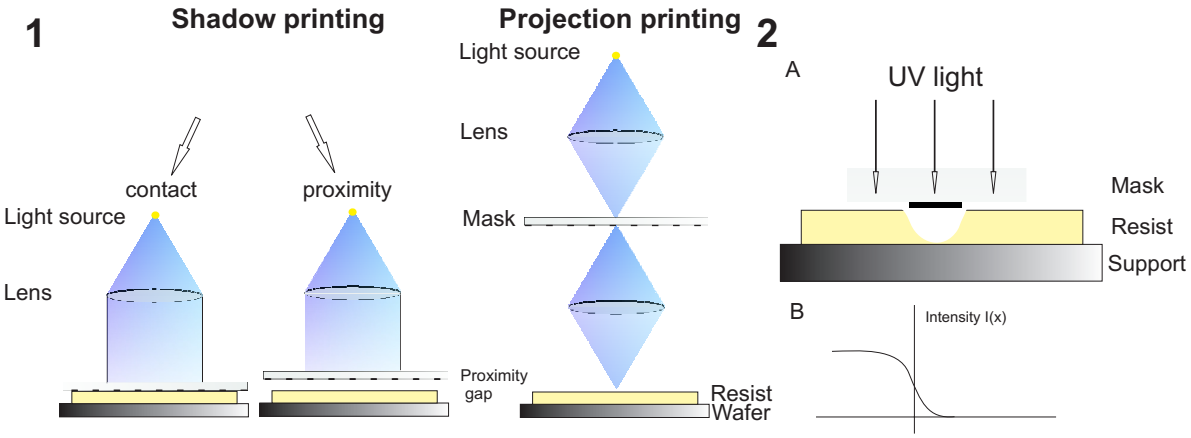

Figure 4.3: Left: Basic two techniques of optical photolithography: Left Shadow printing uses a chromium mask to protect part of the resist from light to get the structure on the photoactive layer. High resolution is achieved only in contact mode with the risk of mask damage. To prevent damage of the mask, the resist is not in close contact (proximity gap), which also results in lower resolution. Right side: Today's 90 nm Intel and AMD chips are produced in projection mode, where the structure of the mask is projected to the resist through an objective. Right A: Resulting geometry of a negative photoresist caused by the diffraction limit. B: Intensity profile of the UV-light using contact printing with a finite proximity gap.

resolution structures) methods. To imprint the structure to a photo-reactive resist (substrate) the mask can be in close contact to the substrate (contact printing) or placed with a gap (d_{prox}) of a few microns over the substrate (proximity printing).The limitation is given by:

$$2b_{min} = \sqrt[3]{\lambda(s + \frac{z}{2})} \tag{4.1}$$

where λ is the wavelength (365nm for i-line), $2b_{min}$ is the periodicity of the structure, s is the gap between mask and resist layer (in case of contact printing s=0) and z is the resist thickness. For SU-8 thick-film lithography using 365 nm light and z=10 μm the min. resolution is 1.5 μm in theory. Below this value the structure is not imaged correctly. The reason is illustrated in Fig. 4.4 While the intensity profile depends on the wavelength of the light used for exposure and the proximity gap between the mask and the resist could not be infinite, the resist is also exposed in the buried regions. This effect gets predominant with higher aspect-ratios. Above a certain threshold there is no possibility to get well defined structures as seen in Fig. 4.4.

4.2.2 Projection printing lithography

The structure on the mask, which could be 10 times bigger than the resulting structure, is projected through a lens system onto the resist layer with a resolution given by:

$$b_{min} = \frac{\frac{\lambda}{2}}{NA} \tag{4.2}$$

where NA is the numerical aperture of the objective used in the system. The attained increase of resolution is limited only to thin resist layers because the depth of focus can be

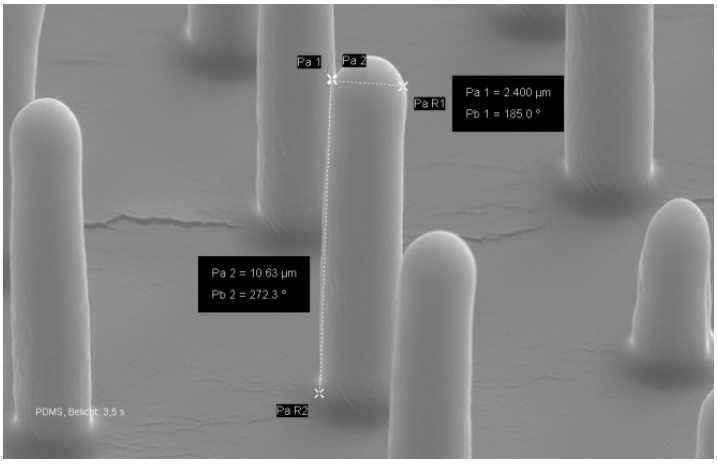

Figure 4.4: SEM image of moulded PDMS pillars with highest aspect-ratio possible produced with standard photolithography. The ends are round shaped because the light is also exposing small areas in the eclipsed part of the resist.

formulated as:

$$\Delta f = \frac{\lambda}{NA^2} \tag{4.3}$$

Today the limiting factor in photolithography is the light source. The latest chip generation is produced with an ArF eximer laser at 193 nm. For lower wavelength (soft X-ray) there is only the cost intensive x-ray lithography to produce structures in the lower nm range. According to Moore´s law [2] in chip production, the use of immersion objectives will be necessary to increase NA over 1 (e.g. oil immersion objective has a NA up to 1.45).

Further on there are some more effects that limit resolution, such as light absorption by the resist material, back-scattering from the support (e.g. highly polished silicon wafers, which is predominant in dense structures with inter-distances smaller than 2 μm), and vibrations during exposure.

[2] doubling of the chip preformance every 24 month

Chapter 5

Superhydrophobic properties of pillar arrays

Wetting of a surface with a liquid depends on the energy of the liquid and substrate surface and on the surface roughness. It can be quantified in the simplest way by contact angle measurements where the angle between the three contact lines, air-liquid, air-surface and surface-liquid is measured (see also Fig. 5.1). Although it has been known for a long time that surface energy affects contact angle only in the last few years, several approaches have been investigated how surface roughness can amplify hydrophobicity in order to produce so called superhydrophobic surfaces [209, 57, 71, 149, 113, 159]. Two requirements are necessary to define a surface superhydrophobic, a very high water contact angle and very low water roll-off angles[1]. The earliest theoretical work to model the apparent contact angle of a drop on a rough surface can be attributed to Wenzel and Cassie [200, 28]. In nature, several superhydrophobic surfaces are known. The most prominent example is the lotus leaf where water droplets rolls off without wetting the plant surface (see also Fig. 5.2)[2]. From that observation it is know that surface structures inducing superhydrophobicity are built up of micrometer sized asperities with a high surface roughness. Several groups used different techniques to obtain super repellent surfaces[3] such as negative photolithography (SU-8 photoresist), structuring of silicon surfaces by dry etching or dicing and deposition of polymers with high surface area[183, 103, 109, 54]. The best defined substrates to explain the theory established by Cassie and Baxter are microstructured surfaces where lateral distance and structural height can easily be controlled. Wetting on rough surfaces may assume either of two regimes: homogeneous wetting (Fig. 5.1 A), where the liquid completely penetrates the roughness grooves, or heterogeneous wetting (Fig. 5.1 A), where air (or another fluid) is trapped underneath the liquid inside grooves. The transition between these regimes plays a major role in superhydrophobicity [121]. The apparent contact angle on a rough surface in the homogeneous regime, Θ_W, is given by the Wenzel equation [200]:

$$cos\Theta_W = rcos\Theta_Y \tag{5.1}$$

[1] the roll-off angle is defined as an angle were a drop applied to a tilted surface starts to roll off.

[2] beside superhydrophobicity the lotus leaf has also self cleaning properties; dirt will be uptaken from the rolling water drops which results in clean dust free surfaces after a rain shower

[3] surfaces are not only superhydrophobic but also can repel non polar liquids [33, 182].

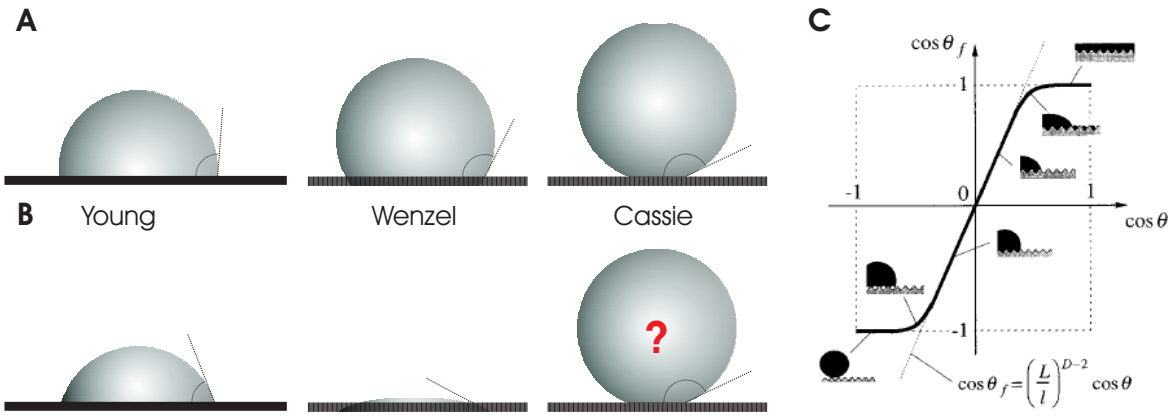

Figure 5.1: A: Different surface roughness from material with $\Theta_Y > \pi/2$ result in superhydrophobic behaviour (Cassie's regime). The contact angel of water easily exceeds 170°and the drop can role over the surface (self cleaning surfaces [21]). B: In contrast, surfaces having contact angels $\Theta_Y < \pi/2$ the roughness is enhancing wettability (see also C on the right part of the diagram). A superhydrophobic surface from materials with $\Theta_Y < \pi/2$ was predicted by Herminghaus and Patankar [86, 148] and also found in vivo. C: Graphical illustration of Wenzel's law. It shows the dependency of $cos\Theta_W$ from $cos\Theta_Y$. It is not predicting the hydrophobicity for hydrophilic ($\Theta_Y < \pi/2$) materials.

where Θ_Y is the ideal Young contact angle:

$$cos\Theta_Y = \gamma_{SV} - \gamma_{SL}/\gamma_{LV} \tag{5.2}$$

and r is the roughness ratio, defined as the ratio of the true area of the solid surface to its projection area. Since r is always > 1, the wetting gets better in hydrophilic situations ($\Theta_W < \Theta_Y$ for $\Theta_Y < \pi/2$) and worse in hydrophobic ones ($\Theta_W > \Theta_Y$ for $\Theta_Y > \pi/2$) [100]. Heterogeneous wetting results from the lower surface energy of dry solids when $\Theta_Y > \pi/2$ compared to a wet solid ($\gamma_{SV} > \gamma_{SL}$). The contact line does not follow the accidents of the solid surface, as supposed for establishing Eq.5.1. In this case, the drop is rather laid on a composite surface, a patchwork of solid and air. Cassie and Baxter proposed an equation describing the contact angle Θ_C at a heterogeneous surface composed of two different materials with surface fractions ϕ_1 for material 1 and ϕ_2 for material 2 [28]:

$$cos\Theta_C = \phi_1 * cos\Theta_1 + \phi_2 * cos\Theta_2 \tag{5.3}$$

If one of the surfaces is just air, the cosine of the contact angle on this surface is -1, and in this case the Cassie-Baxter equation (Eq.5.3) can be simplified to:

$$cos\Theta_C = -1 + \phi_s(cos\Theta_Y + 1) \tag{5.4}$$

where ϕ_s is the fraction of the solid surface. Fig. 5.1 is illustrating the different wetting conditions on smooth and structured surfaces: The switch from Cassie's regime to Wenzel's regime is controlled by the fraction of solid surface area, by the weight of the drop (gravity force must be equal to surface force) and by the height of the surface asperities [46]. The surface enhanced hydrophobicity based on Cassie's equation is only valid for surfaces with $\Theta_Y > \pi/2$, but in nature many superhydrophobic surfaces exists (leaves from *Nelumbo nucifera, Cotinus coggygria Scop., Ginkgo biloba L. or Cercis siliquastrum L.*) where the material building up

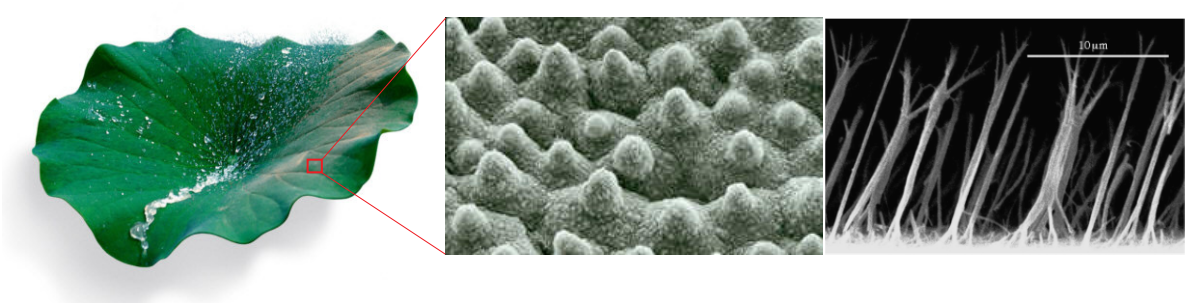

Figure 5.2: A lotus leaf with superhydrophobic and self cleaning properties and its microstructured surface imaged with SEM. The microstructures on the leaf are decorated with epicuticular waxes, witch results in a hierarchical roughness. On the right a artificial surface was generated by nanoembossing PVA polymer through a nano-porous aluminum membrane. The Θ_Y of PVA is 72°on the smooth surface. After nanotexturing the surface, the contact angle raised to 171°.

the structured surface has $\Theta_Y < \pi/2$. All these surfaces showed a hierarchical roughness with nanometer-scale decoration of micrometer-sized spikes (see Fig. 5.2). For such surfaces, Herminghaus derived an argument that a hierarchical structure of the roughness could render any surface (independent of contact angle Θ_Y) non-wettable [86, 148]. Experiments on hierarchical surfaces made from nanoembossed PVA[4] polymer or fractal polymer surfaces, yielded in $\Theta_H > 170°$ for water drops indicating a contribution of the hierarchical structure to the superhydrophobic properties of such surfaces (see Fig. 5.2) [64, 182].

[4]PolyVinylAlcohol

Chapter 6

Materials and Methods

6.1 Mold Fabrication

To fabricate molds with holes of defined height and diameter, it is necessary to get a homogeneous thick layer of photoreactive polymers, which defines the structural height, onto a solid support, like pieces of silicon wafers. Therefore the epoxy based SU-8 resin (Microresist Technologies, Germany) is spin coated under clean room conditions [1]onto a clean silicon wafer with a defined speed (for more details see Tab.6.1). Afterwards the solvent is evaporated by a two step baking process. The wafer is cut into 1 × 1 cm pieces and exposed to uv light through a custom-made negative chromium mask. Thereafter, the photoinitiated ring opening reaction is accomplished at 95°C on a hotplate. To reduce the stress inside the thick resist layer, the structure is cooled slowly for 10 min to RT. Developing is preformed in propylenglycol-monoethylether-acetate containing developer (mr-Dev.600, Microresist Technologies, Germany) for 1 min. The protocol is explained in detail for a 10 μm thick resist:

- Before spincoating, the silicon wafer (Ø100 mm) was dried on a hotplate at 150° C for 20 min. Immediately after cooling to 60 ° C, 3 ml of photoresist was spun on with a two step process. To control resist thickness the residual speed is set as listed in Tab.6.1 In the described case for 10 μm thickness a SU-8 10 [2]resist is spun on with 2700 rpm for 30 sec. resulting in film thickness of 10 μm.

- Softbake and cutting: Evaporate the solvent in two steps, generates a stress-reduced non sticky polymer layer ready to exposure with uv light. In example a wafer with 10 μm resist is heated on a hotplate with a heating rate of 30 °C up to 95 °C and hold for 6 min. After cooling for 10 min. to RT the wafer is cut with a wafer cuter in 1×1 cm pieces and cleaned with a stream of pure nitrogen.

- UV-exposure is preformed on a mask aligner (MJB3, Karl Suess, Germany) equipped with a 400 W mercury lamp.[3] Exposure time depends on resist thickness and varies from 3 to 4.5 sec. (see Tab.6.1).

[1]all work has been carried out in a class 100 cleanroom

[2]The declaration of the resist indicate the medial resist thickness available. It is adjusted by changing the viscosity of resin (epoxy to solvent ratio). There are also SU8-2 (2 μm), SU8-25 (25 μm)and SU-8 100(100 μm)

[3]The build in optics generates a power density of 22 mW/cm^2. The company recommends $100mJ/cm^2$ for 10μm thick resists which is according to 4.5 sec. exposure time. [30]

- To complete crosslinking in the exposed areas the wafer chips are heated up to 95° C [4] for 2 min and cooled to RT for about 10 min.

- For developing the structures it is necessary to redissolve the unexposed parts in PGMEA for up to 1 min. while shaking. The structure is blown dry with a stream of nitrogen and baked for 20 min. at 150°C on a hotplate.

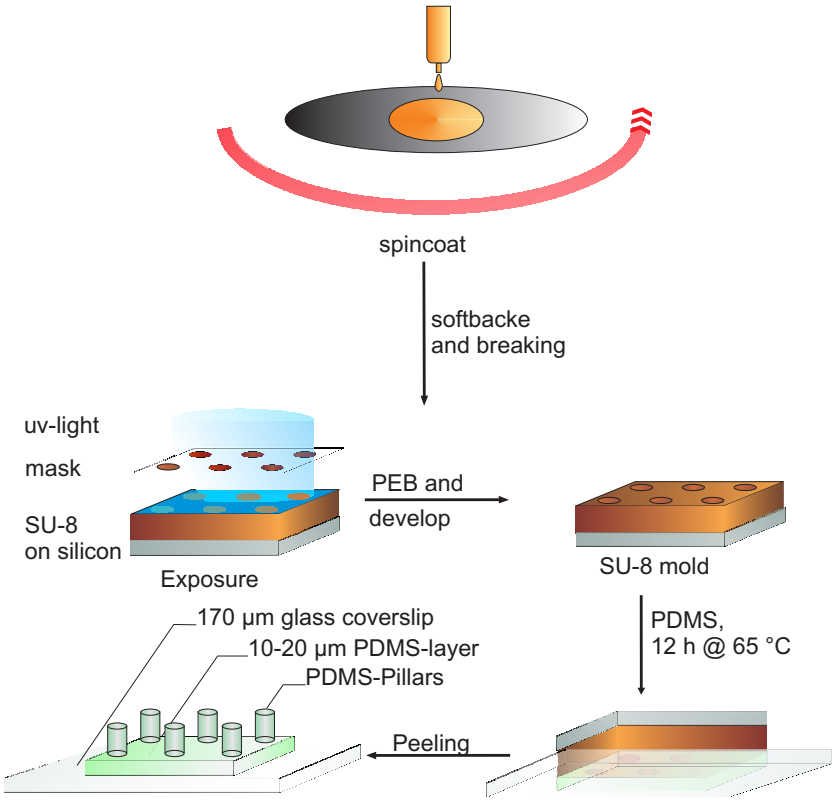

Figure 6.1: Scheme of array formation with spincoating to distribute the resist to homogeneous layer of the desired thickness, exposure to start the polymerisation reaction and development to generate the holes in the resist layer. Pouring the PDMS and pressing the mold to a coverslip gives a suitable device ready for use in standard cell culture

6.2 Casting PDMS

The PDMS used for sensor array formation is from Dow Corning [5]. It consist of a vinyl-terminated 250 siloxane unit prepolymer (18500 g/mol) that is crosslinked via a short hydrosilane crosslinker (50% hydrosilane (4-5), 50% methyl; 684 g/mol and a platinum catalyst. In the well mixed crude state PDMS is a honey-like viscous liquid wich polymerizes at 65°C to a transparent elastic polymer with a Young's modulus of 1.0-2.5 MPa [6]. [ht]

[4] with the same heating rate as for the soft bake to reduce stress inside the polymer layer
[5] Sylgard 184
[6] when is mixed with the crosslinker in the ratio 1:10

Step	Process	Parameters
RESIST COATING	① surface cleaning	bake for 20 min. at 150°C
	② spincoating	SU8-10, 500 rpm,7s., 1500 rpm,30s.⇒ 15μm thickness SU8-10, 500 rpm,7s., 3000 rpm,30s.⇒ 10μm thickness SU8-25, 500 rpm,7s., 2000 rpm,30s.⇒ 18μm thickness SU8-25, 500 rpm,7s., 3500 rpm,30s.⇒ 12μm thickness
	③ softbake	• 10μm: 1 min. 65°; 5 min. 95° • 12μm: 1 min. 65°; 6 min. 95° • 15μm: 1 min. 65°; 7 min. 95° • 18μm: 1 min. 65°; 8 min. 95°
EXPOSURE	① uv-light Exposure	3-4.5 s., hard contact
	② post exposure bake (PEB)	• 10μm: 1 min. 65°; 2 min. 95° • 12μm: 1 min. 65°; 2 min. 95° • 15μm: 1 min. 65°; 3 min. 95° • 18μm: 1 min. 65°; 4 min. 95°
DEVELOPMENT	① resolve unexp. resist	PGMEA 1 min.
	② rinsing and drying	10 s. fresh PGMEA, nitrogen stream
	③ hardbake	20 min. 150°

Table 6.1: Parameters for resist coating, UV exposure and development

After vigorous mixing of crosslinker and base, the PDMS is poured over the molds. To remove trapped air the molds are degassed for 1h under vacuum at $7 \times 10^{-}2$ mbar. The molds are pressed upside down onto 24×24 mm coverslips [9] and cured for 16 h at 65°C. After cooling to RT, the substrates were peeled with an razor blade and overlapping PDMS residues were removed .

6.3 Contact angle measurements

For contact angle measurements, a goniometer from Karl Suess equipped with a video camera was used. Drops were either deposited with a micropipette (at least 20 μl) or was sprayed or condensated onto the surfaces. Drop shape analysis was done with ImageJ. For confocal imaging of water drops on the microstructure, tetramethyl-rhodamine was dissolved in water

[9] to ensure stability of the thin PDMS films and for better handling in cell culture and fluorescence microscopy.

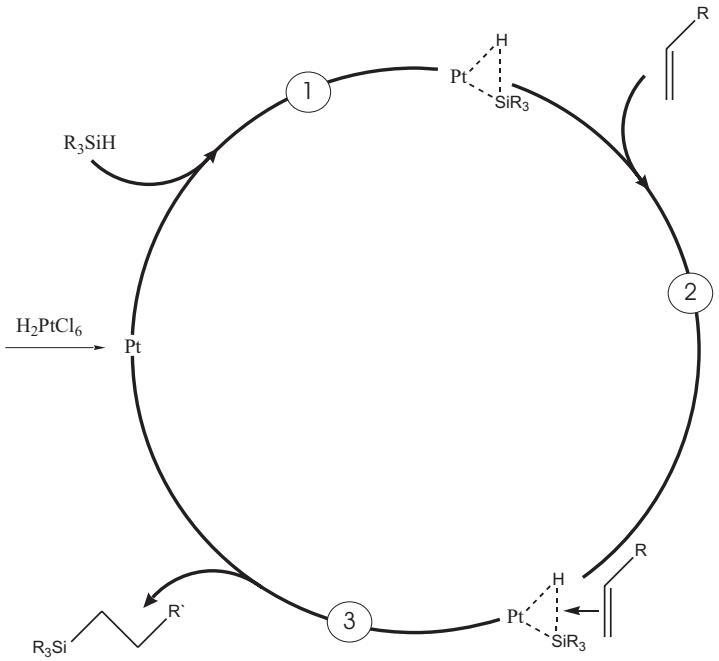

Figure 6.2: The catalytic cycle starts with complexing the hydrosilane to the platinum catalyst ① [8] In the next step the vinyl-terminated oligo-dimethylsiloxane is also complexed ②and the single bond between the silicon atoms is formed after releasing from the catalyst ③.

and imaged in fluorescence and reflection mode using a 40x water immersion objective (N.A. 1.2).

6.4 Calibration and image analysis

Calibration was carried out in two independent ways. Firstly, the measured bulk Young's modulus of PDMS is used to calculate k_{pillar} from pillar dimensions obtained from sem images. In detail, stripes with a rectangular footprint [10] were cut out from PDMS, cured at 65°C and measured at different time points of curing with a spring loaded balance[11]. Dimensions were obtained from microscopy images taken with 10x magnification. Length before stretch and during elongation was measured manually with an calliper (Mitutoyo, Japan). The elastic stress-strain curves were plotted and the Young's modulus fitted according to $E = \sigma/\epsilon$, where σ is the tension (in force per unit area) and ϵ is the strain (relative change in length). Each timepoint was measured twice and the maximal strain from which the PDMS stripes could return to their basic length was shown to be 50% (concerning Hooks's law). For direct calibration of individual pillars a micromanipulator was build onto an inverted microscope. Single pillar bending was performed using calibrated AFM cantilever (see also insert in Fig. 7.3). To characterize the stiffness of a cantilever the thermal fluctuation is measured with an

[10] Areas between $4.8\times10^{-7}m^2$ and $9.1\times10^{-7}m^2$ were analysed to get an appropriate material compliance.
[11] The balance is designed for loadings up to 30 N with a total accuracy of ±0.3%; PESOLA AG, Switzerland.

AFM. The distribution of thermal noise is described by (Boltzmann distribution):

$$lnp = -\frac{kx^2}{2k_BT} + lnA \tag{6.1}$$

After fitting of a second-order polynomal function and background subtraction k can be calculated:

$$k = -C2k_BT \tag{6.2}$$

In a second step the cantilever is approached to a hard surface and the photodiode current is plotted against the distance from the surface. Thereby it is possible to correlate photodiode current and the cantilever displacement. This cantilever is then approached to the microstructured surface in order to laterally bend single pillars. In detail, the microstructures were assembled on a glass bottom petridish and placed on an inverted microscope equipped with a highly precise x, y, z stage (Nanomotion; Applied Precision, USA). The cantilever is mounted with x, y, z micrometer screws to the body of the microscope. After manual approaching the tip to the pillars top, the stage is moved with 0.1 μm steps laterally and images are taken between each step with an 60× water immersion objective [12] and a ccd camera with 1024×1024 pixels in phase contrast. To reduce electrostatic interactions between the PDMS and the cantilever, all measurements are performed in aqueous solution (PBS). Because of the great influence of L on the calculated value of k_{pillar}, it is important to measure all calibrations at the same height, except those where the height dependence is measured explicity (see Fig. 7.5). Overall, a lateral movement of 10 μm is analysed for each pillar (100 datapoints). Position determination from video microscopy is done with sub pixel accuracy using an algorithm written by Wouter Roos in IDL (Interpreted Data Language; RSI, USA). This automated program is based on an analysis method called cross correlation and is described in [75]. It will find the position of a structure marked in one image taken at t_0 from an image taken at timepoint t_1. As the cantilever is concealing the pillar of interest, it is not possible to track the position of the pillar itself. Therefore the difference of the movement from an unaffected pillar and the movement of the tip is plotted against the tip-movement. From the slope (m_{fit}) of the linear fit (see Fig. 7.2.2) the stiffness of the bended pillar can be calculated as:

$$k_{pillar} = m_{fit}k_{tip} \tag{6.3}$$

[12] Objective is from Olympus, N.A. 1.2; camera is from Photometrix, CoolsnapHQ with a resulting pixel size of 0.1103 μm

Chapter 7

Results

7.1 Dimensions

The obtained structures from the molds and after demolding the PDMS are shown in Fig. 7.1. It can be clearly seen that the sidewalls are not parallel. This results from low exposure times and use of soda lime glass as mask blanks which has a slight transmission below 350 nm where the epoxy resist has a high actinic absorption leading to an overexposure of the top portion of the resist film [30]. The dimension and the resulting k_{pillar} values used in this course are listed in Tab. 7.2.1

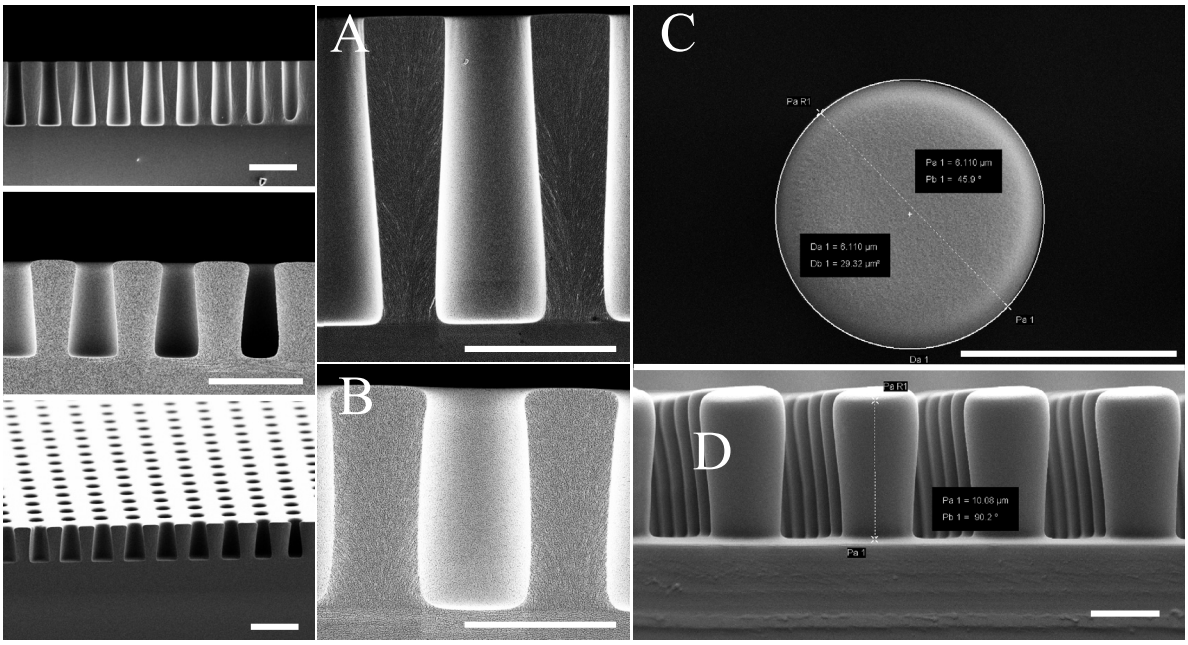

Figure 7.1: A, B: Side view of molding masks with different heights. The resulting structure sizes are A: Ø=5.97 μm, L =11.7 μm; B: Ø=6.8 μm, L= 18.9 μm. bar 10 μm C, D: Molded PDMS Pillars generated from mask B. Bar 5 μm

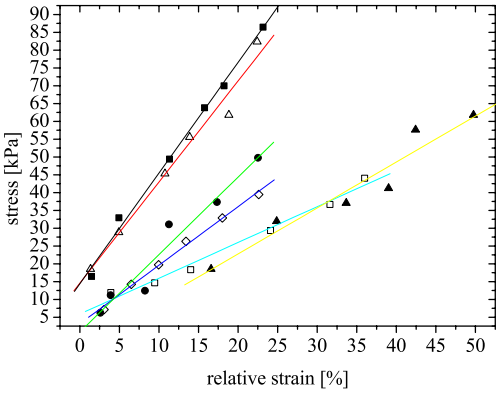

Height L	k_{pillar}
10	0.306
12	0.177
15	0.09
18	0.05

symbol	T[°C]	t[ht]	E[MPa]
□	65	3	1.00±0.06
▲	65	8	1.29±0.18
◇	65	12	1.65±0.06
●	65	24	2.17±0.25
△	65/180	8/2	2.84±0.21
■	65/180	8/12	3.11±0.12

T curing temperature
t curing time
E Young's modulus

Figure 7.2: Left: Experimental stress-strain curves of PDMS under different curing conditions. The parameters used are listed in the table on the right. Top, right: calibrated k_{pillar} values for the pillars used in this course. The changing parameter was L while r kept constant.

7.2 Calibration

7.2.1 Calibration from known Young's modulus

As the pillars are used for measuring forces applied to them only on the pillar ends, it is necessary to find an appropriate method for calibration. Tow independent ways were used as described in the experimental section. Young's modulus of bulk PDMS stripes were measured with a force gauge at different time points of curing. Fig. 7.2.1 summarize the Young's modi taken at different curing times. A variation from 1 MPa up to 3 MPa could be obtained from different curing conditions. With the measured Young's modulus and Eq.3.2, the stiffness k_{pillar} of the pillars shown in Fig. 7.1 can be calculated to $0.17 N/m$ for the lower and to 0.07 N/m for the higher structure. The main errors result from friction caused by sliding inside the force gauge and by size variation of the measured stripes.

7.2.2 Single pillar calibration

For calibrating single pillars, at least 10 different measurements were preformed for one pillar geometry. An average stiffness of $k_{pillar} = 0.218 \pm 0.042 N/m$ is calculated [1]. Fig. 7.2.2 compares the height dependence calculated from theory with the experimental data. After non-linear curve fitting, a $L^{2.5}$ dependence could be estimated. Therefore the experimental data give a slightly reduced value of k_{pillar}. A reason could be, that the pillars are not of cylindrical shape with straight sidewalls as assumed in theory. It is also possible that the

[1] Error is calculated from standard deviation

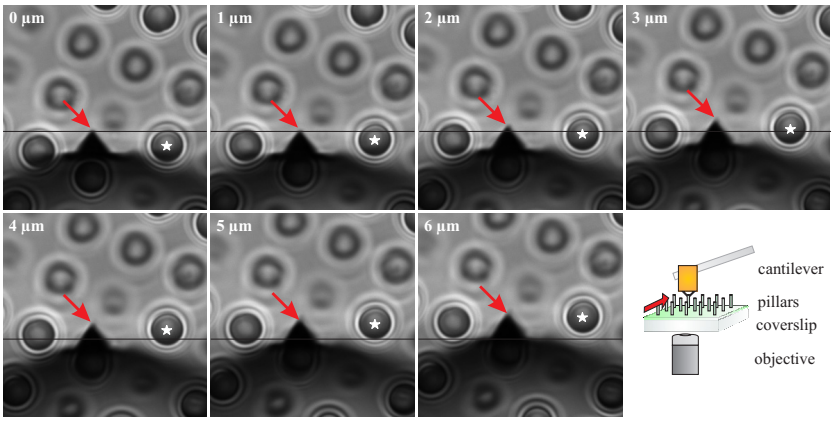

Figure 7.3: Left: Image sequence taken during pillar calibration. Arrow indicates tip of fixed cantilever; asterix indicate a moving pillar in phase contrast. Bottom right: Scheme of pillar calibration with a calibrated AFM cantilever. Arrow indicates moving direction of the microscopy stage. To calculate k_{pillar} the movement from the array is compared with the tip movement of the cantilever. From the resulting difference it is possible to calculate k_{pillar}.

Young's modulus varies depending on the mixing and curing condition (see Fig. 7.2.1). But the biggest error is due to the fact, that in phase-contrast microscopy the z focus could not be set properly [2] and the position of the cantilever along the pillars height could thus not be estimated correctly . As a result k_{pillar} has an error of at least 10 % .

7.3 Superhydrophobicity

The structural size and the contact angle of smooth PDMS (120°) used to build the force sensor arrays are in the range where superhydrophobicity is predominant. The criteria for structures to be superhydrophobic are discussed in the work of C.W.Extrand [46]. In conclusion a contact line density and asperity height criterion must be met in order to show super repellence of the surfaces. As surface forces acting around the perimeter of asperities they must be greater than body forces and directed upward suspending the drop. Also, asperities must be tall enough that liquid protruding between them does not contact the base of the solid, causing the liquid to be drawn downward, leading to collapse. Quantitatively, this requires that values of contact line density and asperity height determined from surface geometry must exceed critical values calculated from properties of the liquid, solid, and their interfacial interactions. Contact angles on the microstructured surfaces are in the range of 150°and 170°. The variation depends on the fraction of solid interface to the entire projected interface and also on the drop size. Drops below the capillary length (water has a capillary length of around 1mm) lie only on the top of the asperities, creating a surface contact angle $\geq 170°$[3]. If the drop size exceeds the capillary length, body weight dominates and the drop tends to penetrate the pillars as seen in Fig. 7.7. To look in detail at the tension line at the air water interface connecting the pillars, rhodamin labelled drops of water were applied onto the microstructure and imaged using a confocal

[2]The PDMS is translucent and the pillar geometry generates many fringes in the collected images
[3]small drops of water can only be deposited on the microstructure by condensation of humified air to the cold surface or by spraying water onto the surface.

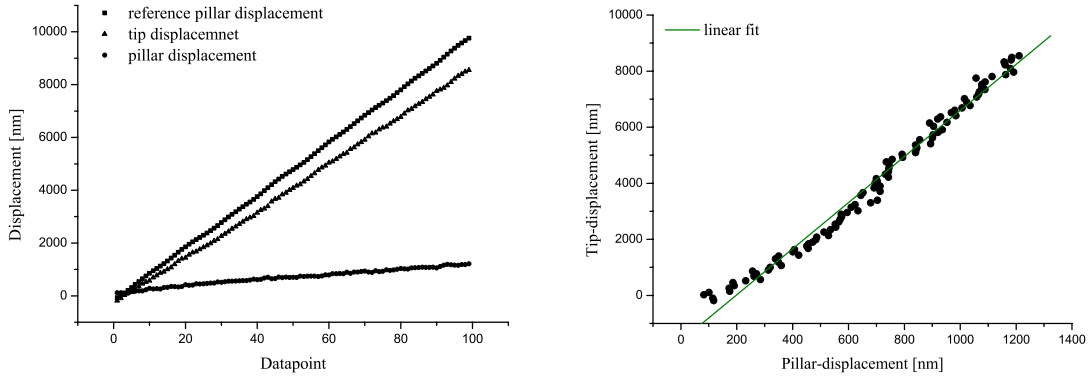

Figure 7.4: Left: Reference pillar and tip movement resulting from image analysis. Right: Pillar- vs. tip-displacement and linear fit. The slope defines the pillar stiffness k_{pillar}.

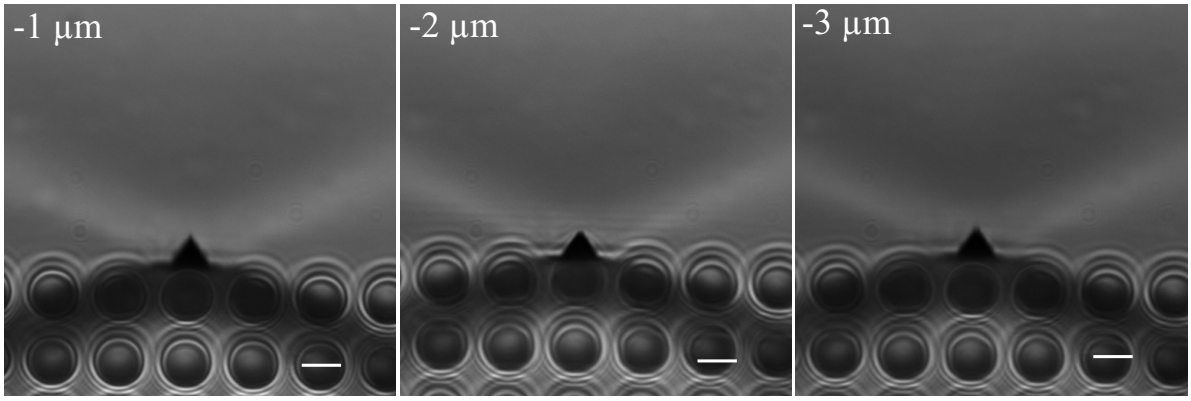

Figure 7.5: Image series for measuring the height dependence of k_{pillar}. Note that the pillars seem to be in focus in all images, although the z focus-plane is moved about 3 μm.

microscope. From Fig. 7.7 it is seen that the pillars are wetted over about 1/4 of their entire length and the air water interface has a convex shape between the pillars.

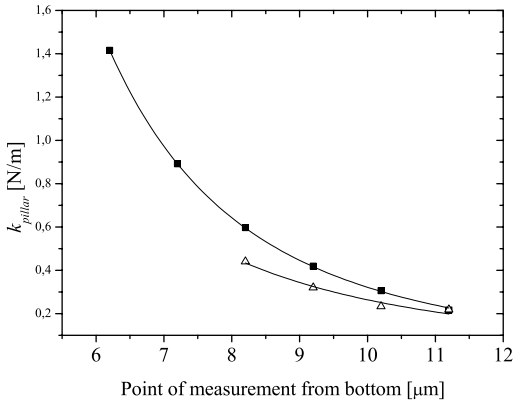

Fitting Parameters	■Theory	▵Exp.
$y = ab^x$		
a	406.31± 14.98	85.19± 54.43
b	-3.1± 0.19	-2.5± 0.29
R^2	0.99989	0.97541

Figure 7.6: Left: Experimental stress-strain curves of PDMS under different curing conditions. The parameters used are listed in the table on the right.

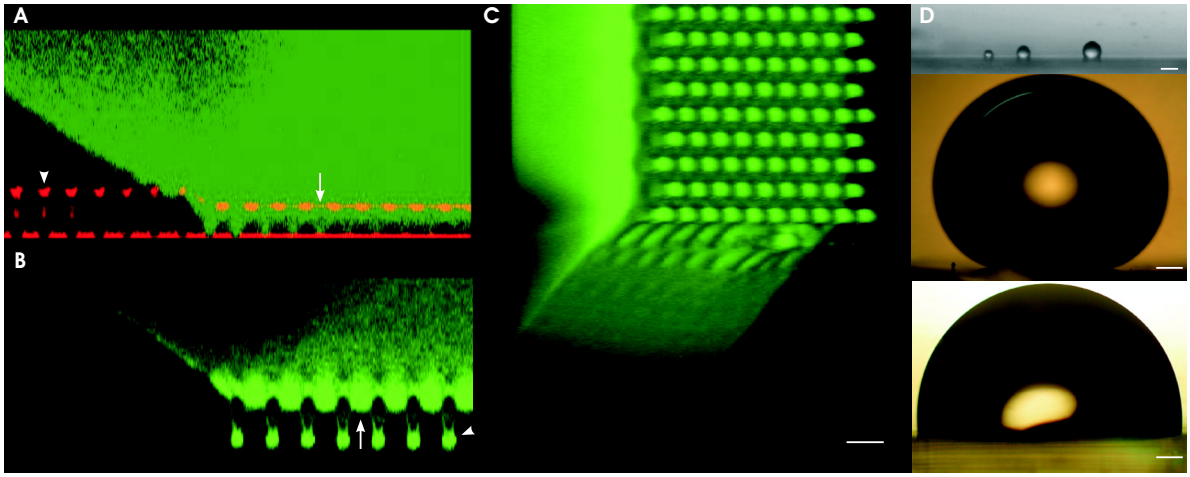

Figure 7.7: A: Side view of a rhodamin labelled drop suspended on the microstructure imaged with a confocal microscope in fluorescence (green) and reflection (red) mode. The reflection of the air-water interface (arrow) is slightly below the pillar ends (arrow heads). B: The suspended drop has a curved interface (arrow) between the pillars (arrowhead) C: 3D reconstructing allows viewing the drop from the bottom. The penetration depth of the water drop corresponds with drop size, here approximately 1.5 mm. Even smaller drops could not be deposited because the adhesion to the pipette tip was stronger than that to the microstructured surface. D: A series of differently sized drops on the microstructure, imaged during contact angle measurement. The small drops on the top row show a near spherical shape (Θ_C near 180°) If drop size is increased the shape gets flattened (Θ_C 160°) and the water is penetrating the surface until it contacts the pillar basement (Θ_W 90°). The scale bars for the confocal images are 10 μm and those for the video microscopy images are 100 μm.

Chapter 8

Discussion

As shown in the last sections, it is possible to fabricate reproducible force sensor arrays using standard photolithographic techniques. The dimensions are in the range of 2.5μm to 6 μm in diameter and up to 20 μm in height. The stiffness can be varied two orders of magnitude (from $\leq$ 0,4 N/m down to 0.006 N/m). With a nominal resolution of 50-100 nm [1] in image analysis it should be possible to resolve forces down to 0.6 nN. The limitations for structures with high aspect ratios are not only set by the described limitations in standard photolithography, it is also a problem of demolding structures. For removing the pillar array from the mould, high forces are necessary, in particular when the array has a high aspect ratio and the contact area between mould and PDMS is increased [2]. The pillars are stretched extensively and snapping back while they are released from holes. During release high pillars tend to aggregate or even collapse due to their own weight. This is shown in Fig. 8.1, where pillars are released from a high aspect-ratio structure generated with focused ion beam drilling [3]. For measuring forces lower than nN, e.g. generated by single molecular motors, their is the need to change polymer for array formation. Great effort has been invested by our group in polymerising PEG diacrylate inside the SU-8 molds. For releasing the structure it is no longer possible to peel the mold. An appropriate method for demolding is to destroy the mold by swelling the hydrogel in a solvent were SU8 did not change volume [4]. With the PEG pillars it should be possible to measure force generated by single motor proteins to their substrate like myosin II interaction with actin [5]. Roos et al. already used PDMS pillar arrays, to build up a biomimetic 2D actin cortex, to study the interactions involved in muscle contractility. Further work could be done to study interactions during vesicle transport on artificial microtubule [6]networks or the force distribution during mitosis in vitro. Another possibility for the use of microstructure with higher aspect ratios is to investigate surface hydrophobicity of materials where Θ_Y is smaller than $\pi/2$. Therefor a contact angle should also exceed 150°because the slender pillars would protect the water drop against wetting of the entire surface [7][148].

[1] depending which objective was used for image acquisition

[2] At a certain level of aspect ratio, it is impossible to demold the structure without breaking the silicon mould

[3] FIB: Focused Ion Beam use high energy gallium ions to strike out atoms from the silicon surface.

[4] mostly water was used in preliminary experiments

[5] actin is a filament-protein which builds up the intracellular skeleton and plays a major role together with myosin II in muscle contractility

[6] microtubules are involved in transportation of proteins or signal transduction in nerve cells

[7] this phenomena is seen in nature and is called the plastron effect. Insects are able to trap air around their body while diving for hunting. Small hair covering insect's body which are bended at their tips about 90°are

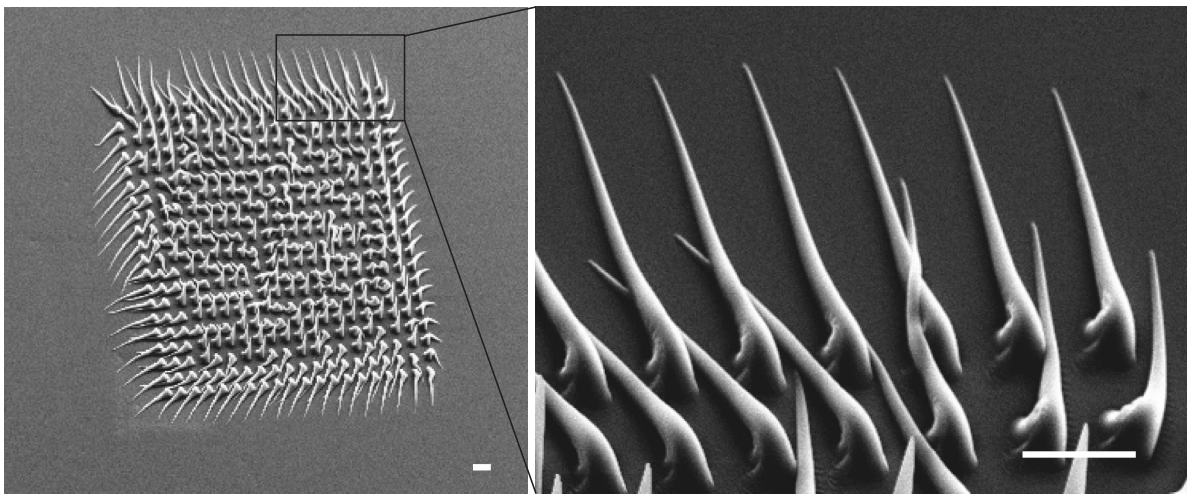

Figure 8.1: PDMS structures molded from a silicon mask generated with focused ion beam. Hole geometry is controlled by the beam shape and structure sizes can be smaller than 1 μm

holding off the water.

Part III

Force Sensors as simple Extracellular Matrix Models

Chapter 9

Introduction

Most mammalian cells are adherent. In order to maintain normal cell function, they need to connect to underlying (epithelial cells) or to thre surrounding (mesenchymal cells) matrix. The biological matrix comprises a collection of insoluble proteins and glycoaminoglycans that are collectively referred to as the extracellular matrix (ECM). A huge amount of these peptide and carbohydrate ligands are recognized by cellular receptors. These receptor-ligand interactions are critical for the maintenance of normal metabolism, proliferation and differentiation and are essential to enable cells to respond appropriately to their environment. The primary function of ECM is to mediate the adhesion of cells [1]. Without adhesion, most cells initiate a program of apoptosis that results in their death, while the loss of adhesion-related signal transduction pathways leads to the growth and spreading of cancerous tumors. The majority of studies on cell adhesion use artificial surfaces like glass, polystyrene and in fewer cases siloxane based elastomers (PDMS), none of which are suitable for cell adhesion. In order to stimulate cell adhesion these surfaces need to be 'activated'. This can be done in a very simple way by incubating the substrates in a physiological solution of cell adhesive proteins, which results however in unspecific adsorption of the proteins with unknown orientation and surface activity. Tailoring proteins, protein fragments or peptide sequences [2] by covalent linkage to the surface is more useful because it is possible to control the amount, spatial distribution and conformational state of the bound molecules [65, 131, 132, 45]. Such surfaces can help to investigate basic aspects of cell adhesion and its regulated processes inside the cells and how different integrin activation is influencing cellular behaviour [6, 110]. There are however some disadvantage for such tailored surfaces. The proteins that mediate cell adhesion are not adsorbed onto flat surfaces in vivo, instead they form a fibrous complex network, to which cells can adhere in a three dimensional fashion. Another drawback is the rigidity of surfaces used in standard cell culture. Since hard surfaces do not exist in vivo,[3] soft and flexible surfaces seem more favorable to control the pliability of cellular vicinities in vitro. For example, it was shown that surface compliance can alter cell morphology on both microscopic and molecular scale. Proliferation and cell spreading was minimized and distribution of focal adhesion was different on soft surfaces compared to rigid ones [150, 43, 195]. However major differences are seen when cells are growing inside a 3D matrix in vitro. Fibroblasts for example have a stellate

[1] It also serves as a mechanical support in connective tissue and strengthens bones due to its fibrous architecture. In cartilage ECM is build up from huge polysaccharides that resist compressive force

[2] which are found in the essential cell binding domains like the RGD sequence in fibronectin

[3] except bone and teeth surfaces

morphology when cultured in a reconstituted soft collagen matrix instead of a ‘pancake-shaped‘ morphology when growing on flat 2D rigid glass substrates [78, 79]. Minimizing such artefacts resulting from non-natural hard surfaces used in cell culture a necessary step is to create new surfaces mimicking structural and molecular composition as well as the pliability of ECM. In this part a new method is described to generate defined fibrous matrix protein networks supported by a soft microstructured surface as introduced in the previous part. By combining all the advantages of both systems, the flat surfaces and the 3D gels into one substrate it is possible to create a powerful tool for the investigative cell biology.

Chapter 10

Theory

10.1 The ECM

The extracellular matrix is composed of five classes of macromolecules: collagens, elastin, proteoglycans, hyaluronan and adhesive glycoproteins, which all together present a rich variety of different organization with vastly different mechanical properties. As a result, the ECM in different tissues is adapted to particular functional requirements, which are as different as, tendons, blood vessel walls, cartilage, bone, the vitreous body of the eye and the subcutaneous fat. The ECM molecules secreted and self-assembled into the immediate cellular environment are linked to one another by multiple binding regions and with specific receptor molecules in the plasma membrane of cells into an organized multifunctional network present in extracellular spaces. The ECM consists of a meshwork of fibers embedded in a gel-like ground substance. The ground substance consists of glycosaminoglycans and proteoglycans, which form extended random coils that hold water by osmotic pressure. The fibrous extracellular matrix components are glycoproteins that reinforce the ground substance and resist its expansive forces. Beyond providing mechanical support, the extracellular matrix also strongly influences embryonic development, provides pathways for cellular migration and sequesters important growth factors.

10.1.1 Glycosaminoglycans

Glycosaminoglycans are long polysaccharides made up of repeating disaccharide units, usually a hexuronic acid and a hexosamine. Apart from hyaluronan, all GAGs are synthesised as covalent, post-translational modifications of a core protein inside the cell [1] resulting in proteglycans. Hyaluronan, a linear polymer, that which often exceeds 20,000 disaccharide repeat units is released without further post-synthetic modification from membrane localised enzymes into the extracellular space. Hyaluronan and proteoglycans are highly charged polyanions (each hydrophilic disaccharide unit bears a carboxyl or sulfate group) that extend themselves by electrostatic repulsion in solution and attract up to 50 g of water per gram of proteoglycane. Retention of water by hyaluronan and aggrecan [2] is essential in cartilage, where compressive

[1] The core protein is synthesised in the ER and glycosylation takes place between ER and the trans-Golgi apparatus

[2] a composite of a hyaluronan backbone with attached proteoclycanes consisting of chondroitin sulfate and keratan sulfate

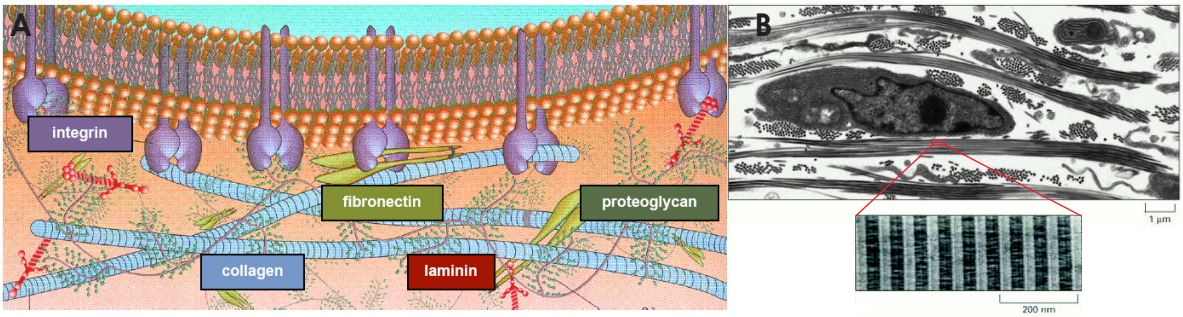

Figure 10.1: A: schematic view of the extracellular matrix network in connective tissue. The proteins are linked to cells via transmembrane receptors which bind to adhesion-mediating ligands such as collagen, laminin or fibronectin. B: TEM image of a fibroblast surrounded by collagen fibrils, seen as black dots (perpendicular) and lines (in plane to image axis). In higher magnification the typical striated morphology of collagen I fibers appears. images are taken from [117, 4].

forces are high. In other tissues, networks of hyaluronan restrict water flow, limit diffusion of solutes, and impede the passage of micro-organisms. Hyaluronan also acts as lubricant in joint cavities [3]. Beside the space filling properties, proteoglycans and hyaluronan are also present at the cell surface, building up the glycocalix. Syndecan, the most common proteoglycan present at plasma membranes of living cells, has for example different functions. Among these functions its heparan sulfate chains at the extracellular domain binds to fibrous proteins (collagen or fibronectin) and the cytoplasmic tail can interact with the actin cytoskeleton. Another class of cell surface proteoglycanes are selectins which play an important role in adhesion of leukocytes to endothelial cells during inflammation (for reviews see [164, 97]).

10.1.2 Collagen

Collagen is the major insoluble fibrous protein in the extra-cellular matrix of connective tissue. It is the most abundant protein found in the animal kingdom. At least 16 different types of collagens are known, but 80-90 % of the collagen in the body consists of the fibrous types I, II, III collagens. Whereas type IV collagen is forming a 2D reticulum, the basal lamina. The typical collagen I base unit consists of a 300 nm long and 1.5 nm thin triple helical structure. It arises from the unusual abundance of three amino acids: glycin, prolin and hydroxyproline, where glycin occupies every third place in the single chain. Collagen is synthesised from cells as a long precursor protein, the procollagen. Enzymatic cleavage of the propeptides in the extracellular space assembles the collagen triple helicals to fibrils [155, 104]). This entropically driven process is completed by crosslinking of oxidised lysine residues with free amino groups (mainly from non-oxidised lysin). Fiber morphology (length and diameter) is controlled by collagen associated proteins and proteoglycans, like collagen type V, type IX, decorin or Fibromodulin [19, 108].

10.1.3 Glycoproteins

Glycoproteins are a class of insoluble, highly glycosylated multiadhesive proteins in extracellular space (e.g. laminin, elastin, fibronectin). They are and long flexible molecules that

[3] recently hyaluronan has been used as a lubricant for arthritic patients

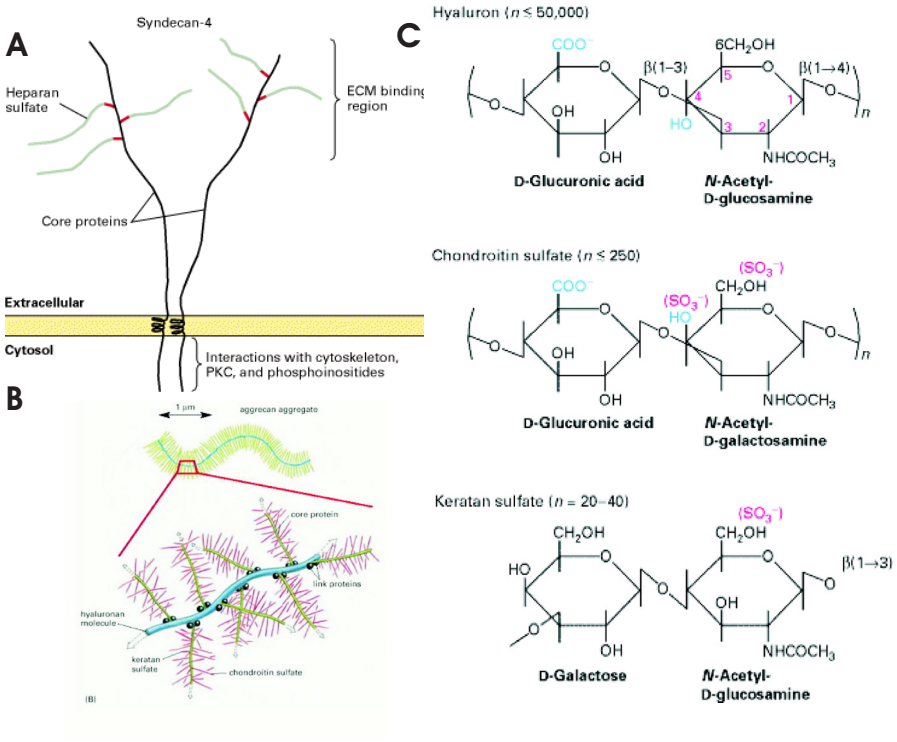

Figure 10.2: A: Structure of the cell surface receptor sydecan, a proteoglycan with heparan sulfate side chains, which can bind to matrix proteins. B: Aggrecan aggregates, an extracellular macromolecule found in cartilage and as space filler in the connective tissue is build up from hyaluronan with attached aggrecan proteoglycan. Its structure, characterized by branches and by the negative charged side chains is responsible for the highly hydrated state of the polymer in vivo. Images are from [117, 157].

contain domains responsible for binding a variety of collagens, other matrix proteins and proteoglycans, cell-surface receptors and signalling molecules such as growth factors and hormones. Their major role is to attach cells to the extracellular matrix. In epithelium-matrix connections laminin is one of the major binding proteins found in the basal lamina. Together with collagen IV it forms a flexible thin (40-120 nm) mat of specialised matrix that underlies all epithelial cell sheets and tubes. The basal lamina thus separates epithelial cells from the underlying or surrounding connective tissue and is determining cell polarity during embryogenesis. It also influences cell metabolism and regulates apoptosis, proliferation or differentiation during organ development. Moreover it can serve as a highly selective filter in the kidney glomerulus (see also Part IV) or direct cell migration. Laminin is a cross-shaped heterotrimeric protein with a total MW of 820 kD which can self-assemble in vitro into a felt-like sheet, largely through interactions between the ends of the laminin arms.

10.1.4 Fibronectin

Fibronectin (FN) is a large, protein consisting of two polypeptides of about 235 kD linked by two disulfide bonds near their C-termini. Each polypeptide chain is a linear array of three types domains, the F-I, F-II, F-III. Each of them has different amounts of repeating units which consist of antiparallel β strands. It exists in two major states, either circulating in

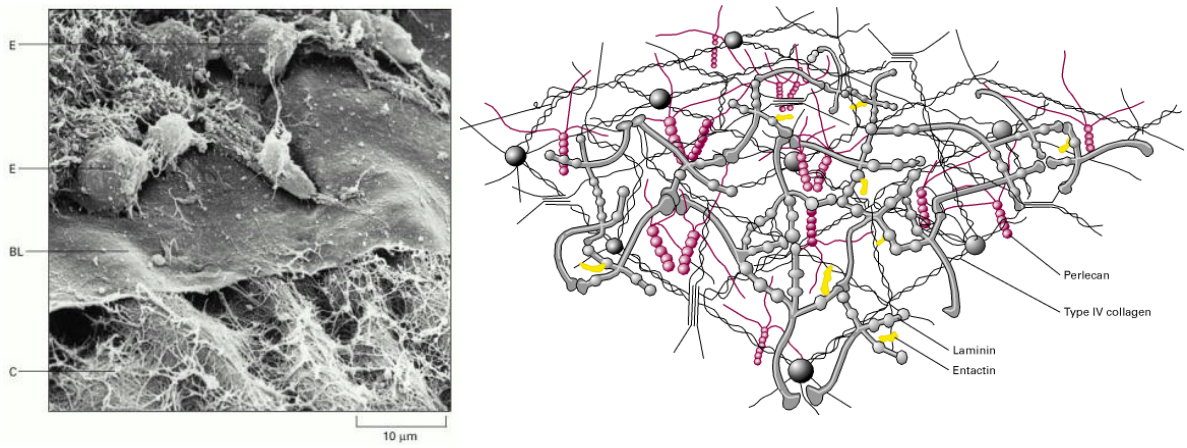

Figure 10.3: The mat-like basal lamina (BL) is protecting the epithelial cells (E) from the underlying connective tissue (C) of fibroblasts embedded in collagen. B: Model of the basal lamina. Images are from [117].

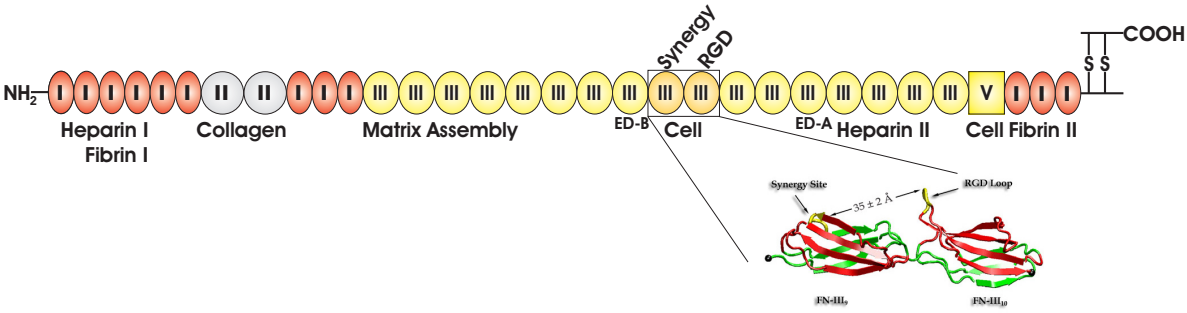

Figure 10.4: Functional sites of fibronectin drawn schematically. In general three types of repeating structural motif are present on the fibronectin chains, termed types I, II, and III. Fibronectin's binding domains and regions involved in its assembly into a fibrillar matrix are delineated along the molecule. Alternative splicing occurs at the ED-A, ED-B, and on the variable (V) sites. A major cell-binding region is present on the 10th repeat unit in the FN III motif. This central cell-binding domain consists of an RGD (arg-gly-asp) site and a synergy site located on FN III_9. A second set of cell-binding sites is located in an alternatively spliced region termed the CS or V region. Scheme is adapted from [127].

blood plasma as a soluble dimeric protein or integrated in the connective tissue as insoluble fibers. Plasma fibronectin is involved in blood clots formation. Binding to fibrin leads to a concentration of the cell binding domains, where activated platelets can bind to (via cell surface receptors). The fibronectin in connective tissue exists exclusively as a fibrous matrix protein interconnecting cells with other matrix proteins. Concerning the functions of a multiadhesive protein, fibronectin has different domains to bind ligands like collagen (located on the FN II domain), heparin I and II (located on the FN I and FN III domains), cell surface receptors (located on the FN III_{9-10} domain), fibrin (located on the FN I domains near the N and C termini) or even to itself (FN recognition site are located on domain FN I_{1-5}[145, 180, 127, 178].

Besides cell adhesion, FN regulates migration, differentiation, and growth during normal wound healing and embryonic development. Loss of FN from the cell surface is a characteristic of many transformed and tumorgenic cells. Restoration of a FN matrix often suppresses the transformed phenotype . Most functions of FN are more evident in the fibrous state compared

to effects of FN in solution. Although much effort has been done to understand the assembly of FN into a matrix, this process is not fully understood. The mechanisms of collagen and laminin fibrillogenesis are well known and confirmed also by cell free experiments [154, 212]. First evidences about the mechanism of FN assembly into fibers were collected from floating cell-populated collagen gels, where a reduced fibrillogenesis of FN was obvious, indicating that forces are needed in order to aggregate FN into fibers [82]. In more detail Zhong et al. have shown that fibrous FN is reduced in serum starved Swiss 3T3 cells. These cells lack active Rho protein - a small GTPase which can induce organization of actin and myosin into stress fibers - and cannot apply tension to the surrounded FN. In contrast FN assembly is enhanced under conditions that activate Rho [220, 206]. From recombinant FN proteins, lacking repeating units 2-5 in the FN III domain and the entire FN I domain near the NH_2 terminus, the essential self binding domain were identified [181, 177]. For example FN III_{2-5} depleted FN did not polymerize when cultured together with CHOα cells, therefore no fibrous FN containing matrix was found in the extracellular space [181]. A possible mechanism was first suggested and considered theoretically by Erickson in 1994, both in the context of FN and for the muscle structural protein titin, which contains many FN III modules and is subject to considerable stretching [62][4]. The structural change of FN III domains under tension may expose a cryptic site for binding additional FN proteins. The energy to unfold a type III module was calculated to be surprisingly small and in the same range as the force generated by one or a few myosin motors interacting with actin [62, 139]. The structural change was also investigated in situ during cell assisted FN matrix assembly. Vogel et al. used a dual-labeled FN monomer and measured FRET [5]values in order to discriminate between compact (high FRET signal) and stretched (low FRET signal) molecules during FN self-assembly. These authors found a stretched conformation of FN in fibrils and a compact conformation of FN on the cell surface and in solution, which is indicating a conformational change during FN aggregation [10, 12]. Additionally several cell-free routes were identified that can promote FN fibril formation, due to the addition of denaturants, reducing agents, or peptidic fragments of the purified protein [130, 89]. FN fibers can also be induced by shear stress in the absence of additives or underneath expanding bilayered phospholipid LB-films [11, 58]. The resulting fibrils exhibit also the high molecular weight characteristic as it is found in the cell-mediated fibrillar networks. However, whether their structure or assembly mechanism is equivalent to that of cellular matrices remains unclear. In both cell-based and cell-free systems, tension seems to play a major role in FN fibrillogenesis. From these results and from SMD[6] simulations of FN unfolding, a general mechanism can be proposed. As illustrated in Fig. 10.5, the assembly of FN into functional matrices can be described by a multistep process. After FN has been secreted in a compact conformation (1), the integrins present on the cell surface binds via the cell binding domain (2). This induces conformational changes that expose FN binding sites and activate the protein to promote intermolecular interactions with other FN dimers (3). Integrin clustering and binding of additional FNs leads to fibril formation, elongation, connections to neighbouring cells, and accumulation into a dense network (4) [178, 72, 41].

[4]while unfolding titin it is protecting the muscle from overstretching. Unfolding of titin is a reversible process unlike applied force is not too high.

[5]Fluorescence Resonance Energy Transfer; the technique is based on the energy transfer between two dyes in a closed vicinity, smaller than 10 nm. If the distance increases the energy transfer efficiency is decreasing by $1/r^6$

[6]SMD: Steered Molecular Dynamics

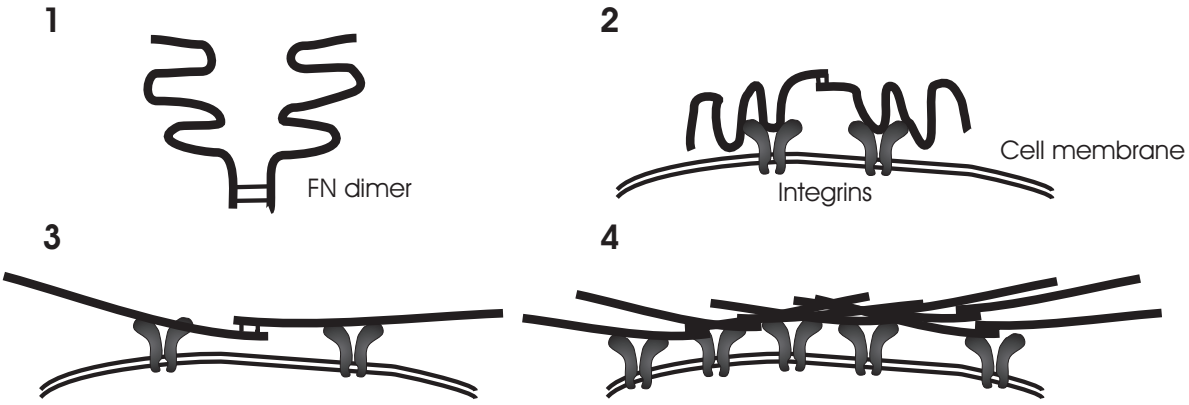

Figure 10.5: Schematic illustration of FN matrix assembly assisted by cell exerted tension. Adapted from [178].

10.2 Protein absorption to interfaces

10.2.1 Native Protein adsorption

Proteins adsorb to essentially all non-natural surfaces [63]. The rate of adsorption is fast [7] and is irreversible on the time scale of routine experiments. All surface adsorbed proteins undergo denaturation. The degree of denaturation is difficult to predict since it depends on many variables, including the structures of the protein and surface, and the composition of the solution (pH, ionic strength, temperature). Denaturation also depends on the concentration of protein in solution; on average, lower concentrations are correlated with greater extents of denaturation since the adsorbed protein has a longer time to denature before the surrounding sites are occupied by neighbouring proteins [185]. Finally, even under ideal conditions, the layer of protein is typically heterogeneous and the determination of distribution in orientation and structure is essentially impossible [8]. Concerning the 3D structure of proteins as shown for FN in Fig. 10.5, proteins should adsorbed to the surface in such a way that the cell binding domains of the adsorbed proteins are accessible for the cell surface receptors [9]. Only in this way can cell adhesion studies lead to results that are comparable to adhesion in vivo. This was shown in studies of FN adsorption to substrates with different surface characteristics (surface energy, surface charge) where differences in the structures of adsorbed proteins (see Fig. 10.6) result in change in the cell morphology, and where the molecular composition of adhesion clusters are obviously different [73, 162, 14, 17, 153, 189, 201, 43].

10.2.2 Alternatives to native protein adsorption

In general, there are some possible ways of controlling the orientation of surface adsorbed proteins. First, it is possible to use only the essential protein sequences mediating cellular adhesion. In the majority of cases a sequence from the cell binding domain found in the FN protein is used, termed RGD (Arginin-Glycin-Aspartate). This small peptide sequence is

[7] for large proteins it can be near the diffusion limit

[8] Therefore it is worth to know how many and in which conformation active ligands are available from the surface adsorbed proteins

[9] Protein structures are normally obtained from x-ray crystallographic methods which may also show a different view of the protein structure compared to the natural one

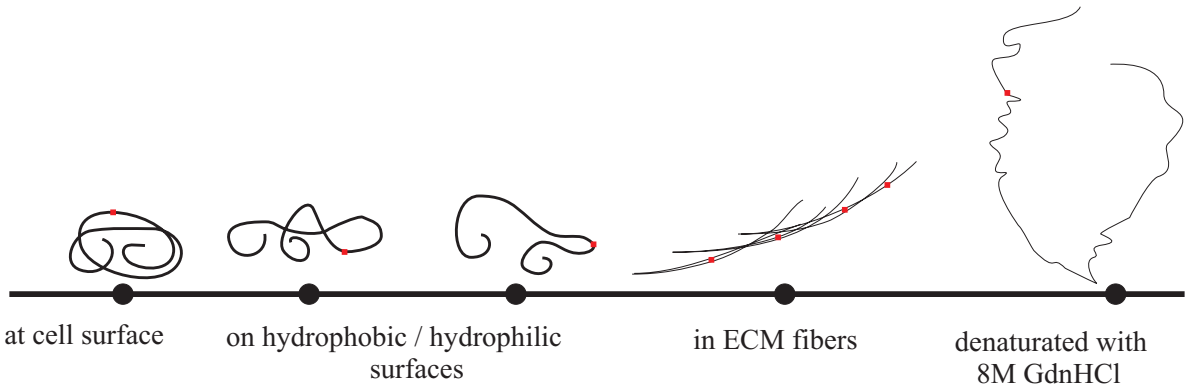

Figure 10.6: Different states of fibronectin conformation in vivo and in vitro. On the left side secreted FN to a cell surface has a compact conformation as well as in physiological solution. Change in surface energy or due to applied force, FN unfolds to a more open configuration. The extreme case of FN unfolding is seen on the right, were FN was totally denaturated in 8 M GdnHCl; tertiary structure is destroyed. The different position of the red marker symbolise the variance in conformation a protein could adsorb onto a surface. Image and data are from [12, 14]

covalently bound to the substrate by reactions shown in Fig. 10.7, generating a surface with known ligand density and orientation [87, 168]. Also the spatial distribution can vary from the nanometer scale, up to homogeneous coatings. Moreover, using different peptides, a organized patterned surface can mimic the spatial distribution of matrix proteins in vivo [6, 52, 135]. Some techniques for surface grafting of small molecules are summarized in the following:

- Co-polymerisation of RGD motif to polymers via acrylates [171]. The small peptide sequence is implemented in the polymerisation reaction or can be added to a existing polymer surface [59].

- Attaching thiolated RGD peptides to gold or silver surfaces forming self assembled monolayers, which are defined in orientation and also in a certain range in spatial distribution [10].

- Chemoselective ligation to premodified surfaces using active ester coupling to amino-terminated RGD derivatives resulting in stable amide bonds [98], or direct coupling of amino-RGD to active hydroxylated surfaces with N,N-disuccinimidyl carbonate in aqueous solution [101]. Bromoacetyl-RGD binding to thiolated surfaces or vice versa [99], quinones which reacts with cyclopentadien generating stable Diels-Alder adducts [210].

- Grafting of RGD peptides to surfaces in a less defined but more general way is done using a photocrosslinker like benzophenone or fluorinated arylic azides. They insert into CH bonds [11] via a photoiduced triplet state (benzophenone) [55] or by a nitren generated from nitrogen cleavage (in case of the arylic azide) [26]. Surface density is not as controlled as in SAM‘s (multilayers are possible but the percentage of coverage can be adjusted by varying the illumination density or the time of irradiation) but the

[10] in the micrometer range spatial RGD concentration can be controlled by softlithographic methods and in the nanometer range by self assembly of gold nanoparticles [135, 133, 134, 91, 6]

[11] a majority of polymers have CH bonds at their interface like PMMA or the chemical inert PDMS

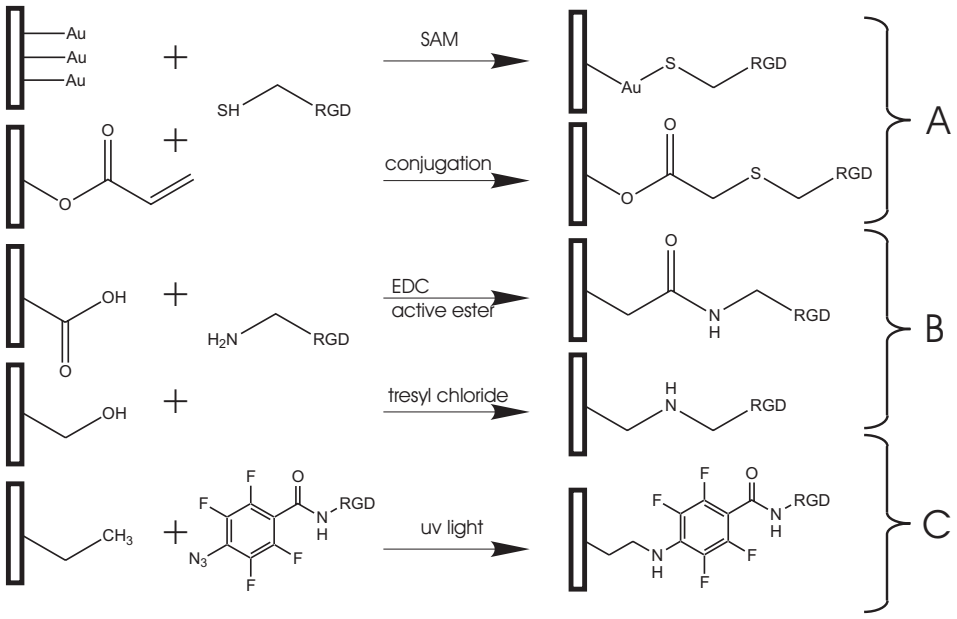

Figure 10.7: Different coupling methods for thiolated (A), aminated (B), and light sensitive (C) RGD peptides to pre modified surfaces. Scheme is adapted from [87]

wide range of usage [12] and the possibility of micropatterning surfaces makes this system more favorable. In Fig. 10.7 some surface reactions known from literature and used for biofunctionalization are summarized.

These tailored surfaces are useful to investigate basic cell behaviour at a low complexity.

To create a more complex system which is closer to in vivo conditions a second approach uses fibrous matrices generated from in vitro polymerisation of different matrix proteins like collagen I, FN, laminin, collagen IV, different GAG's and in combination of the last three together in a mixture called ECM gel (for details in preparation see Part IV of this thesis) [44, 79, 78]. Interestingly cells growing inside 3D matrices which are floating in culture medium behave much different as cells inside a gel connected to a rigid support or growing on a thin layer of protein fibers coated on coverslips [205, 43]. They showed differences in morphology and matrix composition depended integrin usage. Therefore it is necessary to use a system where fibrous protein matrices can be used in combination with controllable rigidity of the substrate [13].

[12] almost all surfaces can be treated

[13] in case of 3D matrix cultures the rigidity can be varied to some extend by the usage of different protein concentrations in the precursor solutions.

Chapter 11

Material and Methods

11.1 Protein labeling

Bovine FN (Sigma, Germany) was fluorescently labelled following a protocol published in [1]. In detail, 0.5 ml of FN solution (1 mg/ml) was first desalted using a size exchange column (Sephadex PD-10, Amersham Bioscience) to remove the Tris-containing buffer [1]. After exchanging the buffer to PBS 10 μg of 5,6-Tetramethylrhodamin-isothiocyanate (TRITC) was added while gently stirring the solution overnight at 4 °C. An 8-fold molar excess of dye molecules was used to get an appropriate degree of labelling. The protein concentration was measured at 280 nm on a UV-Vis spectrometer (Cary scan 500, Varian). The degree of labelling was measured with a fluorescence spectrometer (Cary eclipse, Varian) following the protocol.

11.2 FN at the air water interface

To see how the FN is concentrated at the air water interface, drops of labelled FN (app. 10 $\mu g/ml$ at 10 $\mu g/ml$) were applied to clean coverslips and imaged with a confocal microscope at the border of the drop. In addition a small region was bleached and the fluorescence recovery was imaged over a period of 5 min at 30 sec interval. In Fig. 12.1 C the position of FN bleaching and of image capturing is schematically illustrated. Additionally the FN was deposited also to formvar coated TEM-grids (Plano, Germany) from a 10 $\mu g/ml$ solution. The FN solution was applied to a flat Parafilm and the TEM-grid was laid onto the drop surface. After 5 min. the drop was withdrawn and the grid was washed once with PBS and immediately negative stained with 2 % uranylacetate. Images were captured with a Philips CM12 (Hamburg, Germany)

11.3 FN solutions on superhydrophobic surfaces

FN deposition on the superhydrophobic surfaces was preformed by several approaches. For depositing FN only to the pillar tops small drops (10 μl) of a FN solution in PBS were pipetted carefully to the surfaces and incubated for 2 min at RT. Immediately after withdrawing the

[1] Tris, a primary amine is also reacting with the used dye for labelling FN.

drops with a tissue paper, the surface was wetted with a 70 % solution of Ethanol in double-distilled water (EtOH, Riedel deHaen, Germany) and rinsed with PBS. To generate fibrous FN, the incubation time was increased to 10 min and the FN stock solution was not prediluted but injected into an existing PBS drop sitting alredy on the microarray, resulting in a solution with 10 $\mu g/ml$. After 3 exchanges with PBS the surface was either wetted with 70% EtOH or processed unwetted to get different fiber morphologies. In a different set of experiments, FN was deposited at 10 $\mu g/ml$ in solutions with different ionic strengths and compared to PBS. Two solutions were prepared containing 0.5 M Tris (pH 7.4) and 0.1 M or 1 M NaCl. Deposition was followed by a wetting step with 70 % EtOH and washing with PBS. In the same way bovine FN from two different sources (from Sigma and from Biological Industries) where compared once from its originated buffer diluted to 10 $\mu g/ml$ with PBS or dialysed first overnight in 2 $\times$ 2 l against PBS and then diluted to 10 $\mu g/ml$ in PBS. In addition laminin, a different type of protein from the ECM, was applied in PBS at a concentration of 10 $\mu g/ml$ to the microstructure surface. Wetting and washing steps were the same as for the FN samples. After rinsing the samples, FN or LM was immunoassayed for visualization in fluorescence microscopy. Preincubation for blocking was performed using 0.1 % bovine serum albumin (BSA, Sigma) solution in PBS. A rabbit anti-FN or in the case of laminin a rabbit anti-LM antibody (both 1:100, Sigma) was used as primary antibody followed by incubation of the sec. antibody (Alexa-Fluor488 goat ant-rabbit, 1:50; Molecular Probes). Samples were mounted on objective slides with mowiol 488 (Hoechst, Germany) containing 0.5 % Diaza-bicyclooctan (DABCO, Sigma) and imaged with confocal (Zeiss LSM 5 Pascal) or epi-fluorescence microscopy the DeltaVision Spectris system (Applied Precision Inc., Issaquah, WA, USA).

11.4 Western blot

The cabability of FN fibrillogenesis from soluble FN of different sources was investigated in an additional set of experiments. It is known, that fiber formation only occurs, when the FN molecule is intact, therefore the bovine FN from the two sources was analysed by Western blot following the manufactors protocoll [3]. SDS-PAGE (SDS-polyacrylamide gel electrophoresis) allows the separation of proteins according to their molecular weight. Sodium dodecyl sulfate (SDS) is an anionic detergent, which denatures proteins by ´wrapping around´ the polypeptide backbone and conferring a negative charge to the polypeptide in proportion to its length. It is also necessary to reduce disulphide bridges in proteins with 2-mercaptoethanol or dithiothreitol (DTT) [2], before they adopt the random-coil configuration necessary for separation by size. In denaturing SDS-PAGE separations therefore, migration is determined not by the intrinsic electrical charge of the polypeptide, but by the molecular weight. In a discontinuous system, a non-restrictive large pore gel (stacking gel) is layered on top of a separating gel (resolving gel) to obtain higher resolution of the protein band. For the protein separation, gel electrophoresis is performed using 3-8 % Tris-Acetate pre-cast gels with NuPAGE system (Invitrogen). Protein solutions are reduced with 500 mM DTT and diluted in loading buffer containing glycerin and bromphenolblue (to visualize the run of the protein in the gel). The samples are then incubated for 10 min at 70°C. In each well, a 30 μl volume containing 5 μg of protein sample diluted in loading buffer. The reducing effect is increased by adding an

[2] FN has two disulphide bridges near the c-terminus

antioxidant to the running buffer. Gels are run at 150 V, 110 mA for 1 hr and 10 min. A marker with a protein spectrum between 210-41 kD is used as a molecular weight reference (SeeBlue Plus2 Pre-Stained Standard, Invitrogen). To visualize the different protein bands, the gels were incubated in E-Zinc stain solution (Pirce) for 10 min. and developed for 1.5 min. After washing with PBS, the gels were scanned and digitalized (Epson Perfection 2450 Photo).

11.5 Basement membranes

In order to mimic the basment membrane in vivo, Matrigel was applied at different concentration onto the microarrays by first overlaying the surface with PBS and then injecting the appropriate (100 $\mu g/ml$ and 500 $\mu g/ml$) amount of Matrigel at 4°C. The samples were equilibrated to RT for 10 min and washed gently 3 times. After removing the washing solution, the surface was dried for 2 min and rehydrated with PBS. The samples were critical point dried (CPD 030 Critical point dryer, Bal-Tec, Balzers Liechtenstein) and examined with scanning electron microscope (SEM, Leo 1530, Zeiss, Oberkochen, Germany).

11.6 Single fiber measurement

To measure the elasticity of single FN fibers generated on the microarrays, a solution of 10 $\mu g/ml$ rhodamin labeled FN was applied to the microarray by the injection method as described above. After washing the samples were mounted to a pinched petridish to allow observation through the pillars. To measure the stiffness of single FN fibers a similar setup to that described in Part I for pillar calibration was used. Instead of cantilevers, rigid glass microplates were used to bend the pillars. Images were taken every 100 nm of lateral movement and imaged in fluorescence mode. For analysis the sample was moved 1 μm with 100 nm increments and the stiffness of the analysed pillar (in Fig. 12.6 the pillar marked with *) was set to 0.9 N/m corresponding to the height where the fibers are connected to the pillar sidewalls (about 5 μm from the pillar base). Changes in fiber length were measured from the fluorescence images using ImageJ software (version 1.32j, developed by NIH, Bethesda, USA).

Chapter 12

Results

12.1 FRAP at the air-water interface

In order to construct FN fiber networks on top of pillar surfaces, first a drop of labelled FN solution was placed onto a clean coverslip and examined with confocal microscopy. At the interface the integrated fluorescence intensity was 3 times higher compared to areas inside the drop [1]as seen in Fig. 12.1 A). The stability of this fluorescence intense layer was investigated using FRAP(Fluorescence Recovery After Photobleaching). FRAP is commonly used to estimate protein mobility and turnover in living cells and therefore an ideal tool to investigate the protein diffusion to or from the air-water interface (for review see [161]). A spot at the interface was bleached by a focused laser beam. The rate of fluorescence recovery in this area is plotted in Fig. 12.1. Recovery was in the range of minutes ($I_{FRAP1/2} = 330$sec). For freely diffusing proteins towards and from an air-water interface a diffusion rate in the millisecond range should be expected [126].

12.2 TEM of FN at the air-water interface

Using a pipette tip, it proved possible to pull out thin fibers from the stable interconected network of FN that was lying as a membrane at the air-water interface. By transferring the membrane from the drop surface of a protein solution to a TEM grid, the proteins from the interface were investigated in mor detail. Using electron microscopy randomly orientated FN molecules and orientated fibrils which had dimensions of several 100nm in length and 20 nm in width were observed (see Fig. 12.2). A slight periodicity along fibrils is observed in Fig. 12.2 B. This periodicity was also observed on FN aggregates produced by adding Anastellin [2] to a FN solution. It may result from partially unfolded FN modules along the fiber [123].

12.3 Restricted protein adsorption

By placing a drop of FN in buffered solution (10 $\mu g/ml$) on the surface for only 2 min, followed by completely withdrawing the drop, only the pillars top were immersed in the solution due to

[1]in drops were only rhodamin was dissolved a near uniform intensity distribution was found.
[2]$FNIII_1$ fragment of FN

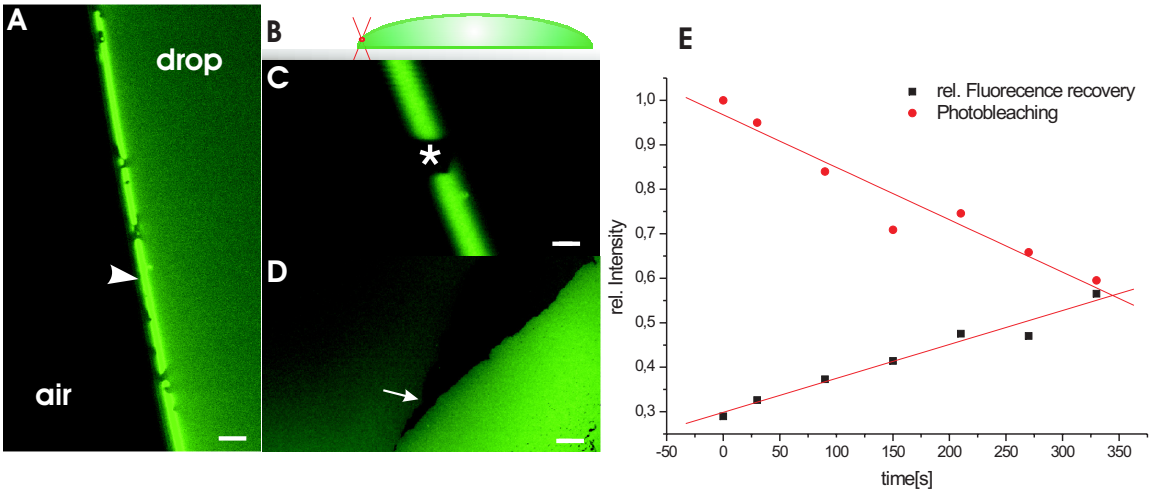

Figure 12.1: A: A drop of labelled FN placed on a coverslip and imaged with a confocal microscope 10 μm above the coverslip. High FN concentration is indicated by an arrow at the air water interface. B: Scheme of bleaching position at the air water interface. C: The bleached area at the air water interface is marked with *. D: Image of a flat drop which was afterwards expanded by injecting 5μl of buffer solution. The stable FN membrane was ripped apart. E: Plotted fluorescence recovery after photobleaching and the absolute photobleaching during image acquisition. The scale bar is 5 μm.

the superhydrophobic properties of the pillar surface. The area of coating was thus restricted to the flat tops of the pillars. The incubation time was kept to a minimum because the solution tends to penetrate the microarray a. The drop sticks to the microarray and after withdrawal a thin liquid film is observed. This leads to deposition of FN-fibers and FN-sheets interconnecting pillar tops (see Fig. 12.3 A-C which are all from the same sample). If the FN is injected into an existing drop of buffer solution in contact with the microarray, resulting in a final concentration of 10 $\mu g/ml$, and incubated at RT for more than 5 min, a dense fibrous network was deposited at the non-wetted areas (see Fig. 12.5 C). This matrix tends to form aligned fibers among major tension lines where the FN molecules are stretched. Tension was increased when the solution had begun to sink slowly inside the pillars [3](see Fig. 12.5D). Defects such as missing pillars allow the solution to penetrate the array and cover the pillars entirely. Along the interface of wetted and non-wetted areas, the fibers are formed. In Fig. 12.5 A the retracted interface is seen leaving behind fibers interconnecting the pillars. The unidirectional orientation of wetting, the substrate was wetted line by line, was responsible of the direction of the highly oriented FN fibers.

12.4 FN fibrillogenesis depends on the protein integrity

In further experiments two different sources of FN [4] were used to see how buffer content is affecting Fn fibrillogenesis. FN from stock solution containing 0.5 M NaCl and 0.05 M Tris was diluted to 10 $\mu g/ml$ with PBS or first dialysed against PBS extensively to remove the origin buffer contents and then diluted with PBS. In the same way FN dissolved in 0.05 M Tris

[3]some networks were tend to sink about half of the entire length of the pillar towards the bottom.
[4]both were bovine FN but from different companies one from Sigma and the other one from Biological Industries

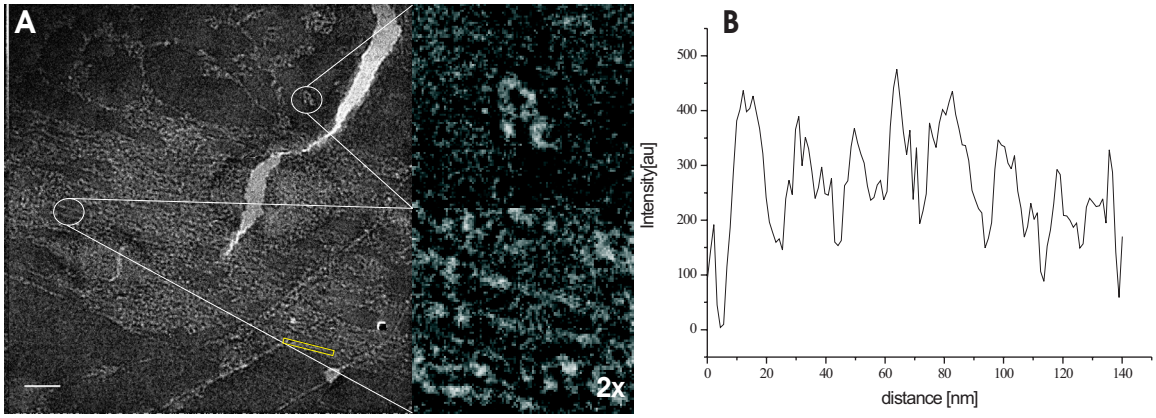

Figure 12.2: A:TEM image of FN deposited on formvar coated grids. Randomly orientated single molecules or aligned strands of several molecules are magnified. A line scan taken from the encircled area with a repetition of intensity every 20-30 nm. Scale bare is 100 nm.

and 2 M Urea was used. Interestingly, FN solutions that originated from the 2M Urea solution did not form FN fibers whereas FN from the 0.5 M NaCl buffer solution showed fibrillogenesis on the microarrays in both cases (the normal diluted and the dialysed solutions). Western blot analysis of the proteins showed a single line at 200 kD for the Sigma FN whereas the FN from Biological Industries was fragmented (two bands at 28 kD) and no band at 200 kD was observed. For fibrillogenesis the need of an intact FN molecule is apparent (see Fig. 12.4).

12.5 Effect of ionic strength to FN fibrillogenesis

The effect of fibrillogenesis on the conformational state of FN molecules in solution was investigated by diluting the FN solutions in buffer with different ionic strenght. From literature it is know that fibronectin unfolds if the ionic strength of the solution is raised [189]. Therefore solutions of 10 $\mu g/ml$ of FN with different salt concentrations were prepared and casted onto the microstructured surfaces (0.1M NaCl or 1M NaCl). No effect of different salt concentration on FN fibrillogenesis was observed (data not shown).

12.6 Other matrix proteins

Other proteins were also tested to see whether fiber formation is unique to FN. Instead of FN, LM was used under same conditions either the 2 min. approach or adding LM to an existing drop suspended by the microarray and incubated for 10 min. No fibers between the pillar were visible and the coating was restricted to the pillar heads as seen in Fig. 12.4 E. LM was slightly visible at the sidewalls if the incubation time was raised to 10min. (compare also Fig. 22.4 in Part IV). To generate a fibrous matrix from non FN-containing proteins or protein blends which was suspended by the microarray a thin diluted protein solution (in this case Matrigel was used) with at least 100 $\mu g/ml$ protein content was slightly dried on the pillar array and rehydrated with PBS. The fibrous matrix was concentrated either as a thin film

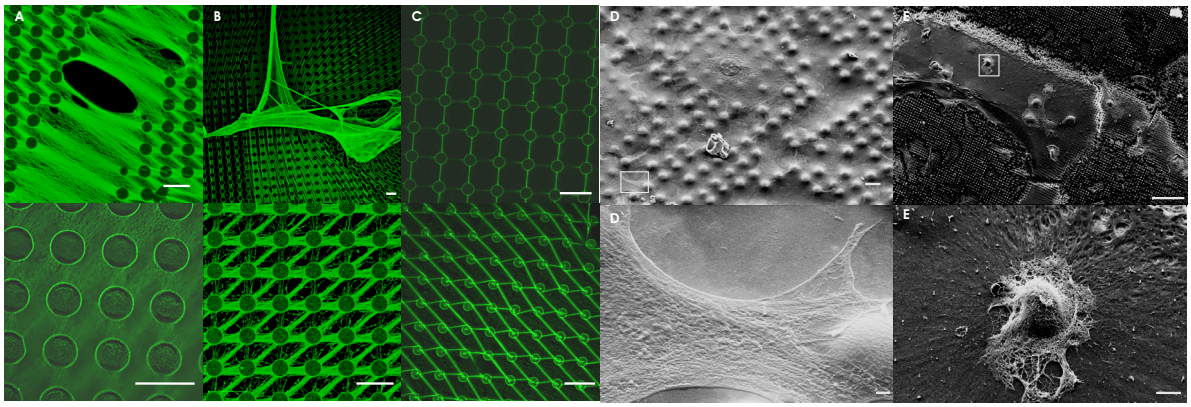

Figure 12.3: A-C: A series of image taken from the same sample. A drop of FN solution was incubated for 10 min. and removed. After wetting and fluorescent labelling, different FN morphologies are visible. Starting from dense fibrous sheets (A) over intermediate fibrous bundles (B) to thin interconnecting fibers (C). The overlaying mats in C are located at the point where the FN solution was detached from the surface. D: Thin ECM layer supported by the microarray casted from a solution. Cultured cells tend to spread out as on flat rigid surfaces. If a higher concentration is used (500 $\mu g/ml$, E) the layer becomes more softer. Cultured cells have a more compact morphology. D‘ and E‘ are images magnified from inserts. Scale bars in the fluorescence images are always 10 μm. In the SEM images D and D‘ scale bar is 10 resp. 1 μm and in E, E‘ it is 100, 10 μm.

(less than 1 μm [5]) or as a 10-20 μm thick hydrated gel depending on the concentration of the applied protein solution.

12.7 Single fiber elasticity

To measure the elasticity of the FN fibers thin fibrils were connected between two pillars as seen in Fig. 12.6 by placing labelled FN solution on top of pillars. A fiber, which was suspended between tow pillar, was choosen to preform the elasticity measurements. One pillar was bent and the movement of the connected pillar was tracked according to the procedure described for pillar calibration. A linear fit of the force distance curves results in a stiffness k_{FN} of $3.45 \pm 1.3 mN/m$ which is two orders of magnitude less than k_{pillar}. Therefore the measured values could only provide a rough estimate of the fiber stiffness.

[5] data from SEM image

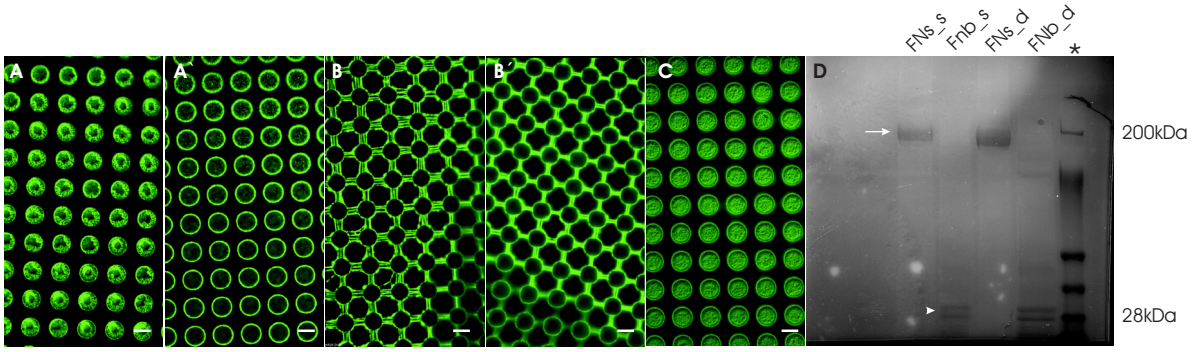

Figure 12.4: A, A': Images of deposited FNb (at 10 $\mu g/ml$) either from stock or dialysed against PBS. B, B': FNs was used under same conditions resulting in fiber Formation. E: Image of FN deposited from a drop with 2min. incubation time resulting in top coating of pillar ends (see also Chapter 3 Fig. 22.4 A). Images are taken in epifluorescence and the scale bar is 5 μm. D: Western blot analysis of the different protein sources. The stock solution was either used without change (FNs_s or FNb_s) or dialysed against PBS (FNs_d or FNb_d), where FNs or FNb is indicating the different source of FN. For FNs a single band is observed at 200 kD (arrow). Whereas, when FNb is used, two bands are observed at 28 kD, indicating fragmentation of the protein (arrowhead). No band at 200 kD was visible.

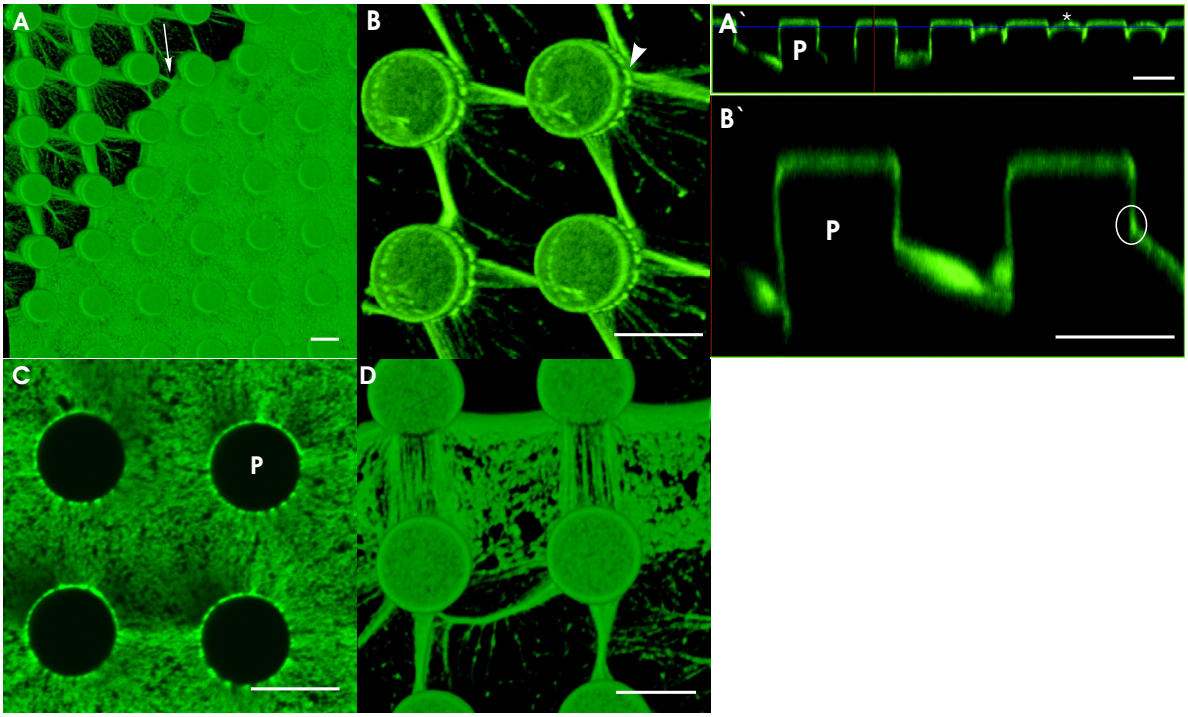

Figure 12.5: A: Image of a sample during fibrous FN deposition. The sample was mounted during wetting. The air water interface , where the fibers are pulled out while the air retracts, is indicated by an arrow. B: 3D reconstruction of the z stack imaged in A. The arrow indicates an area where FN is highly concentrated and the fibers are connected to the pillars sidewall. C: Single z-plane image from the non-wetted area. A random network of interconnected FN aggregates is visible. The dark areas are the pillars which are not fluorescently labelled. D: If tension is applied on the FN network fibrils appeared to be orientated along the major stress lines. B': Side view of B, P is indicating the pillar position to which the FN fibers are connected to (white circle). A': Side view of A with wetted and non-wetted areas (from left to right, P is indicating the pillars). The membrane has a concave shape because the non-wetted area was sealed from surrounded solution. The increased Laplace pressure pushed the membrane upwards against the weight of the solution (see *). Scale bar is 5 μm.

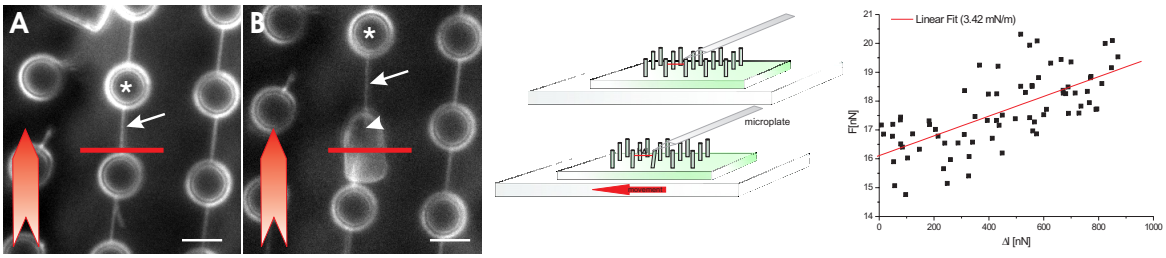

Figure 12.6: Force measurement on a single FN fiber. One side of the fiber (arrow) is fixed by a microplate (position marked with a red line) and the stage is moved laterally about 1 μm (indicated in A and B by the red arrow). For the calculation, the position of the fiber connection is needed (arrowhead in B).The schematical drawing illustrates the experimental setup. The stiffness k_{FN} was calculated to be $3.42mN/m$.

Chapter 13

Discussion

Generation of FN fibers can be generated by different approaches. In the literature, stirring and pulling out a pipette tip from a concentrated FN solution ahve been described [58, 25]. Orientation is poor and the mechanism of fiber formation in vitro is not yet fully understood. From the approach described within this chapter some aspects of fibrillogenesis can be understood. It is apparent that force was needed to aggregate FN into fibrills. The fiber formation on the microarray was fast (fibers develop during wetting or remove of droplets [11]). Fibrillogenesis was in most cases a result of shear forces, which were either from the proceeding water interface during wetting or caused by withdrawal of the protein solution. How these forces affected the thin layer of proteins at the drop boundary laying on the pillar surface was not investigated in detail, e.g. during wetting, because of the inaccessibility [1]. Along the line of highest tension at the air water interface between the pillars, orientation of the interconnected FN molecules was observed indicating a stretch-induced fibrillogenesis. It is worth mentioning that use of a protein from a different company results in no fibrillogenesis in vitro. From Western blot analysis it could be concluded that the entire fully functional protein is necessary to produce fibers. If FN is fragmented no fibers were obvious on the microarray. Fragmentation could be a result of wrong storage conditions or even of a different purification procedure. Which epitope in the protein sequence was responsible for fibrillogenesis was not investigated but one can propose to use recombinant proteins lacking different FN modules and check whether they can form force induced fibrils in the future [181]. While fibrillogenesis from solutions of different ionic strength resulted in the same fiber morphology, the initial conformation of the FN molecules is not important[2]. This may a result of the strong hydrophobic character of the air water interface to which proteins can adsorb such that the original conformation in solution plays a minor role. This artificial model of FN fiber formation could be useful for the full understandings how selfassembly of FN molecules takes place. In combination with techniques like FRET or AFM [3] which can measure stiffness of single fibers and by investigation of the crystal structure of the fibrils by TEM, a model of formation and the molecular/structural composition should be available. It could also be useful to study how a defined structural environment can affect cellular behaviour in vitro and how this well controlled support changes biochemical signals and gene expression (see also Part III, where

[1] air water interfaces and the PDMS are disturbing fluorescence microscopy, and even the fast process of wetting makes it difficult to achieve good images for quantification

[2] change in pH was not investigated.

[3] Atomic Force Microscopy

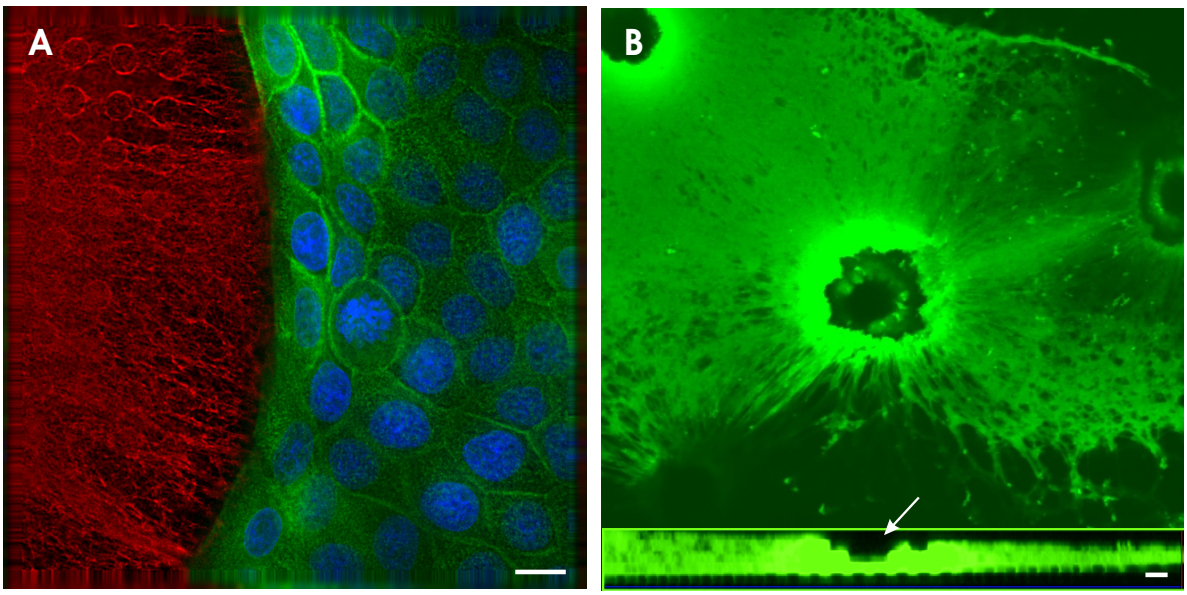

Figure 13.1: A: Epithelial cells (stained for actin, green and nuclei, blue) are growing in a dense monolayer on top of ECM (stained for laminin, red) coated pillars, which is mimicking the basal lamina. Also it should be possible to generate co-cultures where mesenchymal cells are growing inside the microarray and epithelial are laid on top. B: Cells growing inside a thick gel which is supported by the microarray, which could serve as an additional model to study invasive characteristics of tumorgenic cells.

such surfaces were used in combination with adhesion studies). Also dense fibrous mats with well defined physical and chemical properties can be used as a model system of the basal layer between epithelial and mesenchymal cells. So far, no artificial model systems exists, where the molecular composition and tphysical properties of the surface are combined into one system. This enables for example, ephitelial cells to grow as polarised sheets of cells as also found in vivo (compare also Part IV and Fig. 13.1).

Part IV

Physical properties of single cells

Chapter 14

Introduction

The linkage between cells and their environment, mostly other cells or the ECM is mediated by membrane-localized proteins which are referred to as cell adhesion molecules (CAMs). Those proteins building up cellular junctions are different in nature and function depending where they are localized. Overall five major transmembrane proteins have been shown to be involved in cellular adhesion: cadherins, immunglobuline-superfamily (Ig-superfamily), selectins, mucins and integrins. The interactions are either homophilic (cadherins), which are predominant in cell-cell junctions or heterophilic (integrins) in the case of cell-ECM adhesion.

Both the cell-cell and cell-ECM junctions play an important role in maintaining cellular behaviour at a single cell level during embryogenesis and wound healing and are necessary for shaping and the functionality of multicellular structures. The known junctions in adherent cells can be classified into different functions: occluding junctions seal cells together, for example in epithelial tissue, to prevent small molecules from leaking from one side to the other; communicating junctions mediate the passage of signalling molecules, such as ions and soluble factors, and electrical signals. Anchoring junctions serve to mechanically attach cells to each other and to the extracellular matrix. In particular, anchoring junctions play an essential role in tissue maintenance providing structural cohesion; such junctions are most abundant in tissues subject to constant mechanical stress like skin, connective tissue and heart.

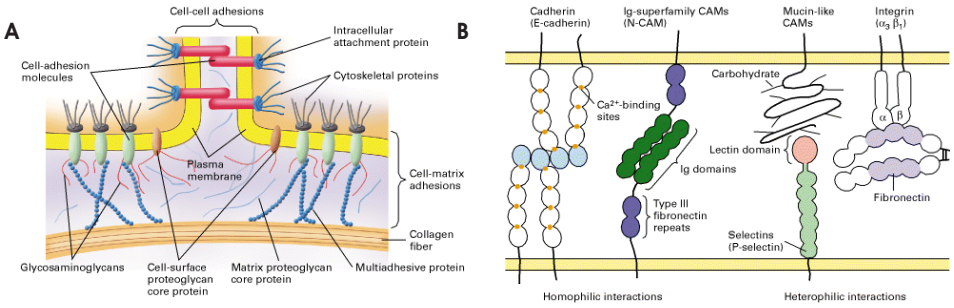

Figure 14.1: Scheme of molecules that are involved in cell-cell and cell-ECM adhesions. Cadherins are essential in maintaining epithelium integrity, whereas integrins link cellular domains to the ECM. Image adapted from [117].

Chapter 15

Theory

15.1 Cell-cell contacts

Stable adhesion in cell-cell interactions are predominantly mediated by homophilically interacting cadherins which have structural (adherens junctions) and signalling (desmosomes and gap junctions) features. In adherens junctions, actin is linked to cadherins through a set of intracellular proteins, such as catenins, vinculin and $\alpha-$actinin forming a contractile bundle which allows the epithelium to be reshaped. Cadherins in tight junctions are not only involved in selective adhesion between embryonic cells but are also primarily responsible for the formation of stable junctions between cells in tissue. For example, E-cadherin is expressed in epithelial cells, so homophilic interactions between E-cadherins lead to the selective adhesion of epithelial cells to one another. It is noteworthy that loss of E-cadherin can lead to the development of cancer derived from epithelial cells, indicating the importance of cell-cell interactions in controlling cell behavior. Different members of the cadherin family, such as N-cadherin (neural cadherin) and P-cadherin (placental cadherin), mediate selective adhesion of other cell types. In desmosomes desmoglein and desmocollin are interconnecting intermediate filaments between cells, forming an intercellular net of great tensile strength. The intermediate filaments are anchored intracellular by linking proteins (plakoglobin and desmoplakin), see Fig. 14.1.

15.2 Cell-ECM contacts in two dimensions

Adhesions to the ECM ligands are mediated by heterophilic interactions with the extracellular domain of integrins. Integrins form a family of receptors that share, as a basic structure, two non-covalently linked type I transmembrane glycoproteins subunits, the α (120-180 kD) and the β (90-110 kD) subunits [94]. The α and the β subunit, which both contribute to ligand-binding specificity, contain a large extracellular domain, a single transmembrane domain and a short cytoplasmic domain, usually 40-50 amino acids long. The β subunit is linked to the cytoskeleton by interacting with actin-binding proteins, such as vinculin and talin. This allows vertebrate cells to use a combinatorial strategy to establish their integrin repertoire. They selectively express a subset of 18 different α chains and 8 β chains. These chains combine to form at least 24 different kinds of dimers, each with different ligand binding specificity (see Fig. 15.1 [117]). Both the α and the β chains participate in binding at least two sites on

JUNCTION TYPE	ADHESION PROTEIN	EXTRACELLULAR LIGAND	INTRACELLULAR CYTOSKELETAL ATTACHMENT	INTRACELLULAR ANCHOR PROTEINS
CELL-CELL				
Adherens junction	E-Cadherin	E-Cadherin	Actin filaments	Catenins, vinculin α-actinin
Desmosome	Desmoglein, desmocollin	Desmoglein, desmocollin	Intermediate filaments	Desmoplakins, plakoglobin
CELL-MATRIX				
Focal adhesion	Integrin	Extracellular matrix proteins	Actin filaments	Talin, vinculin, α-actinin
Hemi-desmosome	Integrin $\alpha_6\beta_4$, BP180	Intermediate filaments proteins	plectin, BP230	

Table 15.1: Anchoring junctions and their components. Table is adapted from [4]

ligands. Integrin $\alpha_5\beta_1$ binds two sites on fibronectin: the RGD loop of FN-III domain 10, and a secondary site on the adjacent FN-III domain 9 (the synergistic site, see also Fig. 10.4) [120]. Integrins generally have a low affinity for their extracellular ligands. The micromolar K_d of integrin $\alpha_5\beta_1$ and fibronectin makes the interaction dynamic. Rapid association and dissociation allow cells to adjust their grip on fibronectin in the matrix as they move through connective tissue [117].

15.2.1 Structure and characterization of contact sites mediated by integrins

When a cell contacts the ECM, several types of structures are formed at the contact side; these structures are assembled according to the type of matrix, the cell type and the stage of cell activity. These sites are termed Focal Adhesion (FA) and consist of clustered integrins, and numerous membrane-associated and cytoplasmic proteins. During cell adhesion integrins are employed in physical anchoring processes as well as in signal transduction. The activity of integrins is regulated from the inside of the cell (inside-out signaling), while the binding of the ECM elicits signals that are transmitted into the cell (outside in signaling) [95]. The principal structural elements of a cell-matrix contact are shown in Fig. 15.2. On the extracellular face, matrix macromolecules bind to specific adhesive receptors, which are typically transmembrane or glycosylphosphatidylinositol-linked glycoproteins. On the intracellular side of the plasma membrane, the cytoplasmic domains of receptor molecules interact with either cytoplasmic proteins which provide linkage to cytoskeletal filaments, or larger sets of cytoplasmic proteins which cluster by protein-protein interactions to form sub-membranous junctional complexes which then interface with cytoskeletal filaments. Progress in microscopy techniques has enabled the characterization and the analysis of the largest and most stable types of contacts which include focal adhesions and fibrillar adhesions (Tab. 15.2). These structures form discrete sites where elements of the matrix co-align with elements of the cytoskeleton, indicating that these are structures specialized in cell anchorage. Other contact structures have been, until recently, less accessible to identification by these criteria because they are smaller, tran-

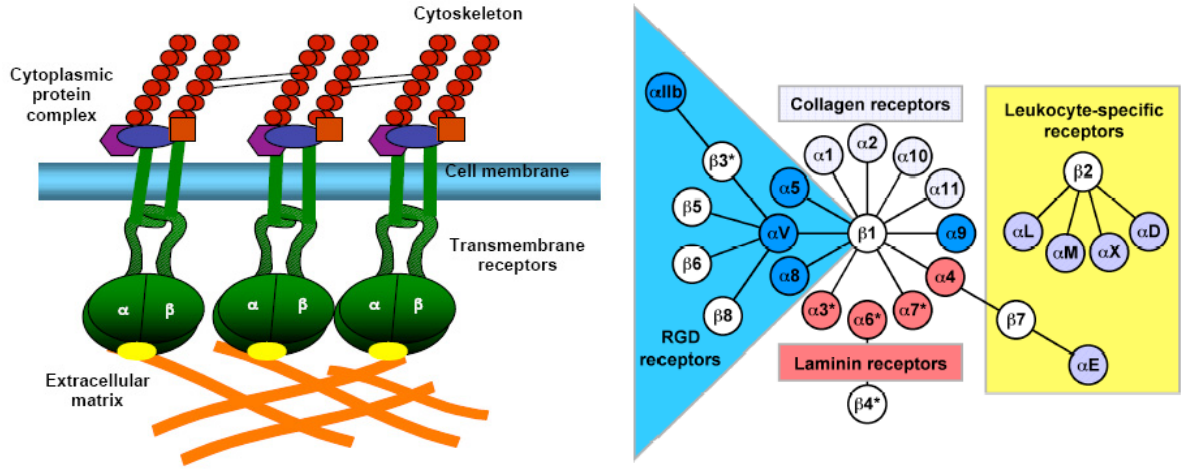

Figure 15.1: Left: The subunit structure of an integrin cell-surface matrix receptor drawn schematically. The α and β subunits are held together by non-covalent bonds in the active state. Right: The integrin family of cell surface receptors and their specific ECM binding partners. Images are adapted from [4, 96].

sient, or have restricted distribution. These include focal complexes, filopodia and microspikes. Progress in microscopy techniques and the recent use of chimeras comprising green fluorescent protein (GFP) attached to various focal adhesion proteins in combination with classical immunohistological methods has made important contributions to our understanding of focal adhesions. Owing to the stoichiometric fusion of GFP to focal adhesion proteins, such GFP chimeras can be used not only as markers for cellular attachment sites but also to provide dynamic and quantitative information about the composition of focal adhesions [216, 217, 8].

CONTACT TYPE	DIMENSION	DISTANCE FROM SURFACE	CHARACTERISTICS
Podosome	0.2-0.4 μm diameter	15-20 nm	Core of Actin perpendicular to surface
Focal complex	0.25-1 μm round	30-50 nm	Submembrane agggregates paralell to F-actin, associated to lamellipodium
Focal adhesion	0.25 μm wide, $\geq$ 1.5μm	10-15 nm	Associated to stress fibers, containing integrin
Fibriar adhesion	3-5 μm long	100 nm	Cables parallel to stress fibers, containing $\alpha_5\beta_1$

Table 15.2: Characterization of cell-ECM contacts mediated by integrins. Table is adapted from [207]

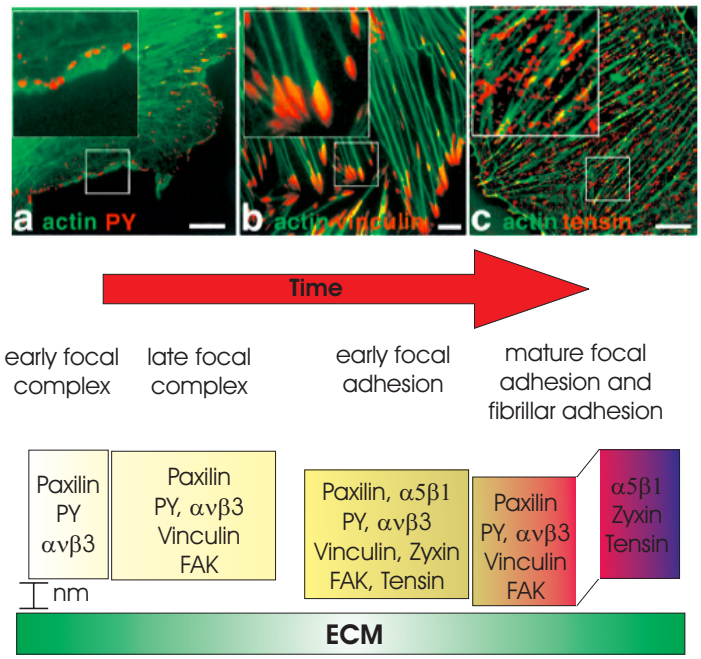

Figure 15.2: Different types of adhesion sites and its temproal stages in the formation and organization of cell-ECM contacts. Images are from [213].

15.2.2 Assembly and dynamics of focal adhesions

Integrin-mediated adhesions have a typical morphology and molecular composition [215]. As a general approach, the structure and dynamics of focal adhesions are described according to their components and their potential interactions; however, more information about spatial and temporal organization is required (Fig. 15.2). A key event in the assembly of focal adhesions is the activation and clustering of ligand-occupied integrins. Specific integrins are recruited according to matrix context: on fibronectin, the major integrin is $\alpha_5\beta_1$, on vitronectin, the major receptor is $\alpha_v\beta_3$ [187]. In the case of fibronectin, concurrent adhesion to both the central cell-binding domain (that contains the RGD site and synergy adhesion sites) and the heparin-binding domain, coupled by recruitment of syndecan-4 to focal adhesions, is required for full assembly of focal adhesions [204, 203]. The assembly of ECM proteins secreted by cells and the physical properties of the matrix are linked to matrix adhesion dynamics. Development of fibronectin fibrils and formation of fibrillar adhesions occur when cells are plated on native fibronectin matrix, whereas cells plated on covalently immobilized fibronectin do not form fibrillar adhesions, and their peripheral focal contacts contain high levels of $\alpha_5\beta_1$ integrin and tensin [106].

Early stages in cell adhesion are mediated by small, dot-like contacts present at the edges of lamellipodia and are termed focal complexes [173]. An 'in vitro wound' introduced into the confluent monolayer of endothelial cells allows the study of the formation of focal complexes under the advancing leading edge [213]. The incorporation of the different components into adhesion sites is a hierarchical process: the earliest observed molecules are $\alpha_v\beta_3$ integrin and phosphotyrosine, followed by talin and paxillin. Later, vinculin and $\alpha-$actinin enter the developing focal complex, along with focal adhesion kinase (FAK) and vasodilator-stimulated

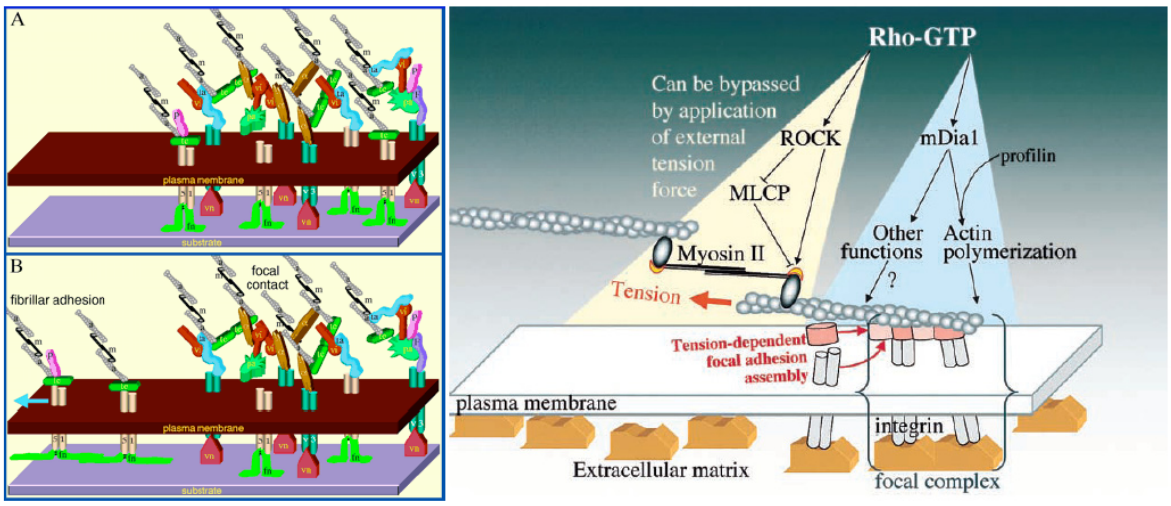

Figure 15.3: A: initial adhesions containing both the $\alpha_v\beta_3$ and the $\alpha_5\beta_1$ integrins. B: Fibrillar adhesion, witch are enriched in $\alpha_5\beta_1$ integrins, are formed because of centripetal sliding due to actomyosin contractility. The figure is also illustrating the molecular complexity of cell-ECM focal adhesion. Image is taken from [215].

phosphoprotein (VASP). Thus, the composition of a focal complex depends on its maturation; however, two components of focal adhesions, zyxin and tensin, are always absent from focal complexes [214]. During the advancement of lamellipodia, focal complexes, with a typical area of 0.25 μm^2, are formed and persist for a few minutes, until the leading edge further advances and new complexes are formed in front of them. This cyclic formation and dissociation of focal complexes persists throughout lamellipodium advancement. The formation of focal complexes is induced by the small Rho-family GTPase, Rac [36]. When the lamella retracts, or even stops protruding, many focal complexes disappear, whereas some of them start growing and transform into definitive focal adhesions. This transformation is not manifested just by a growth in size of the adhesion site, but also by changes in its molecular composition, as mentioned in Fig. 15.2. Thus the formation of FA is accompanied by recruitment of zyxin to the membrane and the concomitant assembly of an actin bundle. Focal complexes develop into focal adhesions as a consequence of Rho activation, or following the application of external forces. This transition seems to be dependent on actomyosin-driven contractility, which applies force at cell-matrix adhesions. This is supported by the observation that myosin light-chain kinase (MLCK) inhibitors enhance lamellipodial protrusions, induce an accumulation of focal complexes close to the cell's edge and block focal adhesion formation [35]. The idea that local mechanical forces activate the growth of focal adhesions is in line with experiments in which local forces are externally applied to matrix adhesions on MLCK inhibited cells. This bypassing of the actomyosin machinery can also induce a rapid growth of the adhesion site [163]. The development of FA is further shown to depend on two downstream targets of Rho, namely Rho kinase, which activates the cellular contractile machinery and mDia, which is involved in the regulation of both actin and tubulin dynamics.

On the intracellular side, focal adhesions contain a large number of structural and signaling molecules (see Fig. 15.2.2). The complexity of interactions and regulatory signals between integrins, focal adhesion components and actin organization is an ongoing field of interest. The

clustering of integrin β subunit cytoplasmic domains provides binding sites for the proximal intracellular components of focal adhesions. Typical focal adhesions present $\alpha_v\beta_3$ integrin, paxillin, vinculin and tyrosine phosphorylated proteins; also, direct binding of talin, $\alpha-$actinin and filamin to β subunit cytoplasmic domains has been reported [42]. A second step in the assembly of focal contacts appears to be the recruitment and unfolding of vinculin. Vinculin monomers exist in a head-to-tail folded conformation, which mask its binding sites for actin and talin [102]. It seems likely that the binding of phosphatidylinositol bis-phosphate (PIP2, a signaling molecule present at increased levels during cell adhesion to fibronectin) to vinculin serves to unfold the protein and to expose the talin-binding site, thus recruiting vinculin into nascent focal contacts and presumably propagating the assembly of other focal adhesion components by molecular interactions [27]. Focal adhesions often appear to slide centripetally, relative to the substratum, due to a polar extension of the adhesion in the direction of the attached stress fibers, and dissociation at the other end (Fig. 15.2). Examination of the molecules at adhesion sites in cultured fibroblasts has revealed an additional dynamic process, characterized by the formation of a new type of adhesion, termed as fibrillar adhesion, where $\alpha_5\beta_1$ integrin associates with fibronectin fibrils [216]. Fibrillar adhesions consist of elongated fibrils or array of dots and are located in more central areas under the cells (Fig. 15.2). While focal adhesions contain $\alpha_v\beta_3$ integrin, high levels of phosphotyrosine, paxillin and vinculin, but display only low levels of tensin, fibrillar adhesions, on the other hand, contain $\alpha_5\beta_1$ integrin, relatively high levels of tensin and little or no phosphotyrosine. The formation of fibrillar adhesions is regulated by the pliability of the ECM, suggesting a role for these structures in matrix reorganization [106] (see also Part II). Focal adhesions contain also many signaling molecules, such as PKC isoforms, FAK, and tyrosine kinases, the activities of which are regulated by matrix adhesion. These molecules regulate important cell functions such as proliferation and growth; moreover, as the closest matrix attachment sites for cells on two-dimensional matrices, focal adhesions participate in the maintenance of isometric tension [174].

15.3 Adhesion in the third dimension

As seen in the last part, integrin-mediated cell adhesion under in vitro conditions show discrete molecular, spatial and temporal compositon with well defined signalling pathways. But the question arises how the artificial vicinity of the flat and rigid surfaces used in tissue culture affects the types of cell-matrix adhesions and the signals they transmit; therefore, a closer approximation to in vivo environments should be attained by growing cells in three-dimensional gels or matrices. Culturing cells within such three-dimensional matrices is not a novel idea. In 1972, Elsdale and Bard described model system for fibroblastic cells in the body using collagen I matrices polymerized in vitro to form a three-dimensional fibrous network [60]. These three-dimensional collagen gels induced morphological changes in fibroblasts that partially mimicked connective tissue cells in vivo. In addition, the importance of 3D ECM for epithelial cells is obvious: 3D environments promote normal epithelial polarity and differentiation (see also Chapter IV). The adhesions formed by fibroblastic, mesenchymal, and neural crest cells to 3D matrices are distinct from both the focal adhesions and the fibrillar adhesions traditionally described and studied in cell culture [43]. These novel 3D matrix adhesions contain many of the same plaque proteins as are found in focal adhesions, such as

Protein	Focal complex	Focal adhesion (mature)	Fibrilar adhesion	3D-matrix adhesion
α_5 integrin	-	-	+	+
β_1 integrin	-	+	+	+
β_3 integrin	+	+	-	-
paxillin	+	+	-	+
tensin	-	+	+	+
talin	-	+	+	+
vinculin	-	+	-	+
phosphotyrosine	+	+	-	+
FAK	-	+	-	+
FAK [Y397]	-	+	-	-

Table 15.3: There are similarities and differences between the molecules found in focal, fibrillar, and 3D-matrix adhesions as indicated in this table showing selected components of these cell-matrix adhesions. Components indicated in black are characteristically present in mature focal adhesions. If that component differs in fibrillar or 3D-matrix adhesions compared to focal adhesions, it is indicated in red. Table is adapted from [207]

paxillin, vinculin, and focal adhesion kinase (FAK). However, they lack the $\alpha_v\beta_3$ integrin, and they are instead based on the $\alpha_5\beta_1$ integrin (see Tab. 15.3). Most intriguingly, unlike the very well studied tyrosine-phosphorylated forms of FAK in focal adhesions, the FAK in 3D matrix adhesions is poorly phosphorylated at its major tyrosine 397 phosphorylation site. This discrepancy in signaling in 2D versus 3D contexts is specific in that paxillin is equally phosphorylated at tyrosine 31 in both 3D-matrix adhesions and focal adhesions. Moreover, the extent of mitogen-activated protein kinase (extracellular signal-regulated kinase, ERK) phosphorylation is moderately elevated, which may help contribute to the enhanced rate of proliferation in 3D matrix [43, 44]. Differences in signaling processes have also been reported in cells suspended in three-dimensional collagen gels when compared to 2D cultures, or under different loading conditions for collagen gel contraction measurements [76, 78].

Chapter 16

Materials and Methods

16.1 Surface Preparation

Microstructured surfaces were prepared as described in Part I. Different types of molds were used starting from 1 μm in height up to 15 μm. All examined areas had the same pillar diameter and the change in bending stiffness can be attributed to the change in length (bending stiffness is proportional to lenght cubed). Surfaces were activated for cell adhesion either by adsorption of 10 $\mu g/ml$ FN (Sigma) in PBS for 2 min or by coupling the central cell recognition motive on the FN, the RGD tri-peptide, termed cRGD due to its cyclic structure that has been created via a hetreobifunctional crosslinker (see Fig. 16.1) [87, 171]. The cyclic structure is mimicking the geometrical orientation of the RGD peptide sequence inside the cell binding domain of the FN protein. Crosslinking biactive molecules to non-reactive polymer surfaces is most efficient when arylic azides are used [208, 221]. Although the simple aryl azides may be initially photolyzed to electron-deficient aryl nitrenes, it has been shown that these rapidly ring-expand to form dehydroazepines-molecules that tend to react with nucleophiles rather than form C-H insertion products [116]. In contrast, Keana and Cai have shown that the photolysis products of the fluorinated aryl azides are clearly aryl nitrenes and undergo characteristic nitrene reactions such as C-H bond insertion with high efficiency [107]. Moreover, conjugates prepared from 4-azido-2,3,5,6-tetrafluoro benzoic acid may have quantum yields for formation of photocrosslinked products that are superior to those

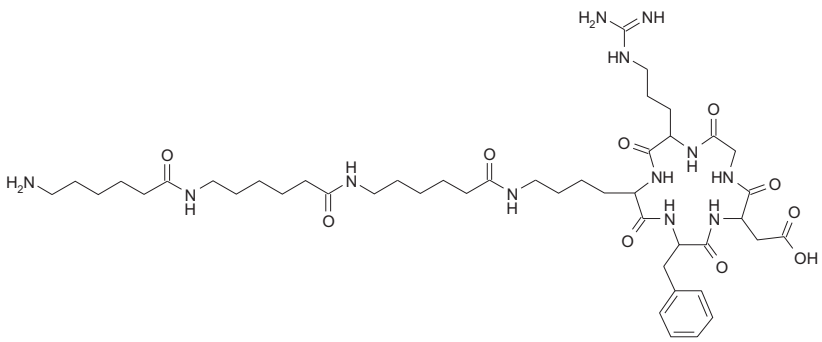

Figure 16.1: Structural formula of the used cyclic RGD tri-peptide.

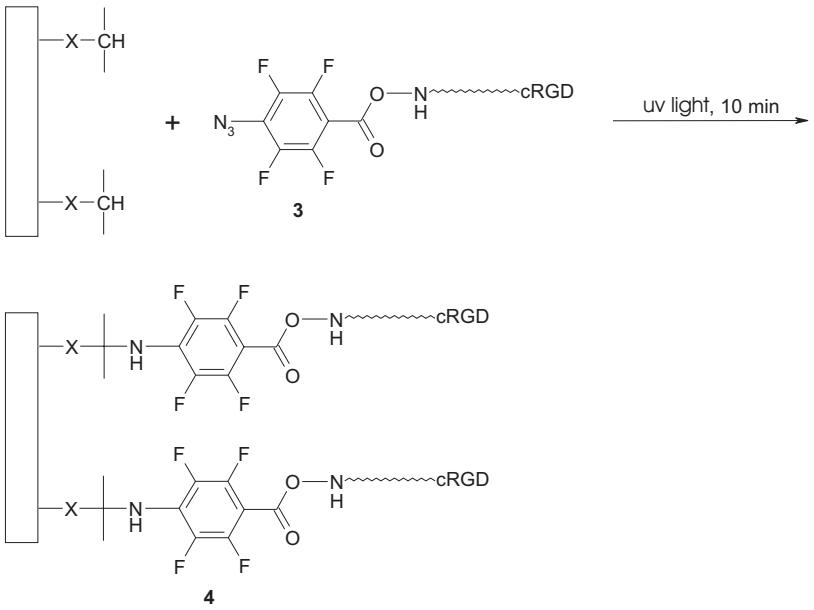

Figure 16.2: Reaction scheme for the coupling of activated cRGD to the PDMS surface.

of the non-fluorinated aryl azides. An important application of these reactive derivatives of 4-azido-2,3,5,6-tetrafluorobenzoic acid is the photofunctionalization of polymer surfaces (see Fig. 16.2).

In detail, a 0.2 mM solution of NH_2 terminated cRGD dissolved in 20 mM Hepes (Roth, Karlsruhe, Germany)at pH 7.2[1], was preincubated with 1.5 μmol of 4-azido-2,3,5,6-tetrafluoro benzoic acid, sulfo-tetraflurophenyl-ester, sodium salt (ATFB, STP ester, Molecular Probes) overnight at 4°C. The solution was used without further purification by placing small drops of the activated cRGD peptide onto the microarray and covered them with fused silica glass slides (Heraeus, Hanau, Germany). The samples were irradiated for 10 min. with uv light at 250 nm (Phillips, Hamburg, Germany). During illumination, nitrogen is cleaved off the azide group generating a highly reactive carbene analogue termed nitrene. This nitrene is stabilized by the four electron withdrawal fluorine groups at the phenyl ring. After extensively washing in PBS[2] the microarrays were washed with 70% EtOH for 30 sec to allow complete wetting of the microarray (see also Part II). The samples were washed extensively with sterile PBS and transferred to 6 well plates (BD Bioscience) containing complete medium. For live cell imaging coverslips carrying the microarray were mounted on pinched 60 mm petri-dishes under sterile conditions. For samples were the cell adhesive area was not restricted to the top end of the pillar head, the microarray was first wetted with 70% EtOH and after rinsing with PBS the protein solution or the cRGD was grafted onto the entire surface allowing the cells to adhere also to the sidewalls and the basement of the pillar arrays.

[1] kindly provided by Horst Kessler (TU Munich, Germany)
[2] the surface was always kept under liquid to prevent dewetting

16.2 Cell culture

16.2.1 General methods for cell culture

To maintain sterility during the experiments with eukariotic cells all steps are performed under a sterile hood (Kendro, Langenselbold, Germany) using sterile techniques and materials. The cells employed in this study are maintained normally in Dulbecco's Modified Essential Medium (DMEM, complete medium in the following) supplemented with 10% fetal bovine serum (FBS) (Invitrogen, Karlsruhe, Germany) and 2mM L-glutamine (Invitrogen). Transfected cells were maintained in complete medium supplemented with the corresponding antibiotics for selection. Cells are cultured at 37°C and 5% CO_2 moistened atmosphere in an incubator (Kendro). The media is changed every 2 days. After the cells have reached confluence, they are first rinsed with a few drops of trypsin-EDTA 2.5% (Invitrogen) and then released with additional trypsin-EDTA solution for 3-5 min. After gently knocking off, diluting in 5-10 ml of complete medium and centrifugation at 1200 rpm for 5 min, the cell pellet is suspended in media and cells are then re-plated in tissue culture flasks (Nunc, Wiesbaden, Germany) or in wells (BD-Bioscience, Heidelberg, Germany) containing the substrates prepared for the adhesion studies.

16.2.2 Primary cell culture

Primary human foreskin fibroblasts (HFF) were kindly provided by Prof. Benjamin Geiger (Weizmann Institute of Science, Rehovot, Israel). They were cultured in complete medium and used between passage 18 and 23.

16.2.3 Fusion proteins and transfection of cells

The REF52 cells (rat embryonic fibroblasts, originated from [66]) expressing β_3-GFP integrin and paxilin-YFP fusion proteins were also a gift from Prof. Benjamin Geiger. The fusion protein was prepared according to Ballestrem et al. (2001). Fusion of the β_3 cDNA coding sequence with pEGFP-N1 (Clontech, Palo-Alto, CA, USA) resulted in full-length β_3-GFP-integrin uing BamHI and EcoRV. Cloning of GFP-paxillin has been described previously (Zamir E, 1999). Paxillin has been re-cloned into pEYFP-C3 (Clontech) using HindIII and XbaI. REF52 fibroblasts are cultured in DMEM supplemented with 10% FBS and 2 mM L-glutamine. Superfect (Qiagen, Hilden, Germany) is used according to the manufacturers' recommendation for stable transfection. Cells are cultured in the presence of 1 mg/ml G418 (Invitrogen) to select for stable β_3-GFP-integrin and in 2 $\mu g/ml$ Puromycin (Invitrogen) for YFP-paxillin expressing clone (REF 52 β_3-GFP and REF 52 paxillin-YFP).

16.2.4 Cell counting

To determine the cell number and the number of vital cells used in the experiments, a cell suspension in DMEM was diluted 1:10 in a 0.05% Trypan blue (Sigma) solution in MQ-water. This colored substance can enter and stain only dead cells. The cell suspension in Trypan blue was then transferred into two hemocytometer chambers (Neubauer counting chamber). By using a 10x objective and light microscopy, the cells were counted in 8 fields (each field having an area of 1 mm^2) and the average number of cells per volume (ml) is calculated (excluding cells stained in blue which are dead).

16.2.5 Cell maintenance for adhesion studies

After trypsinising and counting the cells were plated onto the surfaces in DMEM containing 1% FBS (to minimize the effect of extracellular matrix molecules contained in FBS on cell adhesion and spreading) For fluorescence microscopy and live cell experiments the cell plating density was $1 - 5 \times 10^5$/sample. Time-lapse movies (fluorescent and phase contrast) are acquired whilst maintaining cells on the microscope stage in F12 medium (Invitrogen) [3] supplemented with 1% FBS in 5% CO_2 atmosphere and 37°C.

16.2.6 Immunofluorescence staining and image analysis

Cultured cells are fixed for 25 min. in PBS containing 3.7% paraformaldehyde (Merck) and then are fixed and permeabilized further with 0.1% Triton X-100 (Sigma) and 3.7% paraformaldehyde in PBS for 5 min. Non-specific binding was blocked by incubation with 1% BSA in PBS for 30 min. The cells are then incubated at room temperature (RT) for 30 min. with the primary antibodies at a 1:20-1:100 dilution in PBS containing 0.1% BSA (PBS/BSA); after washing three times for 10 min in PBS, samples are further incubated with the appropriate secondary antibodies at a 1:100 dilution in PBS/BSA for 30 min at RT. The primary antibodies used in this study included: monoclonal antibody (mAb) anti-integrin β_1 and mAb anti-integrin β_3 (both from BD Transduction Laboratories Lexington, KY, USA), mAb anti-vinculin (clone hVin-1, Sigma), mAb anti-pFAK(397) (BD Bioscience), mAb anti-paxilin (Sigma), mAb anti-zyxin (Synaptic Systems, Göttingen, Germany) polyclonal antibody (pAb) anti-zyxin (Sigma), pAb anti-fibronectin (Sigma). Secondary antibodies used were either goat anti-rabbit conjugated to Alexa Fluoro-488 dye (Molecular Probes, Eugene, OR, USA) or goat anti mouse conjugated to Cy5 dye from (Jackson Immuno-Research, West Grove, PA, USA). Phalloidin-TRITC was purchased from Sigma and brought in 1 mg/ml solution with dimethylsulfoxyde (DMSO). The working dilution is 1:250 in PBS. For triple protein staining the fibronectin was visualised using the Zenon technique from Molecular Probes [122]. The other two proteins were stained using classical primary and secondary antibodies derived from different species as mentioned above. Zenon technology is based on the complexation of primary antibodies with dye-labeled Fab fragments of secondary antibodies directed against their Fc regions. The primary antibody types that can be recognized and detected by Zenon labeling reagents are determined by the immunospecificity of the Fab fragments from which they are prepared. 1 $\mu g/ml$ of unconjugated pAb anti-fibronectin were incubated for 5 min. with 5 $\mu g/ml$ rabbit Fc-specific Fab fragments conjugated with AlexaFluor 350, followed by incubation with 5 $\mu g/ml$ non-specific rabbit IgG_1 to block unbound anti-Fc sites. The resulting complex was further diluted with PBS resulting in a 1:100 primary antibody dilution [158] and incubated for 30 min. at RT. Reaction with the Fab labeled pAb anti-fibronection was following the labeling the two other proteins with secondary antibodies.

After extensive washing with PBS (except when Zenon labeling was used the washing after incubation was constricted to 5 min), samples were mounted in Elvanol (Mowiol 4-88, Serafon, Ashdod, Israel) in phosphate buffer containing 0.5% 1,4-diazabicyclo[2.2.2]octane (DABCO, Sigma) to conserve the sample and inhibit photobleaching. Immunofluorescent images are taken with the DeltaVision Spectris system (Applied Precision Inc., Issaquah, WA, USA) on an

[3] F12 medium has nearly the same composition as DMEM except for Riboflavin which has a fluorescent peak in the region where GFP is emitting; resulting in an exceptional high image background.

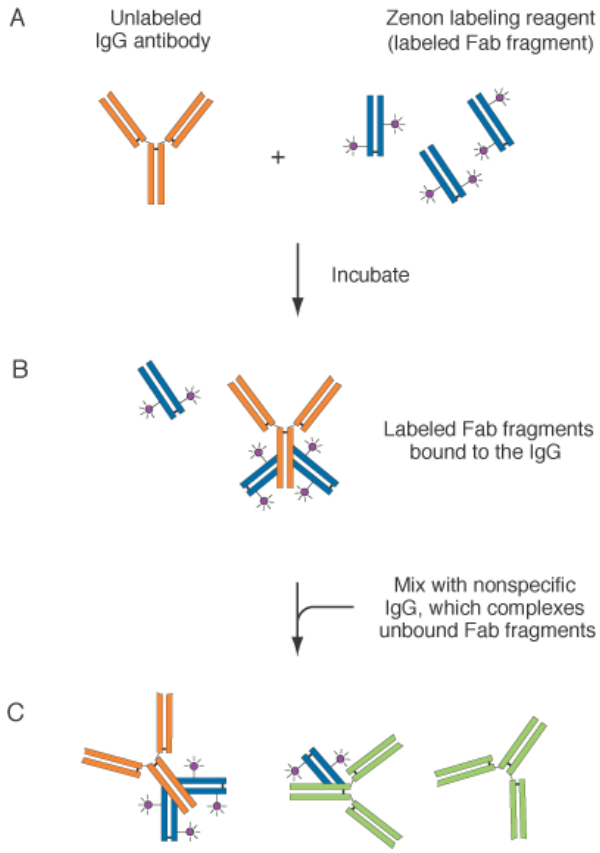

Figure 16.3: The Zenon labeling scheme. An unlabeled IgG is incubated with the Zenon labeling reagent, which contains a fluorophore-labeled Fab fragment (A). The labeled Fab fragment binds to the Fc portion of the IgG antibody (B), and excess Fab fragment is neutralized by the addition of a non-specific IgG (C). The addition of non-specific IgG prevents cross-labeling of the Fab fragment in experiments where multiple primary antibodies of the same type are present. Note that the Fab fragment used for labeling need not be coupled to a fluorophore, but could instead be coupled to an enzyme or to biotin. Image is from [158].

Olympus IX 71 inverted microscope (Olympus, Hamburg, Germany). The DeltaVision system allows optimal illumination and image recording of living and fixed samples providing high resolution even for small samples and faster image acquisition for live-cell studies. To allow time-lapse experiments, the system is equipped with an incubation chamber (heated to 37°C and air humidified). In addition, the CO_2 concentration is controlled with a sensor (Vaisalla, Stuttgart, Germany) and maintained at 5% (v/v). The following objectives are used: 60x oil, 1.4 UPlanApo (Olympus) for fixed samples. Time-lapse movies of the fluorescently-tagged cells are acquired with a 60x water, 1.2 objective at 10-minute intervals for several hours. Images are acquired with cooled CDD camera (Photometrix, Kew, Australia) at a resolution of 1024x1024; each pixel corresponds to 110.3 nm. Image acquisition and processing are controlled by a Linux workstation using the Resolve3D software, and the SoftWorx software for image visualization and deconvolution (Applied Precision Inc). For image analysis, fluorescent images were processed by using high pass filtering and segmentation according to Zamir and coworkers [105]. The program was written in IDL (Version 5.4, Research Systems, Inc.) and kindly provided by Christian Schmitz (University of Heidelberg, Germany). For size

measurements of focal contacts and RGB line profiling, segmented images were loaded and analyzed using ImageJ [4]. For analysis of pillar bending, from each image the non-deflected position of the pillars were subtracted and the resulting differences were plotted against the adhesion area using the software OriginPro (Version 7.0, OriginLabs Corp., Northampton, MA, USA).

16.2.7 Cell proliferation assay

4', 6-Diamidin-2'-phenylindol-dihydrochlorid (DAPI, Sigma) staining is used to determine the total cell number adhering to the substrate. To quantify cells entering the S phase [5], the percentage of cells incorporating 5-bromo-2'-deoxyuridine (BrdU) relative to the control was measured by fluorescence microscopy. Cells on the samples were incubated in medium containing 10 mM BrdU for 18-24 hr and DNA was then denatured with 2N HCl incubation for 20 min. After rinsing with PBS, cells were incubated with mouse monoclonal antibody anti-BrdU (Sigma) and then fluorescently labeled with Alexafluor 488-conjugated goat anti-mouse (Molecular Probes). Samples are mounted and observed by fluorescence microscopy (on the DV Spectris system) using a 20x objective (Olympus). Five different fields per sample are examined and the number of stained nuclei was determined using ImageJ software. The proliferation index is defined to be the ratio of the number of BrdU positive nuclei to the number of DAPI-stained nuclei and was plotted using OriginPro.

16.2.8 Cell adhesion assay

To evaluate the growth rate on the microstructured surfaces different cell types were plated onto the samples at a cell density of 1.5×10^5 cells/ml. After 24 h in culture, samples were fix/permeabilzed and stained for F-actin using Phalloidin conjugated to TRITC (Sigma). Samples are mounted and observed by fluorescence microscopy (on the DV Spectris system) using a 20x objective (Olympus). Ten different fields per sample are examined and the cell area was determined using the cell ouliner plugin implemented in the ImageJ sofware. Only cells were counted that showed a spreading behaviour comparable to flat surfaces, indicating that the attachment is restricted to the pillar heads. For each different sample type, the total average area was plotted using OriginPro software.

16.2.9 Force measurement in vivo and in vitro

The microarrays were calibrated as demonstrated in chapter 2 resulting in a nominal stiffness of 0.17 N/m. Two cell lines, the YFP-paxilin and the β_3-GFP REF52 cells were plated at a density of 1×10^5 either on cRGD or on FN* functionalised force sensor arrays. After incubation of the cells for at least 3h under normal conditions the samples were mounted in Ham/F12 medium upside down onto a glass bottom petridish. A spacer of 50 μm thickness was used to prevent cell damage. Illumination time was kept to a minimum, to reduce cell death and photobleaching. Timelapse videos were captured every 10 min. over a period of 60 min. After rinsing with fresh PBS the samples were fixed/permeabilized and stained for fibronectin and zyxin. After image acquisition, from each sample the focal contact area of a

[4] freely avaliable@http://rsb.info.nih.gov/ij/

[5] During the S phase the cell is synthesizing DNA and is using also the present 5-bromo-2'-deoxyuridine (BrdU) for DNA replication

single cell was estimated using IDL and was correlated with pillar deflection and plotted in OriginPro.

Chapter 17

Results

17.1 Viability of mammalian cells on pillar arrays

17.1.1 Adhesion area depends on surface pliability

Cell viability on the microstructured surfaces was investigated by measuring the cell adhesion area on pillars functionalized with FN or cRGD. Surfaces with different compliances were compared to each other, varying from non structured flat PDMS to 10 μm to 15 μm high microstructures. The spring constant was changed from 10,000 N/m (approximated for the flat surface [188]) to 0.04 N/m for the 15 μm high pillars. The projected cell area are plotted in Fig. 17.1 for primary human fibroblasts (HFF). They show a maximum of cell area at 6h on all surfaces, which is in good agreement with the change in cell polarity after 6-12h. Initially fibroblasts adhering to rigid surfaces have a pancake-like morphology due to formation of lamellipodia. After cell attachment and stress fiber formation (1-3h) the shape was changed to a spindle shaped morphology and the projected cell area was reduced. The effect is more predominant on hard surfaces compared to softer ones, but at later time points the cell shape is comparable to cells growing on the solid support. For rat embryonic fibroblast (REF52) the effect is not as distinct as for the HFF cells. As seen in Fig. 17.2 this cell line retained more or less a pancake-shape. In both cell lines the differently functionalized surfaces had a minor effect on cell spreading, more obvious was the effect of the different surface pliabilities of the microstructures. At any given time the projected cell area on the soft pillars was around half of those measured on the flat samples, which indicates that cell spreading is closely related to surface stiffness.

The cell shape changed dramatically from a spindle like to a stellate morphology when the area of adhesion was not only restricted to the top part of the microstructures. Complete coating of the microstructures with FN or cRGD allowed the cell to increase its contact area, inducingit to change shape. In Fig. 17.3 several surface conditions are shown from a homogeneous surface to 1 μm and 10 μm of structure length. The cell formed fine filaments containing actin which were several microns long if plated on an array with 10 μm high posts. If the asperities were only 1 μm high, cell shape didn‘t change obviously. The length of extension was maximized when the distance between the posts was increased to 10 μm (compare C and D in the same Figure).

17.1.2 Proliferation of HFF on surfaces with different compliance

The effect of surface pliability on cell proliferation was investigated using HFF on surfaces coated with cRGD in the presence of BrdU. As in previous sections, the stiffness of the pillars was varied by 5 orders of magnitude (a flat PDMS surface was also used). All cell nuclei were stained with DAPI and the relative percentage of proliferating cells was evaluated by immunocytochemistry for BrdU. Only proliferating cells synthesizing DNA incorporate BrdU. As shown in Fig. 17.1 the proliferation rate of human fibroblasts decreased when cells were cultured on soft surfaces for 24 h, and only about 25% of the cells were BrdU positive, indicating that more cells were in quiescent phase. When shorter asperities were used, proliferation was significantly higher. The difference compared to flat and homogeneous coated surface was in the range of 10%.

17.2 Measuring cellular forces

17.2.1 Forces generated by living REF52 YFP-Paxilin cells

In situ force measurements was conducted on calibrated force sensor arrays with a nominal stiffness of 0.17 (N/m) [1]. REF52 stably transfected with YFP-paxilin were used to localize focal adhesions; these cells were plated on cRGD or FN*. Cells spread and develop focal adhesions (Fig. 1f) on these substrates and showed a behaviour comparable to that on flat surfaces. The forces applied by the cells deformed the initially regular pattern of the surface. The position of the center of the posts was recorded together with the fluorescence picture pixels of the focal adhesions, marked by YFP-paxilin, using a high numerical aperture 60x water immersion objective [2]. The pattern was regular and so any deviation from regularity indicates an application of force. The displacements of the posts relative to a non-deflected one next to the investigated cell are determined by setting a threshold the fluorescence images or phase-contrast images in case of cRGD coated force sensors and analysed with imageJ. Once the displacements are mapped (Fig. 17.4), the forces generated at each pillar are compared with the area of focal adhesion for the corresponding pillar. The area of focal contacts was

[1] for each experiment at least 10 pillars were calibrated according to chapter 2.
[2] images where recorded with 1024×1024 resulting in 110.3 nm pixel size.

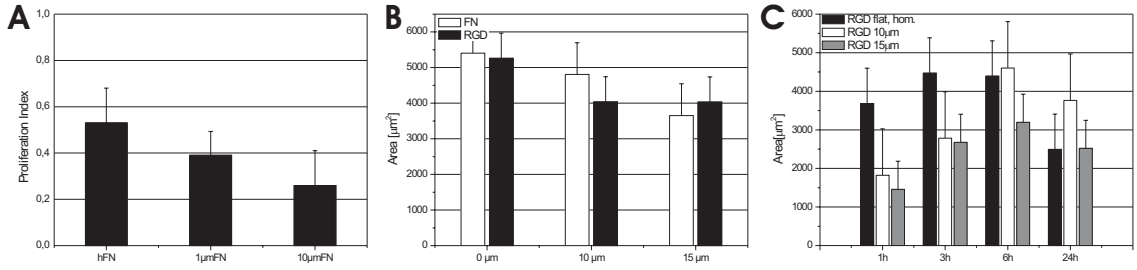

Figure 17.1: A: Cell proliferation was measured by BrdU incorporation and plotted in percent of total cells present at the surface. B: Projected cell area of HFF cells plated on FN or cRGD functionalized microstructures. C: Time coarse of HFF cell spreading on cRGD functionalized surfaces with different compliance.

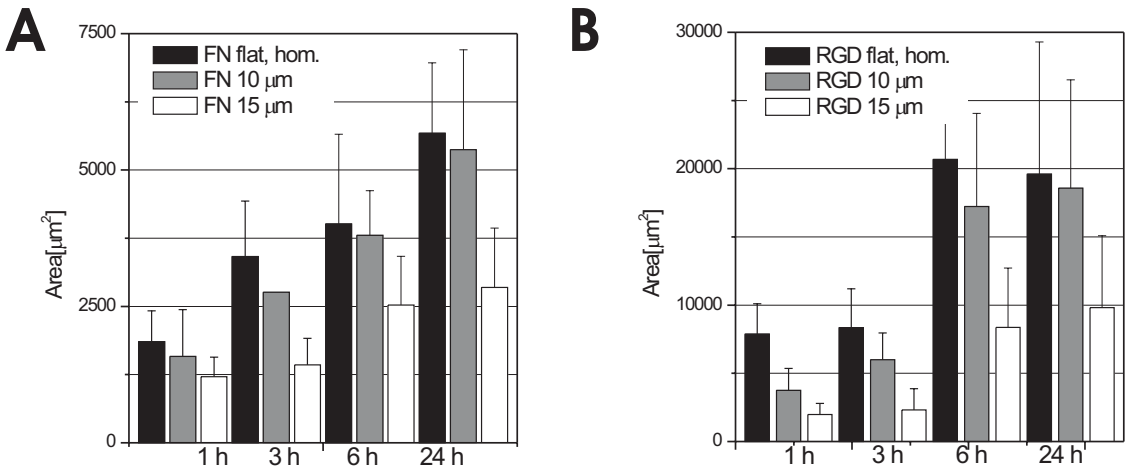

Figure 17.2: Temporal growth of projected cell area of REF52-WT on surfaces with different stiffness coated with FN (A) or with cRGD(B).

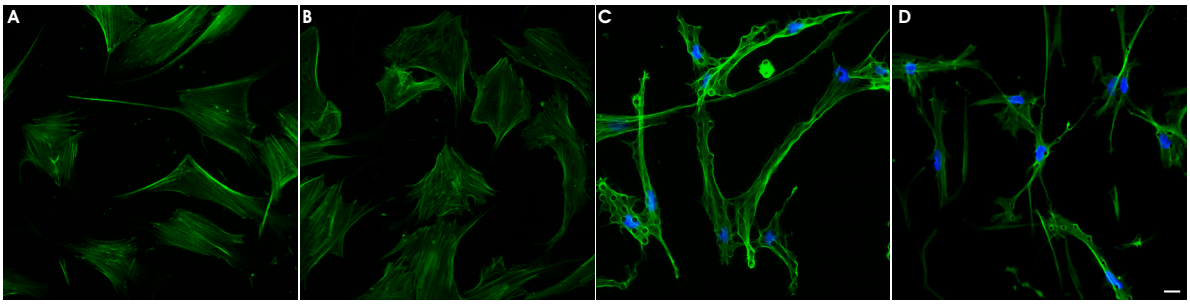

Figure 17.3: Image sequence of HFF cells growing on complete functionalized microstructures, with 0 μm (A), 1 μm (B), 10 μm (C) high structures. In D a sample with a reduced inter-pillar distance was used, resulting in a reduced length of extensions. Scale bar is 15 μm.

analyzed using highpass filtering and a segmentation algorithm (see materials and methods). The temporal force development was plotted against the area of focal contacts. The increase in force, determined by pillar deflection correlated linear with the increasing area of the corresponding focal contact. From a linear fit an average stress of 13 $nN/\mu m^2$ in the cRGD coated force sensors and a slightly increased stress (14.4 nN/μm^2) on the surface coated with FN could be estimated. Maximum force level generated at a single post was up to 100-250 nN with a corresponding total area of focal contacts of 8-16 μm^2 [3]. The orientation of the force was parallel to the direction of the long axis of the focal adhesions, indicating that the increase in area owing to force is not isotropic but occurs mainly in the direction of force application.

[3]force was always estimated as a sum of the focal contacts present on a single pillar. The number of contacts varied from 1-4 FA/pillar.

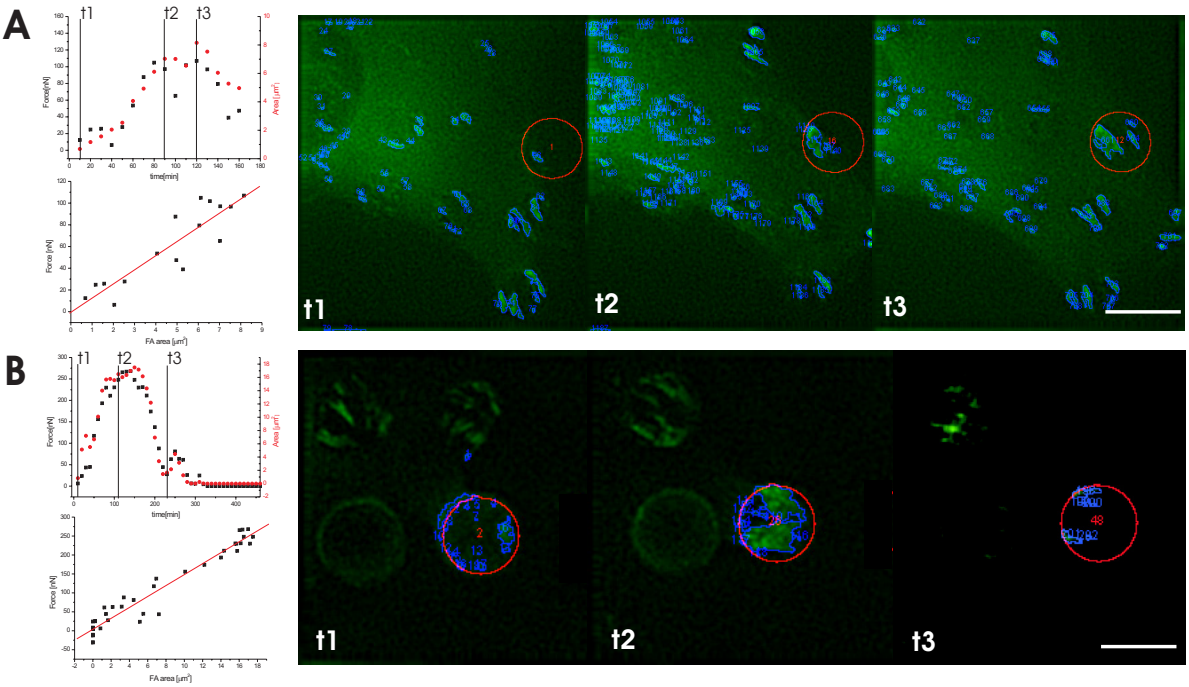

Figure 17.4: REF YFP-Paxilin were imaged during focal contact formation on cRGD functionalized (A) and FN* activated microarrays. Three time points are shown which correspond to the marked lines in the force vs. time curves on the left. The pillars are encircled in red, and the area of the patches (green channel) were outlined in blue. Scale bar is 5 μm.

17.2.2 Maximum force generated by different cell lines

To investigate how the overexpression of different proteins inside the focal adhesion affects cell contractility, YFP-paxilin and GFP-integrin β_3 were compared. Both cell types were plated on FN* functionalized and calibrated pillars with the same stiffness as used for the other live-cell experiments. The cells were investigated *in vivo* and after fixation. A marked difference between YFP-Paxilin and GFPβ_3 was visible. The GFPβ_3 exerted much more force to the force sensor array indicated by the average stress value of 115.1 $nN/\mu m^2$. Under the same conditions the YFP-Paxilin cells could only generate 16.1 nN/μm^2. The increased force of the GFPβ_3 cells could not be correlated to a bigger patch size. In contrast the focal adhesions had a distinct smaller area when compared to that of the YFP-Paxilin cells. To see if the patch size is affected by the used fusion proteins both samples were fixed and immunofluorescence stained for zyxin which is also present in focal adhesions. The zyxin labeling in the two cell lines showed a comparable focal adhesion size and the area for the GFPβ_3 cells was in the range of 2-5 $\mu m^2/post$. For YFP-Paxilin cells the area per post was more than two times bigger (up to 16 μm^2) [4] indicating an influence on adhesion morphology of the tagged integrins. From immunofluorescence images, calculated forces were not comparable to those estimated for living cells. Both, YFP-paxilin and GFPβ_3 cells when alive had a 5 to 10 fold higher contractility alive than cells after fixation. In Fig. 17.5 A the force versus focal adhesion area is plotted for GFPβ_3 cells resulting in an average stress of 115.1 $nN/\mu m^2$ when the cells are

[4] total area of the pillars used was 19.6 μm^2

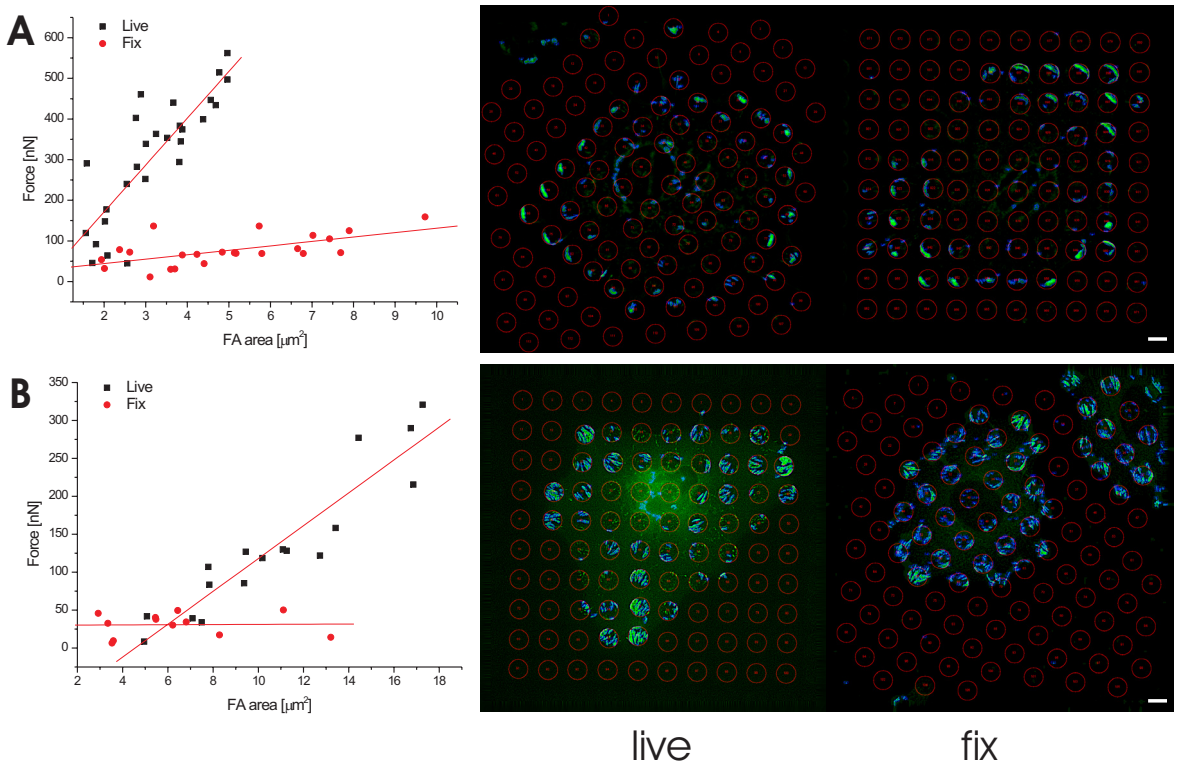

Figure 17.5: Different mutants of REF52 cells plated on calibrated FN* functionalized pillars. The cells were imaged alive or after fixation . Maximal force was obtained with β_3-GFP stably transfected (A). Measured force after fixation was only $1/10$ of the initial value. B: YFP-Paxilin expressing cells generated an average stress of 16.1 $nN/\mu m^2$ and after fixation the measured force was in the range of 0 to 50nN. Scale bar is 5μm.

imaged alive and 10.9 $nN/\mu m^2$ after fixation.

17.3 Molecular assembly of focal contacts

17.3.1 Cluster size dependence on surfaces with different pliability

The molecular composition of the focal adhesions formed on surfaces with different pliability was investigated using HFF cells and immunofluorescent labeling of different plaque proteins always compared to zyxin as a reference protein. It is known that zyxin is not present in initial adhesion sites, the so called focal complexes, and it is therefore a good candidate to discriminate between the different types of adhesion clusters. The HFF cells were plated on substrates with 0 μm, 10 μm, 15 μm-high pillars. All microarrays were functionalized with cRGD to get a uniform and undisturbed pattern [5]. The cells were fixed after 24h in culture and double labeled for vinculin, β_3 integrin, β_1 integrin and zyxin. The axial ratio was measured by fitting an ellipse into each patch of the segmented images. For each analyzed substrate (n>8) the cellular adhesion pattern showed morphological characteristics. On flat surfaces

[5] using FN to functionalize the pillars tend to agglomerate especially for the flexible 15 μm high pillars. The same was noticed for cRGD coating, but a sonification step during preparation could recover uniform array geometry.

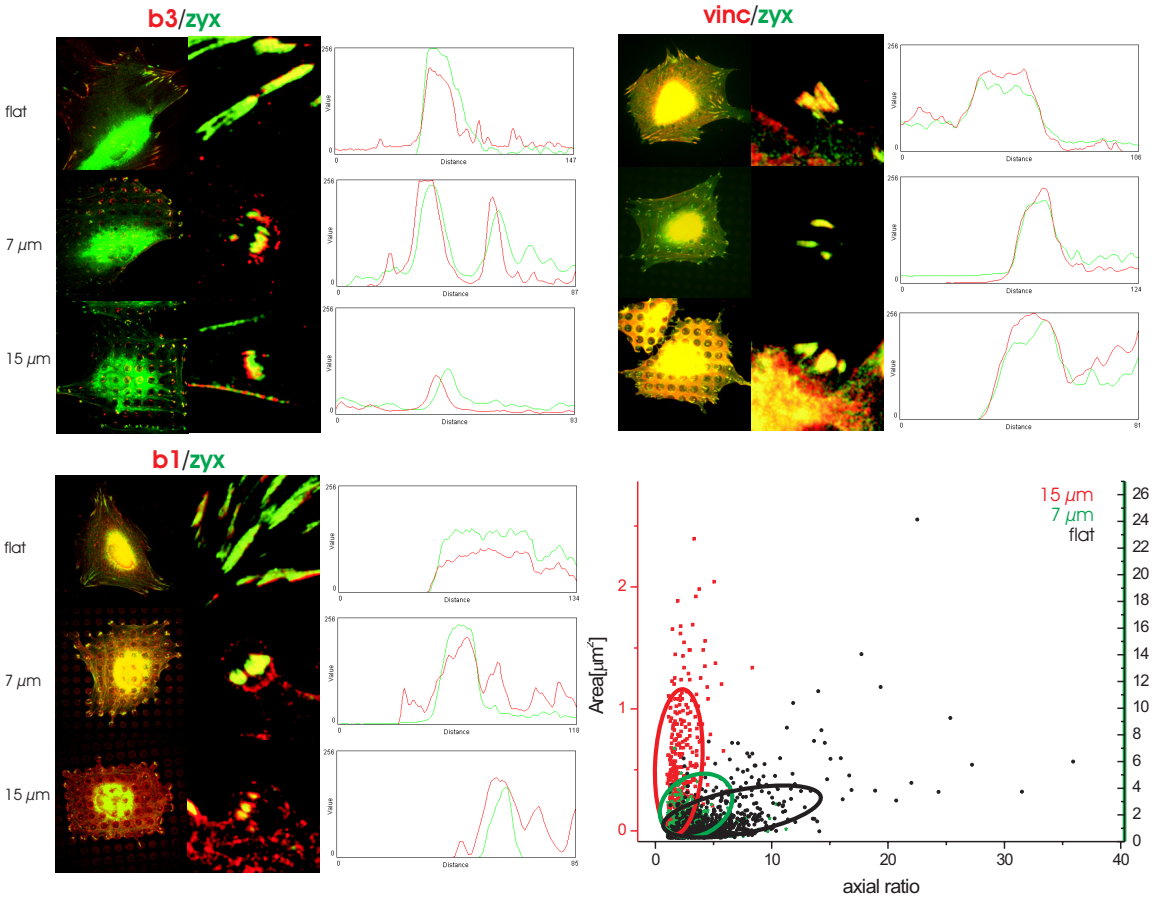

Figure 17.6: Focal adhesion morphology is depended on surface compliance. The axial ratio of the adhesion clusters are plotted against patch area resulting in three distinguished domains. The molecular composition of focal adhesions was investigated by double labeling of HFF cells. Different plaque proteins were compared to zyxin. Line scans of individual focal contacts showed the diversity inside the contact area when the surface pliability was changed.

the adhesion sites are rather elongated with a typical length of 2-5 μm. On the other side the adhesion structures on the very soft surfaces were dot like and the length of single adhesions clusters were below 1 μm. For cells growing on the 10 μm high arrays the cluster size was in between that on the soft and rigid surfaces (see Fig. 17.6).

The molecular composition of the focal contacts developed on surfaces with different pliability was plotted in Fig. 17.6. Looking at the β_3 integrin and zyxin it was ascertained that zyxin was shifted towards the cell center when surface stiffness was lowered. The shift was examined by plotting a line scan for the two fluorophores and by the low colocalization visible in the merged images. For the β_1-zyxin pair the shift was less distinguished but still visible. For the last protein combination there was no visible shift of the two fluorescent markers and the merged image showed a high colocalization. In all three sets of images the cluster size of adherent cells decreased with decreasing surface pliability, indicating a morphological change of focal contact according to the surface stiffness.

17.3.2 Surface specific FA composition on FN coated pillar arrays

For cRGD functionalized pillar arrays, the area of adhesion was always restricted to the solid surface of the pillar top. However in case of FN coated pillars the focal adhesions tend to grow over the solid surface. A closer look in the molecular composition of the extended adhesion area revealed that underneath the extensions dense FN bundles were present. Along this bundles the distribution of different plaque proteins were investigated by double labeling of the different proteins and FN. In case of β_3 integrin staining no antibody labeling was found along the fibrils. The reduced intensity of FN colocalized with β_3 was an artefact of the fixing and permeabilization procedure. The fluorescence signal of pre-labeled FN under focal contacts was significant higher than that of FN labeled via antibodies (datas not shown). This could be due to the low accessibility ot antibodies of the area where the cell came in close contact to the surfaces, in samples that were first fixed and then permeabilized [6]. For β_1, the intensity profile of protein labeling was totally inverted; the integrin colocalized with dense FN fibers but was absent in areas where cells formed focal adhesions. For the last two sets of proteins the intensity profile was nearly identical. On the sites of weak FN labeling the intensity of paxilin and pFAK(397) was increased. Along the fiber, proteins did not colocalize except in the tip where the FN was connected to the intracellular actin.

[6] comment of Prof. Benjamin Geiger

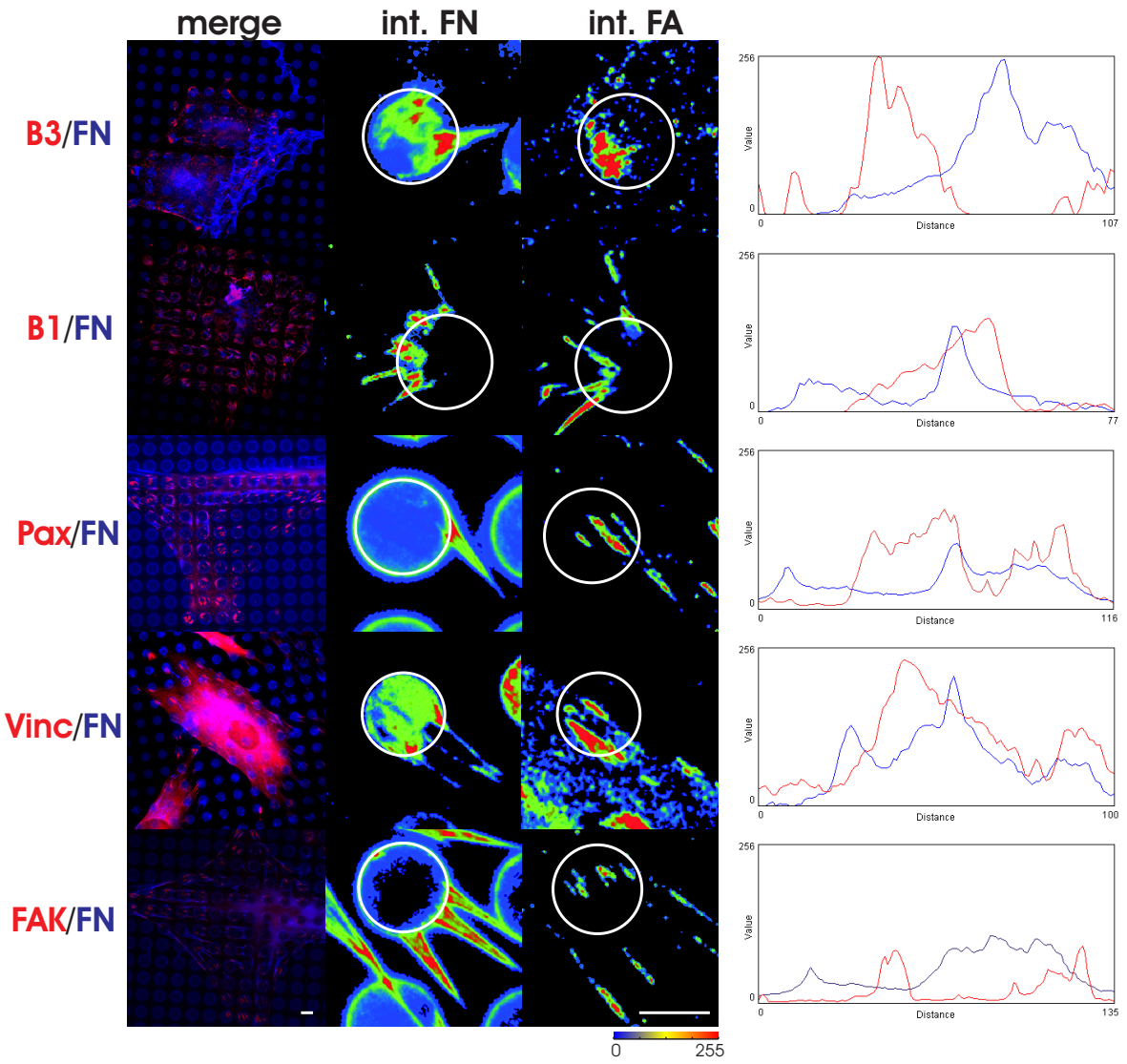

Figure 17.7: HFF plated on FN coated pillars resulting in increase of focal adhesion area over the pillar boundary. Specific proteins present in the focal adhesions showed a typical pattern on this extensions which was also visualized by line scans of individual adhesions. Scale bar in all images is 5 μm.

Chapter 18

Discussion

In this Part, the cellular behaviour, including proliferation and cell morphology, of two REF52 cell lines with focal contact-associated proteins tagged with GFP and HFF cells was investigated on surfaces with different pliability and functionalization. The influence of surface stiffness to the molecular composition of focal adhesion sites in HFF cells was determined, giving new insights on contact assembly. In particular, the cell viability was estimated by measuring the adhesion area on substrates with different adhesion molecules and quantification of proliferating cells by BrdU assay on cRGD functionalized surfaces. That surface pliability can influence cell viability was proved by calculating the rate of proliferation on surfaces with different compliances. The fractin of proliferating cells was reduced by 50% when compared to flat surfaces. This suggests that the assembly of integrins and integrin related proteins inside the focal contacts acts as a local regulatory element that can control the proliferative activity of fibroblasts [195]. Integrins intersect the MAP kinase pathway at multiple points, involving the sequential activation of Ras, Raf, MEK and Erk, ELK-1 and finally Cyclin-D1 transcription. Integrin-mediated adhesion enhances the transmission of this signal at the level of recruitment of RasGAP and regulation of several other proteins inside the pathway [175]

The reduced cell spreading was not affected by the ligand used (either FN or cRGD); rather it was a result of surface pliability. The low cell area on softer surfaces was accomanied by a reduced amount of stress fibers and by the generation of small punctuated focal adhesions. An insufficient maturation of the initial focal complexes into focal contacts could be a contributing effect to explain these observations. In Fig. 17.6 the adhesion sites on the 15 μm substrates functionalised with cRGD still remain dot-like even after 24 h in culture whereas the contacts of cells cultured on flat surfaces are dense and well established. Focal complexes are initially formed at the protrusing areas of the cell - the filopodia and lamellipodia. They are formed in a Rac1- or CDC42-dependent manner [9, 166]. When the cell spreads, the small dot like adhesions normally transform into mature focal contacts in response to RhoA activation and myosin-dependent actin-filament contraction [9, 166]. RhoA activation also affects actin polymerization via its downstream target Diaphanous (mDia) [74, 163]. Together with the activation of Rho kinase, which inhibits the myosin light chain phosphatase resulting in continuous acto-myosin contractility, this effect may regulate the maturation of focal complexes into focal adhesion. Similar results as seen on soft surfaces were obtained by inhibition

of actomyosin contractility with butanedione monoxime, a myosin-ATPase inhibitor or with ML-7 (inhibition of myosin light chain kinase). In summary, if the contractile apparatus is not activated because of surface pliability or because the downstream targets of RhoA are inhibited, the cell is unable mature the initial focal adhesions into focal contacts and is unable to spread.

Interestingly, the substrate stiffness underneath the adhesion plaque of cells growing on the microarrays is the same as for cells growing on flat PDMS surfaces where they can develop focal adhesions. Therefore the change in the micromechanical environment is not the only reason for the inhibition of focal adhesion assembly on the softer pillar array. In addition to their local force-sensing capabilities cells can also sense global stiffness. The regulatory mechanisms behind are unclear and further investigations is needed to prove this idea. Beyond the insufficient maturation of focal contacts on the soft pillars a instability was also detectable. Compared to flat surfaces, zyxin was not colocalized with β_3 integrins in cells growing on 15 μm pillars. Moreover, zyxin was accumulated along actin fibers, indicating a translocation of this protein out of the focal contact. Similar results from cells plated on ligand reduced substrates indicate that focal adhesions from cells cultivated on pliable substrates are unstable [29]. The dynamics of different adhesion cluster morphologies should ideally be investigated in further experiments.

How strong this contractile machinery inside a cell can be, and how it is influenced by overexpressing different plaque proteins, was estimated using different REF52 cell lines (REF YFP-Paxilin and REF GFP-β_3) plated on calibrated microarrays. Functionalization had no effect on stress values exerted by REF YFP-Paxilin cells. A major difference was obtained when β_3 integrins were overexpressed. Not only are that the maximum forces 3 to 6 times higher when compared to the YFP-Paxilin cells, but the area of focal adhesions is also reduced. From the literature it is known that overexpressing β_3 integrin increases activity of Rho and stress fiber formation [125]. This may result in higher contractility and stress values for the GFP-β_3 cells compared to cells overexpressing YFP-Paxilin.

The way in which the mechanical properties of the adhesive support can control the recruitment of different signalling and linking proteins was demonstrated using FN coated microarrays. During cell spreading on surfaces where contractility was not reduced, the FN is pulled toward the cell center in a actomyosin dependend manner [215]. Different regions of protein composition were observed along the fibers. At the point where the cell was forming the focal contacts, proteins like β_3 integrin , pFAK(397), paxilin and vinculin were accumulated. From samples where pre-labeled FN was used, it could be observed that FN was not reduced significantly under focal adhesions. In this region the focal contacts are supported by a rigid surface and the intracellular tension can distort the focal adhesions that is inducing a mechanical signaling. Protein composition varies greatly along the fiber, which can extend several microns over the pillar area. Paxilin, pFAK(397) and β_3 integrin showed reduced intensity, whereas β_1 integrin was increased and colocalized with FN fibers. Interestingly, when the extracellular tension is reduced, focal adhesion sites lose the ability to recruit paxillin, suggesting that continuous generation of intracellular tension is required to maintain focal adhesions. This is supported by the increased amounts of paxillin and pFAK(397) at the tip end of the FN fibers

where tension exerted to FN is maximized. Physical distortion during the contraction of focal adhesions can serve as a mediator to recruit paxillin and pFAK(397) towards the adhesion site [170]. Wehrle-Haller et al. proposed a model for the mechanism of how adherent cells are sensing the mechanical properties of their environment [197]. The pliability of the substrate influences the assembly of focal contacts by regulating the mechanical distortion of integrins and their related proteins. This then activates a signalling cascade which regulates intracellular tension to compensate the external forces. If the extracellular support can withstand the cell mediated forces, more integrins and anchor proteins are recruited to the adhesion plaque. To this model a third mechanism should be added. Mechanosensing is not only restricted to the sites where the cells are forming focal adhesions, but may be also implemented in other signalling pathways.

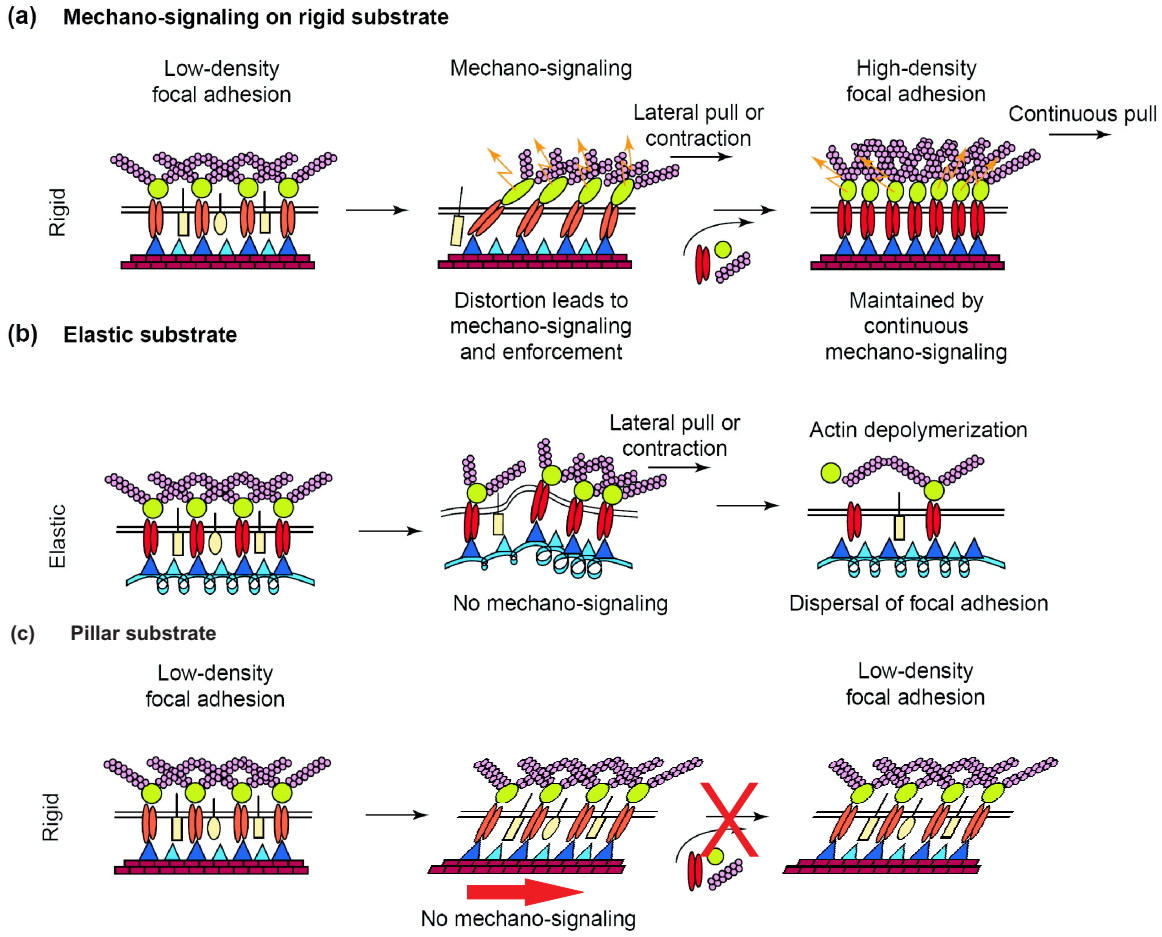

Figure 18.1: The influence of substrate elasticity on focal adhesions formed on rigid [brick wall; (a)], elastic [blue ribbon (b)] and rigid but slender substrates (c). The integrin-binding sites are represented by blue triangles. When focal adhesions are formed within filopodia or lamellipodia, they assume a low-density configuration that does not necessarily occupy all available extracellular-matrix-binding sites (left-hand side). In addition, the loose integrin spacing might leave space for additional non-integrin transmembrane receptors within the adhesion site (yellow). Owing to the absence of acto-myosin contraction, adaptor proteins are in a relaxed configuration (green circles). In response to RhoA activity and increased tension, the actin cytoskeleton will contract, generating a lateral pull. We propose that the distortions created in integrins (red) and adaptor proteins (green ovals) between the rigid extracellular binding sites and the contracting actin cytoskeleton induce mechanical signaling ('zigzag' orange arrows) by exposing so-far unidentified stress-sensitive binding sites for adaptor or signaling proteins. The subsequent recruitment of new integrins and adaptor proteins together with actin polymerization leads to high-density focal adhesions that, however, need to be continuously pulled to maintain mechanical signaling. When the cell establishes a low-density focal adhesion on an elastic substrate, the subsequent acto-myosin dependent contraction was not able to create a distortion within the condensing focal adhesion because of the lack of resistance of the substrate (b). In the absence of a mechanical distortion, no mechanical signaling occurred. The lack of focal adhesion reinforcement results in the dispersal of the focal adhesion site. If the microenvironment behaves like a rigid surface but the entire substrate is deformable as presented in the used pillar array, RhoA activation is lost. The reduced distortion of integrin and their related proteins is permitting the maturation into foacal contacts. Therefore a focal adhesion independent mechanosensor may exist which is measuring the global elasticity around a cell (c). Scheme is adapted from [197].

Part V

Physical properties of multicellular aggregates

Chapter 19

Introduction

Building up organs during embryogenesis is a complex process involving a huge population of different cells. These multicellular structures have to organise their spatial and temporal distribution in such a way, that the resulting organs (kidney, lung, blood vessels) show distinguishable properties. Most organs in human body, but also in other animals and insects are composed of tubes and cavities from 0.1 μm or less in diameter for the smallest insect tracheal tubes to greater than 20 cm for the gut of an adult elephant [119]. They serve as the body's plumbing, transporting critical gases, liquids and cells from one site to another. These biological pipes and collecting ducts are almost invariably composed of living cells, usually attached to one another forming an epitehlium, the inner layer of organs facing the environment. There are many developmental pathways found to be important of building epithelian sheets forming cavities and tubular structures. Most of them are based on specific biochemical signalling from growth factors or receptors, which specify the location, differentiation and patterning of tubular organs [218]. Despite significant progress over the past decade in understanding how tubular organs are patterned during development, we are only now beginning to understand how cells assemble into tubes and how tube size and shape is regulated. But some general rules for cyst formation and tubulogenesis can be formulated and a detailed mechanistic understanding of these processes is important for medicine as well as biology, because many human diseases such as polycystic kidney disease and atherosclerotic heart disease are essentially plumbing defects. A molecular understanding of cysto- and tubulogenesis could lead to new ways of diagnosing and treating these conditions [119].

Chapter 20

Theory

20.1 Epithelization during organogenesis and in kidney development

The aggregation of mesenchymal cells is an essential step in vertebrate development. It is seen in the formation of many tissues including somites, muscles, bones, hair follicles and nephrons[1]. The underlying mechanism of mesenchymal condensation and in the case of nephron development, epithelialization and tube maturation are not well understood (see Fig. 20.1) [13].

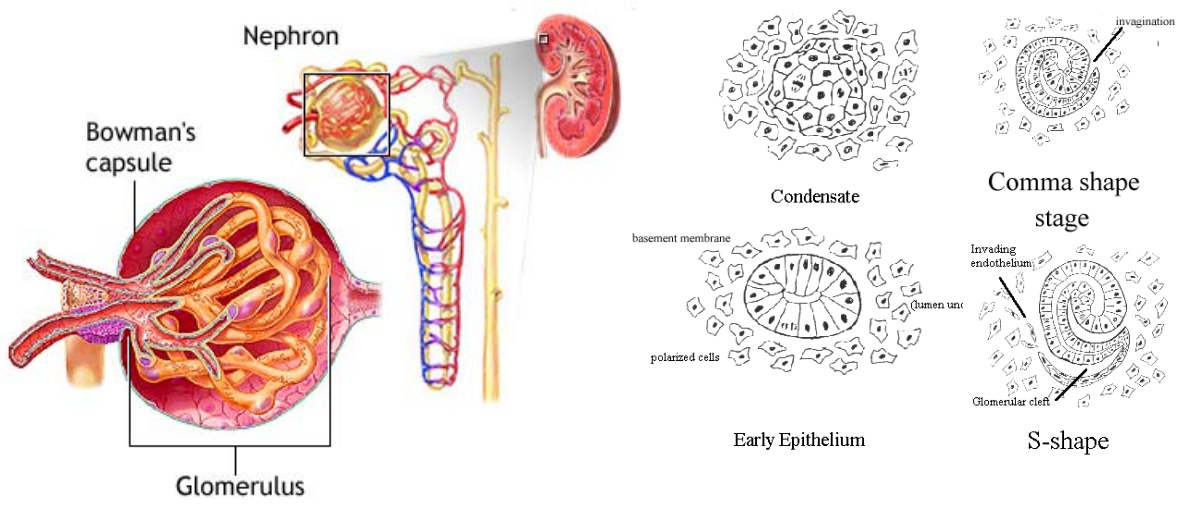

Figure 20.1: Left: Functional units and their localisation inside the kidney. The primary filtration is done in the Brownman's capsule. Nutrient recovery takes place in the so called loop of helene, where electrolytes, glucose and water are reabsorbed from blood vessels. Right: Early stages of nephron development induced by condensation and epithelialization of mesenchymal cells. For more details see [47]. Images were taken from[2].

In vivo tubulogenesis occurs by many different mechanisms, which at least superficially seem distinct [1]. Tubulogenesis is such a widespread and fundamental property of epithelial cells, however, that one could imagine an underlying basic program (or small number of

[1] the functional structures in vertebrate kidneys

programs) for tubule formation, which perhaps might be modified in different organs [3,4]. In vertebrates, tubulogenesis can be described as occurring by one of two broad mechanistic categories: epithelial sheet deformation, or condensation from non-polarised cells [1,51,52]. In epithelial sheet deformation, the cells move as a coherent sheet [2] that invaginates or evaginates. Typically, this involves only a portion of the epithelium, with the tube-forming cells first detach from the basal membrane to form a cervice in the epthelium, then sealing off and separating from the rest of the epithelium, as seen during neural tube formation in many vertebrates . This generates a tube that runs parallel to the plane of the epithelium from which it derives [38]. In condensation, cells that lack epithelial polarity aggregates and arrange themselves into a tubule. The rearrangement starts with the transition from a non-polarised mesnchymal cell state to ephitelial polarity. The change in cell polarity allows the formation of tightly packed sheet of cells. The dense sealing from outer environmental influence is arises from tight-junctions, that separate the cell membrane into two distinct regions. The apical compartment is the free surface (the lumen in kidney cysts and ducts). The basolateral compartment lies between epithelial cells and is continuous with the underlying connective tissue and its blood vessels. This sealing inhibits the diffusion of solutes between the apical and basolateral compartments of the extracellular space. The plasma membrane is also separated into apical and basolateral domains, restricting the movement of integral membrane proteins between these domains [157] (see also Fig. 20.3). After aggregation of mesenchymal cells and the transition to epitelial polarity, cells tend to form a cavity surrounded by a monolayer of cells. Cavities are formed by membrane separation or by clearing lumenal space from cells not facing the extracellular space by apoptosis [3](see also Fig. 20.4) [119, 218].

20.2 In vitro model systems for tissue morphogenisis

To understand the mechanisms that organise the action of single cells during tissue morphogenesis, it is necessary to overcome the barriers that are inherent in carrying out such an investigation *in vivo*. Different model systems were developed during the past 25 years, most notably Madin-Darby Canine Kidney cells (MDCK) [4]. Cultivation of MDCK cells shows very specific behaviour on culture conditions. Epithelial polarisation [5] can be induced by growing the cells on filter supports, were nutrition also takes place from the basal side of the cell [40]. They grow to confluency as tightly packed columnar cells, which are well polarised and show contact inhibition means that they do not pile up on top of each other. This contact inhibition can be dramatically reduced by overlying monolayers of cells with matrix proteins such as collagen I. The mechanism involves induction by apical activation of the collagen receptor $\alpha_2\beta_1$ integrins. The $\alpha_2\beta_1$ integrin is primarily located basolaterally in MDCK cells, but there is also a small, crucial pool at the free apical surface [222]. The $\alpha_2\beta_1$ integrins are normally inactive here, as long as collagen is absent at free surfaces. Overlaying the free membrane with collagen I matrix activates the apical integrins and cause cells to sprout out from the monolayer enclosing a lumen with the existing cells from the epithelial layer to generate new free apical surfaces for recovering epithelial polarity [179]. To investigate morphogenic details

[2] the epithelium can also detach from the underlying surface

[3] apoptosis can be inhibited by ErbB2, Bcl-2 or ECM contact

[4] A human model system from mammary glads (MCF10-A)was also developed.

[5] specific markers for epithelial polarity are gp135, actin for the apical membrane, ZO-1 is a protein located in tight-junctions and p58, laminin are secreted only at the basal membrane [140]

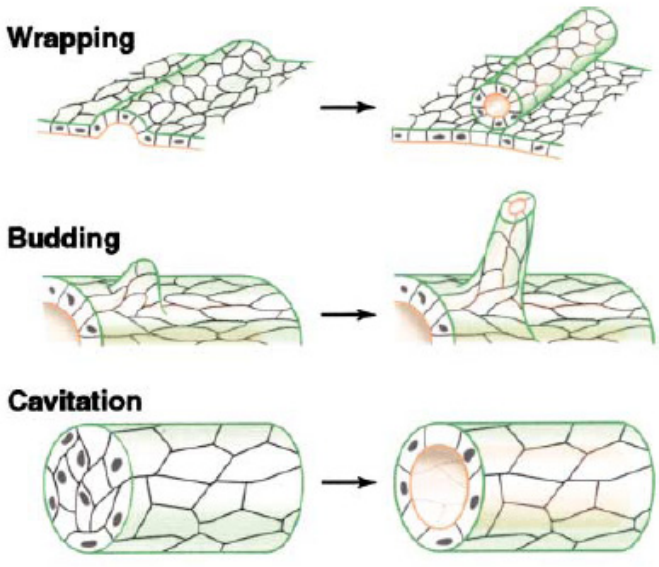

Figure 20.2: Morphological Processes of Tube Formation. Wrapping: a portion of an epithelial sheet invaginate and curls until the edges of the invaginatig region meet an seal, forming a tube that runs parallel to the plane of the sheet. Budding: a group of cells in a existing epithelial tube (or sheet) migrates out and forms a new tube as the bud extends. The new tube is a direct extension of the original tube. This mechanism is described in HGF-induced tubulogenesis of embedded cysts. Cavitation: the central cells, which lack the basal membrane surface-contacting ECM of a solid aggregate are eliminated to convert it into a tube or a hollow sphere. Image taken from [119].

during tissue development it was necessary to extend the standard culture methods with a 3D model system [81, 142, 144, 223]. Single cells, when embedded in a gel build up from reconstituted collagen type I [6], tends to grow as cell aggregates with a central lumen (see Fig. 20.4). This 3D-system has been used extensively to investigate how extracellular factors interact with an intrinsic differentiation programme to specify the architecture of epithelial tissues. Like simple 2D epithelial tissue, cysts - also known as acini in the mammary gland, aveoli in the lung and follicles in the thyroid - are spherical monolayers of polarised cells that enclose a lumen and encircled by a basement membrane. The polarisation is common for self enclosed epithelial layers wherein cells have three distinguished surfaces: a free, apical surface that borders the lumen; a lateral surface that adheres to neighbouring cells; and a basal surface that adheres to the ECM. Because many proteins localise to both the basal and lateral surfaces, these surfaces are often collectively referred to as 'basolateral' (see Fig. 20.3) [141].

With the established 3D model-system, it is also possible to get detailed information during tubulogenesis in vivo and how different biochemical and matrix composition is influencing these mechanisms. It has been known for 15 years that hepatocyte growth factor (HGF) induces tube formation in cells and hollowed cell aggregates embedded in collagen I matrices [18, 23, 128]. It is speculated that HGF initiates new tubule development by inducing a transient epithelial-mesenchymal transition (EMT) that temporarily overrides the driving force for the 'three surfaces' condition. There are several downstream targets which can be affected by HGF, like the cytoskeleton or the basal plasma membrane. The most abundant effect

[6] collagen can be extracted from tendons or skin at pH 2. For gelation and fiber recovery it is necessary to neutralize and warm up the solution

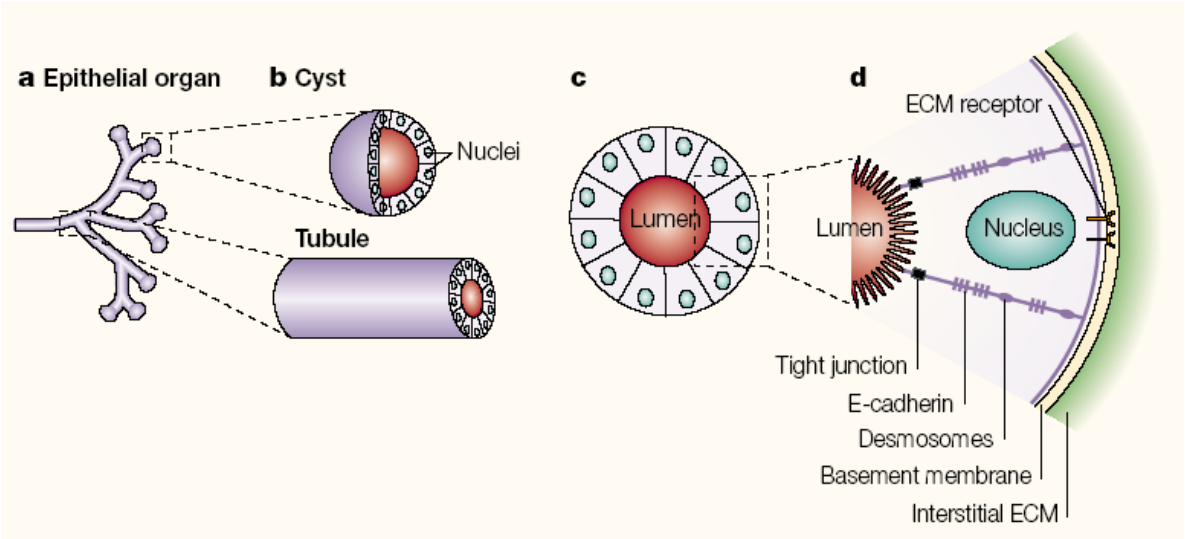

Figure 20.3: Internal epithelial organs (a) consists of two basic building blocks: cysts and tubules(b). c) In cross section, these building blocks are lumen-enclosing monolayers of polarised cells. Each cell in the monolayer has a microvilli-rich, free apical membrane domain that faces the lumen, a lateral membrane domain that facing neighbouring cells, and a basal membrane domain that faces the basement membrane. d) The basement membrane, a specialised extracellular matrix (ECM) that is produced by epithelial cells, forms a layer between the epithelium and the mesenchymally derived interstitial ECM. Cells attach to ECM through integrin and non-integrin receptors and bind to neighbouring cells through tight-junctions, desmosones and homotypic E-caderin interactions. Tight-junction also demarcate the boundary between the apical and basolateral surfaces. Image was taken from [141].

caused by HGF is switching the spindle orientation during cell mitosis [211]. Normally, dividing MDCK cells orient their spindles parallel to the axis of the monolayer [160]. In cells trying to escape the monolayer the spindle might orientate perpendicular to the cyst surface. [7] As the cell is proliferating out from the cyst monolayer, it forms a chain surrounded by ECM proteins. This status is similar to filter supported MDCK monolayers overlaid with collagen as discussed above. To restore normal polarisation, cells again form multilayers and then create small lumens between the layers (membrane separation, see also Fig. 20.4). Therefore tubulogenesis shows features of both basic mechanism: sheet deformation and condensation (see also Fig. 20.2) [156, 90]. The existence of an intermediate situation between sheet deformation and condensation suggests that these two mechanisms are not as dichotomous as is usually assumed, but rather that they are likely to be two ends of a continuous spectrum. That the MDCK/HGF model as a redundant system cannot describe the complexity of lumen formation is evident. For example other proteins or growth factor can inhibit EMT induced by HGF [169, 37]. It is also known that kidney development of HGF-knockout embryos seem normal [192, 172]. Therefore the complex interaction during tissue morphogenesis is not only influenced by different growth factors or other up-/downstream signaling proteins but also by other factors not relatet to biochemistry.

[7] Parallel and perpendicular mitotic axes are specified by APC/EB-1 and Par-3-Par-6 [118, 152, 112]

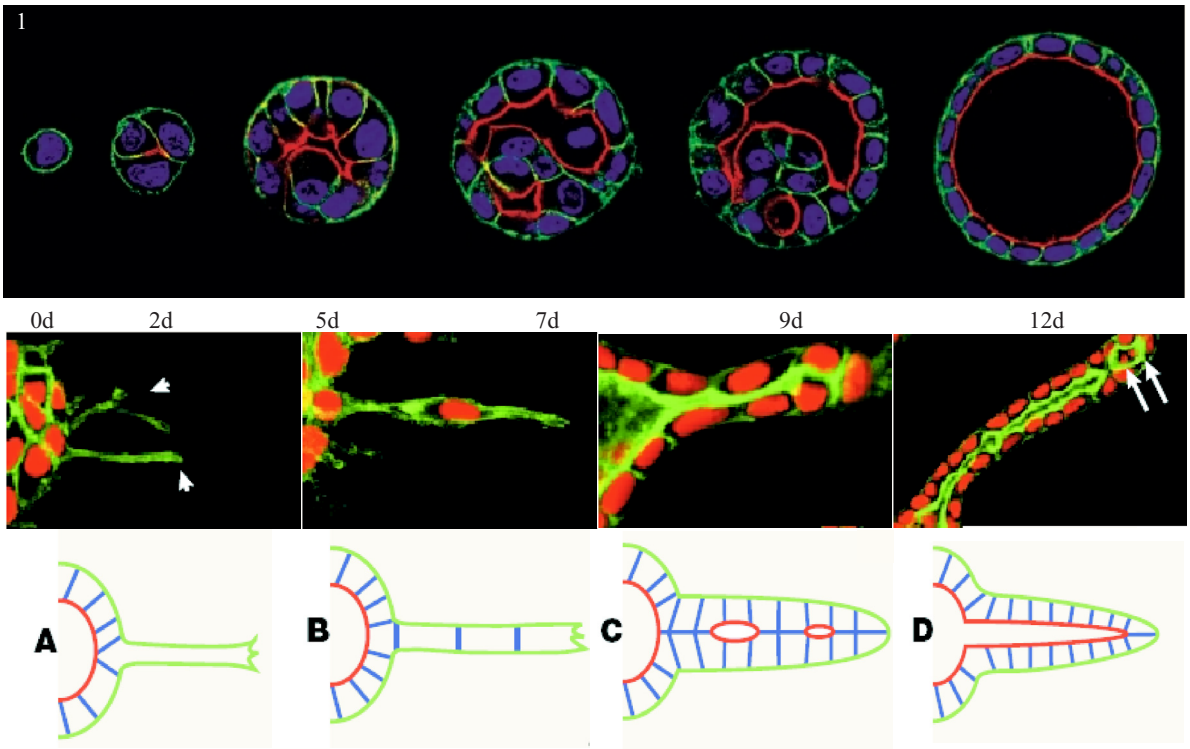

Figure 20.4: 1) Single epithelial cells that are embedded in extracellular matrix (ECM) proliferate to form clonal cysts. Madin-Darby Canine Kidney (MDCK) cyst at 0, 2, 5, 7, 9 and 12 days of development are shown. The lumenal apical domain is stained for actin (red), basal and lateral domains are stained for p58 (green), and the nuclei appear blue. Although each cell in the mature 12-day cyst has a free, lateral and basal membrane surface, cells in immature cyst often lack at least one surface type. Note the apoptotic nuclei in the lumen of the cyst at day 7. 2) MDCK tubules at different stages of development, stained for nuclei(red) and actin (green). In cartoons, blue represents cell-cell contacts, green represents cell-matrix contacts, and red represents free membrane surface. A) After treatment with hepatocyte growth factor (HGF), new tubules initiate when single cells become invasive and project a long, basal-membrane extension into the ECM (arrowheads). B) Cells proliferate to form single file chains, were cells has lost apico-basolateral polarity. C) To recover polarity cells starts to form multilayered cords. Apical membrane surface is re established, as shown by intense actin staining at the interface between cell layers, and new lumen formation is initiated. D) Lumen enlargement provides each cell with a free surface. Note apoptotic nuclei in the developing lumen (arrows). Images were taken from [141].

20.3 Mechanical influences on cystogenesis

During cyst formation, cells in a 3D culture mechanically remodel ECM [151]. A number of studies have suggested that mechanical forces play a role in controlling epithelial morphogenesis [199, 24, 84, 186]. The mechanical forces might also be one of the factors controlling cell proliferation and cyst formation [205]. To elucidate the correlation between mechanical forces and cystogenesis, it is necessary to quantify the mechanical forces between cells and the ECM. Various approaches have been proposed for evaluating the mechanical forces between cells and the ECM, including measurements and calculations using cell-populated matrices, planar elastic substrata in 2D cultures as mentioned in Chapter 1, or differential interference contrast (DIC) images in 3D cultures. When fibroblasts were seeded into a porous matrix, forces generated by the cells could contract the matrix [80]. This has been used in some stud-

ies to measure the force produced by the cell population [111, 49, 67]. In these studies, one end of the matrix was clamped, and a force gage was attached to the other end, so that the mechanical force produced by the cell population in the ECM was monitored. Although cells were present in the 3D culture in these tests, details on forces produced by single cells could not be obtained, except for average values in some cases. Vanni and co-workers presented a technique in which DIC images were used to measure the displacement around a cell in a 3D culture. Visible collagen fibers were tracked in the in-focus plane of DIC images of a cell to derive the displacements caused by the cell [194]. However, the displacements thus derived were essentially 2D, as was the subsequent calculation of stress. To elucidate the correlation between mechanical forces and cystogensis, it is necessary to quantify the mechanical forces between cells and the ECM in 3 dimensions. Elastic substrate methods, which apparently can measure forces at the interface between the cell surface and the ECM in 2D cultures, need to be extended by a computational model of cyst movement in the 3D matrix in order to estimate the 3D force distribution [219].

Chapter 21

Materials and Methods

3D cultures have proven advantages over 2D cultures in studying tissue morphogenesis in vitro [48, 218]. The necessity to develop a method and tools for evaluating the mechanical forces between cells and the ECM, in three dimensions and at the cellular level, is apparent. A 3D computational model complemented by experiments for such a purpose was developed. Stably transfected GHY3-MDCK (YMD in the following) [1] cells expressing the monomeric fluorescent fusion protein Gap-43:mYFP:His6. Gap-43 portion was doubly palmitoylated and targets the monomeric Yellow Fluorescent Protein (YFP) to the membrane lipid rafts. YMD cells were embedded in type I collagen gel. Cells were tracked over time with a confocal microscope to determine the 3D geometry of the cells or aggregates. Displacements at the boundary between the cell aggregate and the ECM were derived by registering two images of the same aggregate taken at two consecutive times. These displacements were taken as boundary conditions at the surface of the aggregate. The ECM was modeled as a viscoelastic material. The finite element method (FEM) was used to compute the stress field around the cell aggregate. To validate the calculated forces resulting from cell aggregate displacement within the ECM an appropriate model system is necessary. It should fulfil several conditions:

- The cells should be able to form multicellular cysts surrounded by a ECM network.
- The force should be measured at the boundary of the aggregate independently from the ECM displacement.
- The system should be capable of being used in conjuction with fluorescence microscopy.

21.1 Surface preparation and cell culture

The ideal tool that fullfills these guidelines is the force sensor arrays introduced in part II. Further improvements were done to ensure preferred cyst growth on the microarray. To evaluate cell behavior on PDMS, flat glass coverslip supporting thin PDMS films and bare coverslips (as a control) were coated with different proteins under various conditions. All proteins were diluted in PBS except reconstituted collagen I. The surfaces were incubated for 2 minutes at RT or overnight at 4°Cwith a protein concentration of 100 μg/ml. To coat the

[1] kindly provided by Dr. D. A. Zacharias (The Whitney Laboratory for Marine Bioscience, University of Florida. Gainesville, FL, USA)

microarry, the pillars supported on a 24×24 mm coverslip were incubated in a neutralized acetic solution of collagen I with a final concentration of 100 μg/ml at RT for 2 minutes. RGD was grafted as described in the previous part. After washing in PBS the samples were mounted with vacuum grease on a punched 60 mm petridish and uv-sterilized for 2 minutes.

21.2 Cell plating

YMD cells were used to achieve better visualization of the cyst geometry during force measurements. A single cell suspension was generated by trypsinizing a sub-confluent YMD 2D culture with 0.05% Trypsin and 0.53 mM EDTA for 20 minutes at 37 °C. Cells were resuspended in DMEM suppl. with 1% glutamine, 1% penicillin/streptomycin and 10% FBS to obtain a final cell density of 12500 cells/ml. After one day of incubation a solution of reconstituted collagen I (1mg/ml)in DMEM or diluted gfr-Matrigel (BD-Bioscience, Heidelberg, Germany)[2] was allowed to polymerize on top of the cells for 1 h at 37°C. After polymerization was complete, 5 ml of complete cell culture medium was added. After 4 days, cyst-like cell aggregates had developed on the microarrays. One sample was fixied for immunofluorescence labeling. Fixation was performed in PBS containing 3.7 % PFA for 30-40 minutes. For permeabilization, the sample was incubated for 10 min. in 0.1 % Triton X-100 solution (diluted in PBS) and washed thoroughly 3 times with PBS. In general all antibodies used for immunostaining were incubated in a 0.1 % BSA -PBS solution for 30 minutes at RT. A washing step was included during the staining procedure between primary and secondary antibody (3 times á 10 min. in PBS). Samples were mounted on objective slides with elvanol to prevent photobleaching. For detection of adsorbed proteins on the microarrays, primary monoclonal mouse anti-collagen I antibody (1:400, Sigma) was used in combination with secondary goat anti-mouse Alexafluor 488 (1:100, Molecular Probes). The cysts were stained for laminin (polyclonal, rabbit anti-laminin, 1:400, Sigma, together with goat anti-rabbit conjugated to Cy5, Jackson ImmunoResearch), actin was visualized with TRITC conjugated Phalloidin (1:100, Sigma) and DNA was stained using DAPI (Sigma, 1:50). Three coloured images were taken with a wide field epi-fluorescence microscope (DeltaVision, Spectris) equipped with a 60X water immersion Plan Apochromat objective (NA 1.2) to keep spherical aberration minimized. Fluorescence was excited with a 100 W mercury lamp. All excitation and emmision filters were from chroma (Rockingham, VT, USA). Image restoration was performed on a workstation running a deconvolution software (SoftWorX, version 3.2) from Applied Precision. For higher resolution and 3D reconstruction of the cyst images were captured with a '5 Pascal' confocal microscope (Zeiss, Goettingen, Germany).

21.3 Image acquisition and analysis

Images from the flat surfaces for evaluating the best protein combination were taken on a inverted microscope (Axiovert 25, Zeiss) equipped with a CCD camera (Axiovision,Zeiss) and a 20X LD Ph1 objective (N.A. 0.5; Zeiss). Image acquisition of growing cysts was performed

[2]Matrigel is a mixture of laminin, collagen type IV, entactin, and other proteglycans derived from Engelbreth-Holm-Swarm (EHS) mouse sarcoma. It gelates to a matrix that resembles the basal membrane. Here it was used with reduced growth-factors to minimize the biochemical influence of ECM. Dilution (1:1) was done with DMEM supplemented with 10% FBS.

on a DeltaVision Spectris system equipped with a environmental chamber and LD 20× (N.A. 0.6) objective and a resulting pixel size of 0.3313 μm. Images were taken every 10 min. over a period of 8 h. YFP was excited at 510 nm selected from a 100 W mercury lamp and the Pillar movement was acquired in phase contrast. Seven images from different time points were aligned manually using NHI ImageJ to remove thermal drift between the images. Manual contrast enhancement of each pillar was done in Corel Photopaint (Ver.11, Corel Corp., Ontario, Canada). Analysis of pillar movement was done in ImageJ. From each image a threshold image was generated and the center of mass from each particle (pillar) was recorded. An image of undeflected pillars was also analysed using the same protocol. Force calculations were preformed in OriginPro (Version 7.0, OriginLabs Corp., Northampton, MA, USA) and the resulting force was addressed as false color to each pillar position as shown in Fig. 22.6 for three images representing the entire stack. Two pillars were also tracked over the whole 47 images, one is underlying the cyst($*$) and the other lies outside ($+$). In Fig. 22.6 C the movement of those pillars is plotted as force over time curves. The microarrays used were calibrated before cell plating as described in Chapter 1. The k_{pillar} was calculated to be 0.089 N/m.

Chapter 22

Results

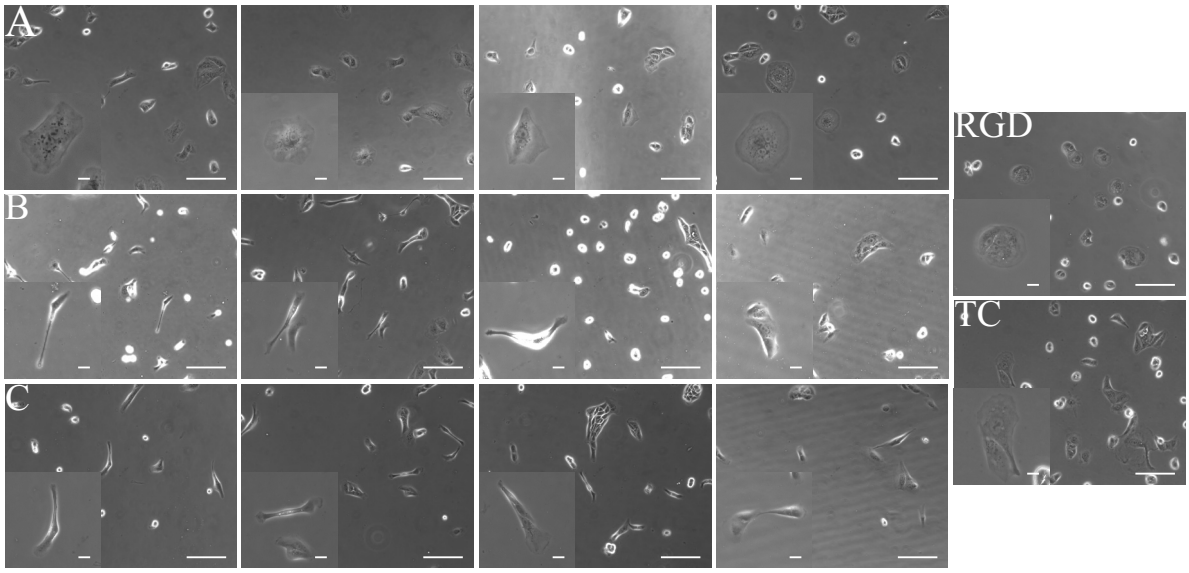

Figure 22.1: Changing cell morphology by different surface conditions. A: Glass surfaces were coated for 5 minutes at RT with different proteins: collagen I, collagen IV, laminin, and fibronectin. B: The same coating conditions were used to functionalise thin PDMS films supported on glass coverslips. C: Incubation of the different proteins on PDMS was extended to 12 h for saturation of surface adsorbed protein molecules to maximum. Last column: for selective activation of the $\alpha_2\beta_3$ integrins a cyclic RGD was crafted on the PDMS surface. As a control images were also taken from bare tissue culture plates. Scale bar corresponds to 100 μm in panels and 10 μm in inserts.

22.1 Influence of protein type on cell morphogenesis

To assay polarized cyst formation several protein combinations and media supplements were tested as promoters for the defined cell adhesion necessary for cyst development on PDMS. In Figure 22.1, flat PDMS coated coverslips were incubated for 2 min with different protein solutions at a concentration of 100 μg/ml and compared to coated glass coverslips. The most relevant difference can be seen on collagen type I coated PDMS surfaces when compared to the glass surfaces. After one day, cell spreading is not as distinctive as for cells on collagen-coated

glass. Rather the cells assume a more elongated morphology. To rule out the possibility of a reduced surface adsorption of collagen type I on PDMS compared to glass the surfaces were incubated with the same collagen concentrations overnight at 4 °C. There was no evident coating difference between the short and the prolonged incubation time of collagen type I on PDMS. After 4 days in culture the cells formed a confluent layer and the incipiently visible difference between glass and PDMS surfaces was no longer predominant. Unlike the protein-coated substrates, confluent monolayers on RGD terminated surfaces, start to detach from the surface and form loops of single cell monolayers. This peculiar behaviour was never detected on collagen or fibronectin coated glass or PDMS surfaces (see Fig. 22.2).

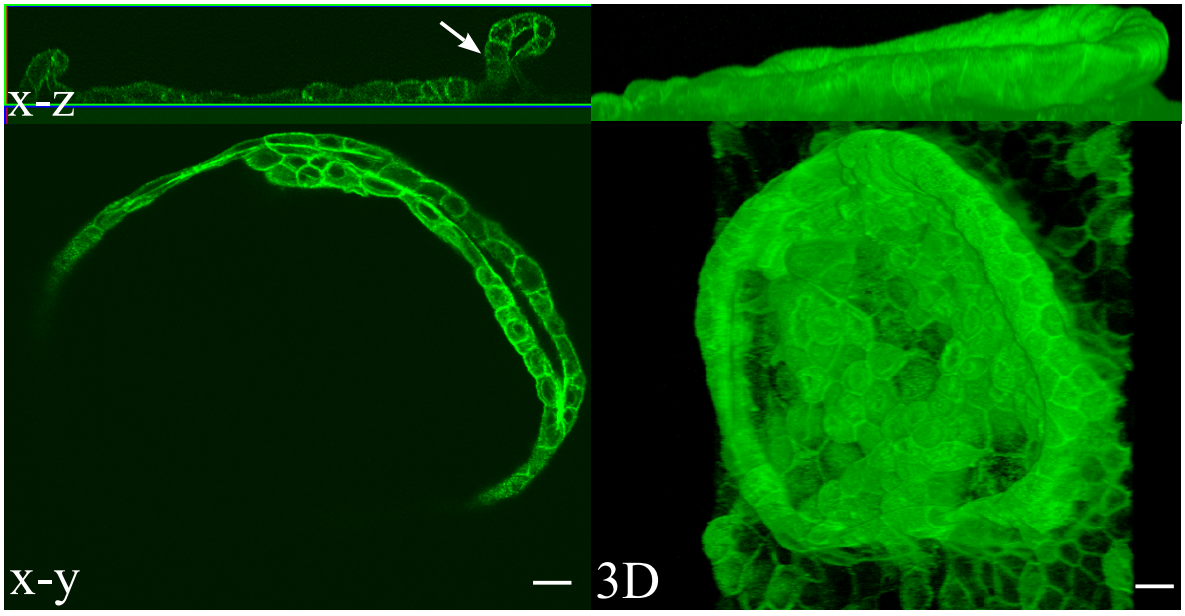

Figure 22.2: After growing to confluency on a RGD terminated surface, YMD cells detaches from the surface on a circular area and form a single layered loop (arrow). This morphology never appeared on protein adsorbed surfaces. The reconstructed 3D image on the right was rendered from confocal z slices. Scale bar 10 μm.

22.2 Enabling 3D growth on 2D substrates

As known from the literature [81], embedding MDCK cells in an ECM matrix initiates cyst formation. Cells growing on different protein-coated surfaces were overlaid with either collagen I (1 mg/ml) or gfr-Matrigel (diluted in a 1:1 ratio with DMEM). Fig. 22.3 shows the effects of the different ECM proteins to MDCK cyst formation. Only when the cells are overlayed with gfr-Matrigel they start to aggregate and to form small cysts within 4-5 days in culture. Overlaying the cells with collagen I matrix did not induce cyst formation. It was also seen that cell proliferation was reduced when matrix proteins were present at the apical surface of the cells. After 4 days in culture, monolayers were formed on non-overlaid samples and on overlaid glass substrates. Cells on PDMS surfaces still remain as cell islands (data not shown). From other experiments it was known that the microarrays reduce cell proliferation. This preliminary result was used in order to optimize cytogenesis onto microstructured surfaces [22].

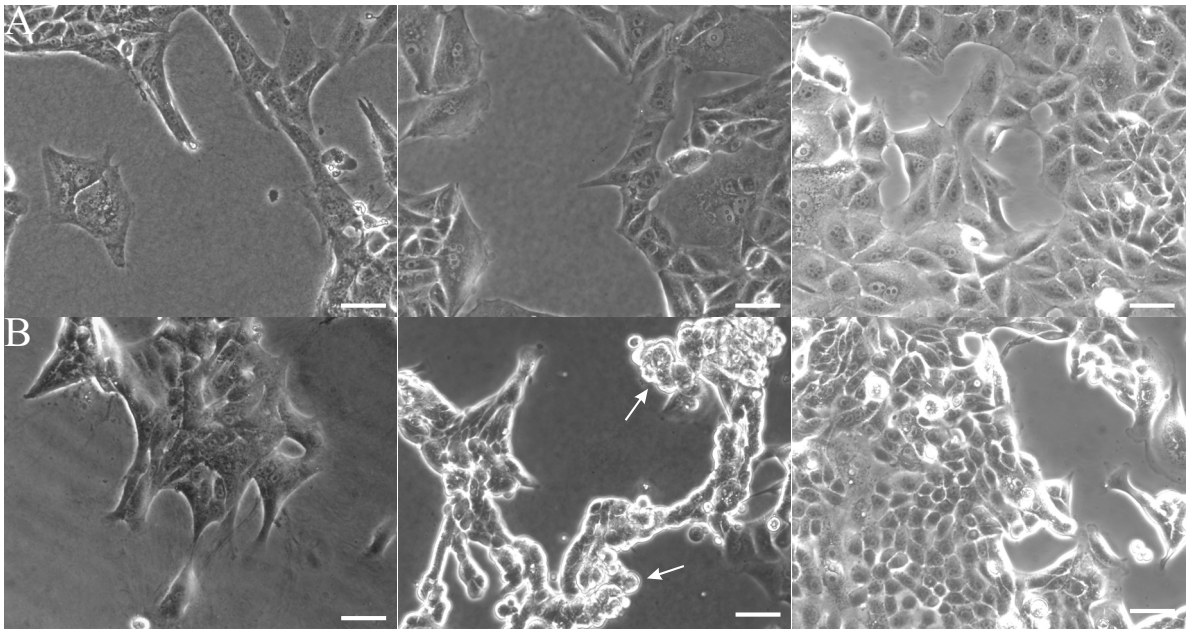

Figure 22.3: Influence of different matrix overlays in flat MDCK cultures after 4 days in culture. A: Glass surfaces were collagen type I coated and after one day cells were overlaid with either reconstituted collagen type I at a concentration of 1 μg/ ml (column 1) or with gfr-Matrigel diluted with one part of complete medium (colum2). B: The cells were cultured on flat PDMS instead of coated glass coverslips. Only in the case of gfr-Matrigel overlay, cells started to leave the surface and to grow inside the gel (arrows). The control is shown in column 3 were the cells were cultured w/o matrix overlay. Cells growing on PDMS had a roundish unspread morphology even after 4 days, whereas the cells on glass showed a well spread phenotype. Scale bar corresponds to 20 μm

22.2.1 Cystogenesis on force sensor arrays

The reason for keeping the incubation time at minimum, is shown in Figure22.4. When the microarray is coated for only two minutes, the majority of collagen was adsorbed to the pillars top. If the incubation time is extended to 30 minutes, the protein solution is adsorbed also to the sidewalls. In this case the repellent properties of bare PDMS to cell adhesion vanished. The resulting increase of cell-substrate adhesion inhibits cystogenesis. The cells are growing as a multilayer incorporating the pillars. Spherical cysts did not develop at any time point under these conditions(see Fig. 22.4 C).

After cells were embedded in gfr-Matrigel, they started to form multicellular aggregates with a central lumen. Small cysts of 50 to 100 μm developed within 5 days in culture. They were composed of a cell monolayer enclosing a central lumen where the cells showed distinct polarization. Actin (green in Fig. 22.5 A) is concentrated to the apical membrane in actin-rich microvilli [129]. Laminin (red in Fig. 22.5 A), the major protein in the basal lamina, is secreted only to the basal surface and is not present in lumenal space. Cysts were only attached with the basal side to the top of the microarray as seen in Figure22.5 C.

22.3 Force measurements

In this configuration it was possible to measure forces exerted by the cell aggregate on the pillar array. In Fig. 22.6 three representative images are displayed from time lapse imaging

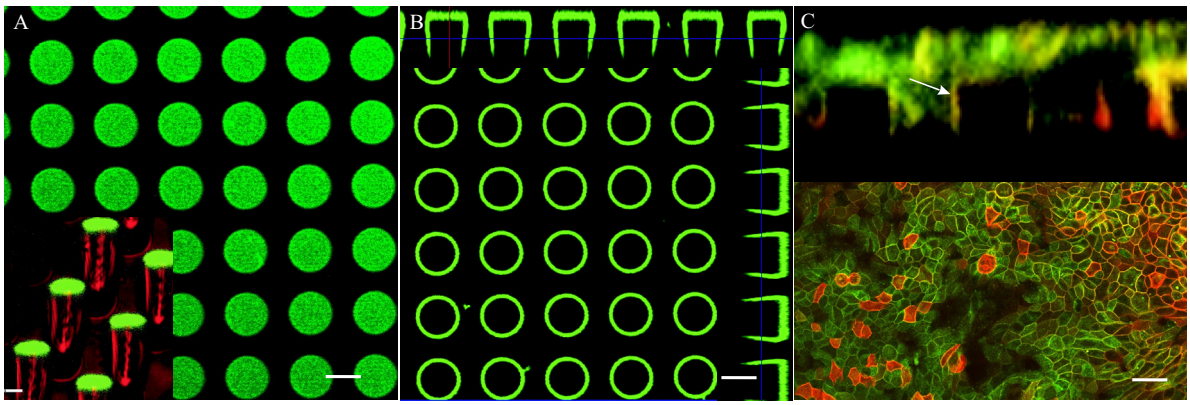

Figure 22.4: A: Collagen type I was incubated for two minutes on the micro array and visualized by immunofluorescence labeling and confocal imaging. From the insert were bended pillars are imaged, it is clearly seen that the protein layer (shown in green) is restricted only to the top of the pillars, which were visualized in reflection. B: If incubation time is extended to 30 minutes the protein solution is also wetting the sidewalls of the micro array as seen in the x, z and y, z sections of the confocal z-stack. C: Cells growing on entire coated micro arrays as shown in B forming mono- or multilayers without lumen incorporating the pillars (arrow). Cells were immunostained for actin (red) and YFP is shown in green. Scale bar correspond to 5 μm in A/B and to 15 μm in C.

of a growing cyst. From phase contrast images, the pillar bending was tracked manually and the exerted force is displayed using false colors at the corresponding pillar position (see Fig. 22.6 B. The white circles in the images symbolize the initial position of each pillar in the field. Two pillars (marked with $*$ and $+$) were tracked throughout the experiment (in total cyst development was recorded over a period of 8h) and force was plotted over time (see Fig. 22.6 C). Three time points from picture A and B were marked as lines in the graph. The initial force values decrease over time as the cyst is growing and moving. At the beginning the pillar underneath the cell aggregate is near the center were the cyst is adherent to the force sensors. The area of adhesion is encircled in Fig. 22.6 B. After 8 h the cyst moved and the pillar of interest was tracking the force at the cyst boundary where adhesion was weaker. Pillars next to the aggregate were also bent, because the attached fibers of the model ECM serve as force transducers. The average force value applied to the pillar marked with $+$ was around 1/3 lower than forces exerted directly to the force sensors (marked with $*$).

22.4 Anisotropy induce cyst polarization

The micro array used to measure forces generates an isotropic environment [3] for the cell aggregates. It was important to know how cystogenesis was affected by changing environmental conditions, because previous investigations in this directions considered only biochemical signals [141, 211, 169]. To answer this question anisotropic microarrays were used instead of circular pillars with equal stiffness in x and y direction. The cells were plated under the same conditions as for the isotropic microarray. Under these conditions cells could recognise the anisotropic environment provided by the pillar surface. Some of the cyst altered their shape from spherical to cylindrical and grew as tubes on the arrays (see Fig. 22.7 E, F). Polarity did not change dramatically, actin was still concentrated at the apical surface and laminin

[3] not taking into account that interfaces in general generates an anisotropic vicinity

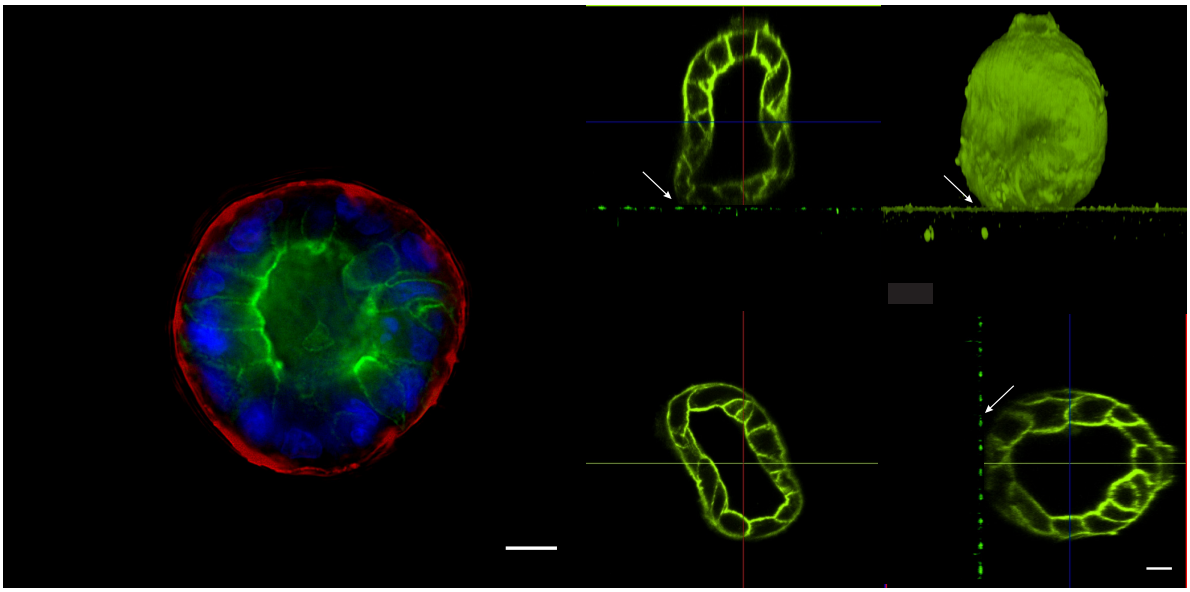

Figure 22.5: Left: Image of a cyst, immunostained for laminin (red), actin (green), nuclei (blue). The images were extracted from a deconvolved z-stack at the plane of biggest cyst diameter. Cells forming a cyst segregate laminin only to the basal membrane while actin is concentrated on the apical surface in small extension (the microvilli), typical of polarized epithelial cells. Right: Different plans through a cyst stained for actin. The z-stack was collected with a confocal microscope [2]. Arrows indicate the points in which the cyst adheres to the pillar surface. The freestanding cyst surface was surrounded by gfr-Matrigel which was removed during fixation and immunostaining procedure. The reconstructed 3D image in the upper right corner was rendered from confocal z-slices. Scale bar is 10 μm.

was secreted exclusively to the basal membrane. How this contact guidance was influenced by the matrix overlay could not be investigated, because of matrix removal during the staining procedure [56]. To draw more attention to the influence of matrix remodelling, cells were plated on flat PDMS surfaces and overlaid with a collagen type I matrix.

22.4.1 Basic mechanism of Cyst reorientation

It is known from the literature that overlaid MDCK cells can be cultured [4]. Therefore the cells cultured on PDMS should have an intermediate morphology between epithelial and mesenchymal. Collagen type I can induce a change in cell differentiation from epithelial to mesenchymal (see also Fig. 22.1) [223]. The transition from epithelial polarity to migratory polarity causes matrix reorganisation of the surrounding fiber network [39, 190, 77]. The cells condense and align the fibers along the direction of highest tension between two separated cell islands. This fiber condensation guides cell growth. In the first panel of Fig. 22.8, two cell cords growing against each other directed by the aligned fibers between them are shown. The arrows are indicating small extensions which may guide growth direction. Furthermore on Panel B a migrating cell is changing direction when reaching an area of collagen matrix fibers orientated perpendicular to the migration axis. This well known contact guidance show how sensitive cellular recognition of the surrounding matrix is. In the same field, a round cell island (marked

[4] MDCK cells growing on solid supports are much less polarised as cells growing inside a 3D culture or on filter supports [40]

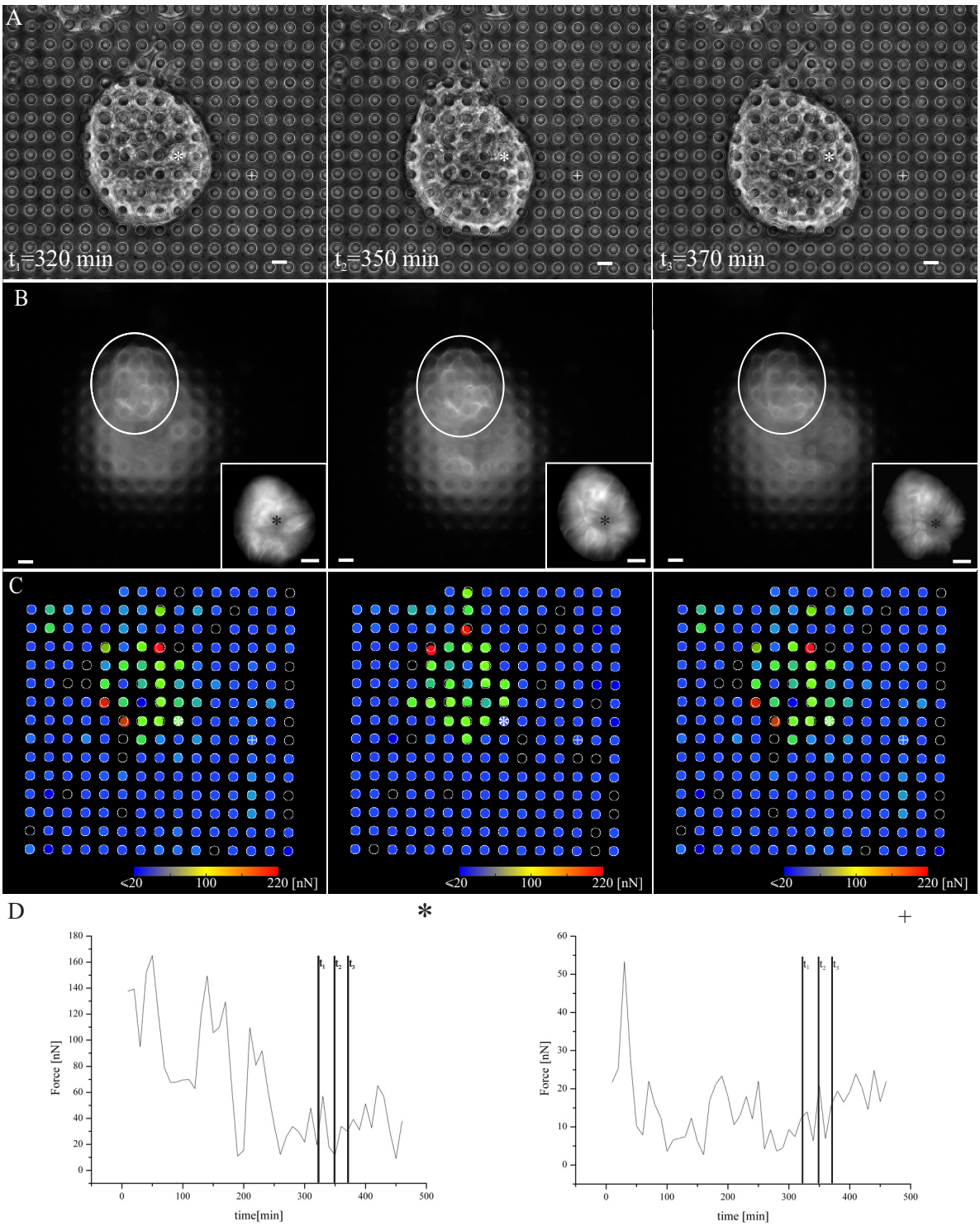

Figure 22.6: A: After 4 days in culture cysts, developed on 15 μm height posts. Images were taken at the cyst pillar interface every 10 minutes over a period of 8 h in phase contrast. In panel B the corresponding fluorescence images are displayed and the area of adhesion is encircled in white. Images shown in inserts were taken 12μm above the surface at biggest cyst diameter. Lumen is marked with $*$. The corresponding bending of each pillar is shown by the false color (B). Circles illustrate the undeflected position of the corresponding posts. Circles were no color is present are below the threshold of 10 nN. C: The two pillars marked with $*$ or $+$ in A and B were tracked throughout the experiment and the resulting force was plotted over time. The three selected time points from A and B are marked as lines in the graph. Scale bar corresponds to 10 μm and to 20 μm in the inserts.

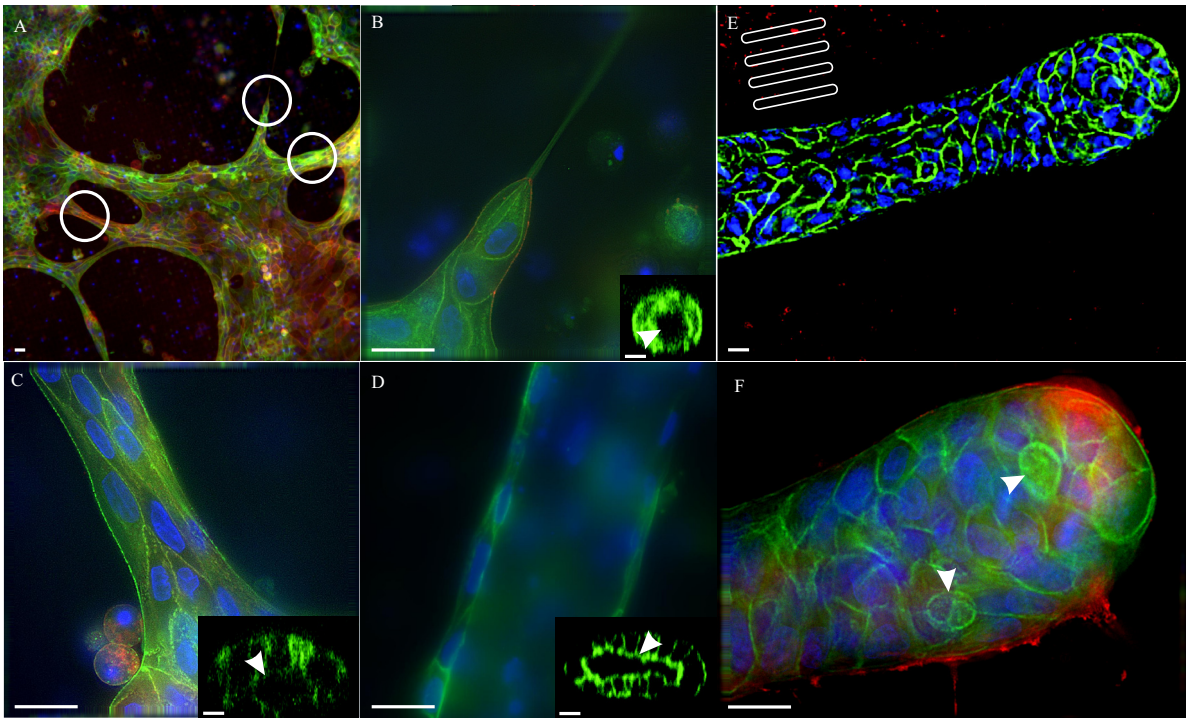

Figure 22.7: Different stages of tubule development of MDCK cells growing on the microarrays with a matrix overlay. The different stages were taken from the sample shown at low magnification in (A). Cell nuclei are stained in blue, actin is green and laminin appears red (except of image D were laminin was not stained). Encircled areas are shown in B, C, D at higher magnification. Along the protrusions (which can be over 50 μm long) the cells are growing as a thin nearly single cell cord with small vacuoles at the tip (B). In the multilayered string of cells, the vacuoles grow to localised lumen in order to create new apical membrane (C). As the mature tube the lumen is extended over the whole length. The inserts are x−z sections of confocal images taken on the same areas as for the widefield deconvolved images. To orient the growth direction of the tube, cells were also plated on anisotropic pillars (see encircled pillar, E). The cells are recognising the given direction and forming a tube within the same orientation. Small vacuoles are generated at the tip of the growing tube to get a free surface for proper polarization. Scale bars are 10 μm and in the inserts 5 μm.

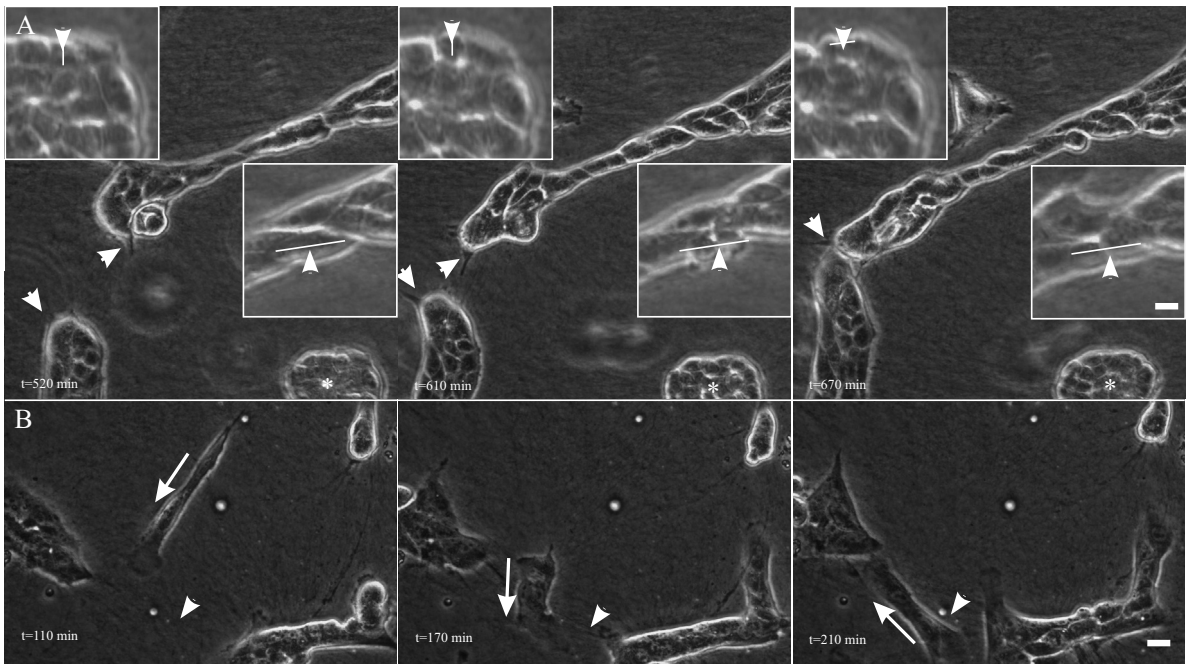

Figure 22.8: A: MDCK cells growing on collagen type I coated PDMS overlaid with matrix. Cell protrusions (arrows) may guide the growth direction concentrating the fibrils by means of higher tension. The round cell aggregate (arrowheads) did not alter morphology during 8 h of observation. Cell division was observed in both structures. For the single cell wires the dividing cells orientate their axis along the migration axis, which is defined by the aligned fibers. For the round cell aggregate the axis of division was turned of 90 °. The change of mitosis axe orientation kept the daughter cells inside the cell assembly (see inserts). This difference in the division axes is known from cells which change morphology from epithelial to mesenchymal cell state [211]. B: In the mesenchymal state, cells become more motile and show fibroblastic polarization. They have reduced cell-cell contacts and can detach from cell monolayers. During migration the cell is always sensing its surrounding and change migration direction (arrow) depending on extracellular cues (arrowheads).

with ∗) showed only small protrusions during 8h of investigation (arrow heads), without cell outgrow. The fiber alignment around the perimeter was evenly distributed and not as oriented as for cells growing in cords. Therefore, directed growth is not predominant in this state of cell morphology. This may be an effect of the dense cell packing inside the circular cell island compared to the cells in the cord. The different behaviour of the two cell stages (epithelial and mesenchymal) was also investigated during cell mitosis (see inserts in Fig. 22.8). In the cell cord built up from highly motile cells, the division axes are not changed and they are orientated along the direction of migration. Inside the small island of cells (marked with ∗) the axis of mitosis is tilted of about 90 ° to keep the daughter cells inside the monolayer. In combination with the microarray, the cells cultured with matrix overlay did not form a closed monolayer after incubation even after several days in culture. Instead they grew as interconnected cords and tubules connecting separated cell islands. Different evolution stages could be observed from single cell cords and multilayered strings with small lumens through to mature tubules between formerly separated cell islands (see Fig. 22.7). The orientation of tubules was randomly distributed and directed by aligned matrix fibers. In contrast the cells growing on anisotropic arrays showed a distinct growth direction along the long axis of the posts (see Fig. 22.7 E,F).

Chapter 23

Disscusion

It was shown that cultivating epithelial cells inside a 3D environment drives cells to form lumen-enclosing structures [81, 142, 144, 223, 205]. In order to get 3D structures near a surface, where the cell-exerted forces can be measured via the force sensor arrays, culture conditions were adapted in such a way, that complete matrix embedding was no longer necessary. It could be shown that MDCK cells growing on collagen type I coated flat PDMS surfaces had a reduced proliferation rate. The cells showed a reduced spreading and a marked fibroblastic polarization. An explanation could be that the amount of collagen type I present on the surface was lower on PDMS than on glass surfaces [50, 73]. The cell spreading was was further reduced when cells were grown on collagen type I coated microarrays [1]. When gfr-Matrigel was polymerized on top of the substrate, cells started to grow as multilayered aggregates on the flat surfaces and then formed lumen-enclosed cysts on the microarrays. Several publications discussed the influence of the small GTPase Rho and its effector ROCK to cyst formation [205, 211]. They predicted a down regulation of Rho in soft collagen gels due to the missing feedback from ROCK. Rho inactivation is in turn influencing FAK phosphorylation (a central event in creating cell adhesion, and migrations; [32, 83]) and cell proliferation [43]. Rho activity is also influenced by integrin $\alpha_2\beta_1$ activation [2] [125]. Reduction of surface present collagen type I should also influence the morphology of epithelial cells. In the case of MDCK . The samcells cultured in suspension where collagen is not present, hollowed 3D aggregates with inverted polarity was generated[143]e cellular behaviour was established on surfaces without coated adhesion-promoting proteins (see Fig. 23.1 B).

23.1 Strategies

From these experiments a strategy was developed to achieve 3D growth on the microarrays. First the surfaces should have the capability to allow cell adhesion while keeping cell spreading to a minimum. To maintain cell polarity with an apical membrane facing the lumen and a basolateral surface directed to the ECM, it was also necessary to overlay the cells with a gel of gfr-Matrigel (compare Fig. 23.1 B with Fig. 22.5). It has been known for 25 years that the application of matrix proteins to the apical membrane changes cellular behaviour and morphology [81]. The usage of reconstituted collagen type I gel did not promote cyst grow,

[1] in this case only a partial adhesion is available on the pillar array compared to flat surfaces

[2] integrins are the cellular actors at the cell-ECM interface. Their signalling affects also Rho activity

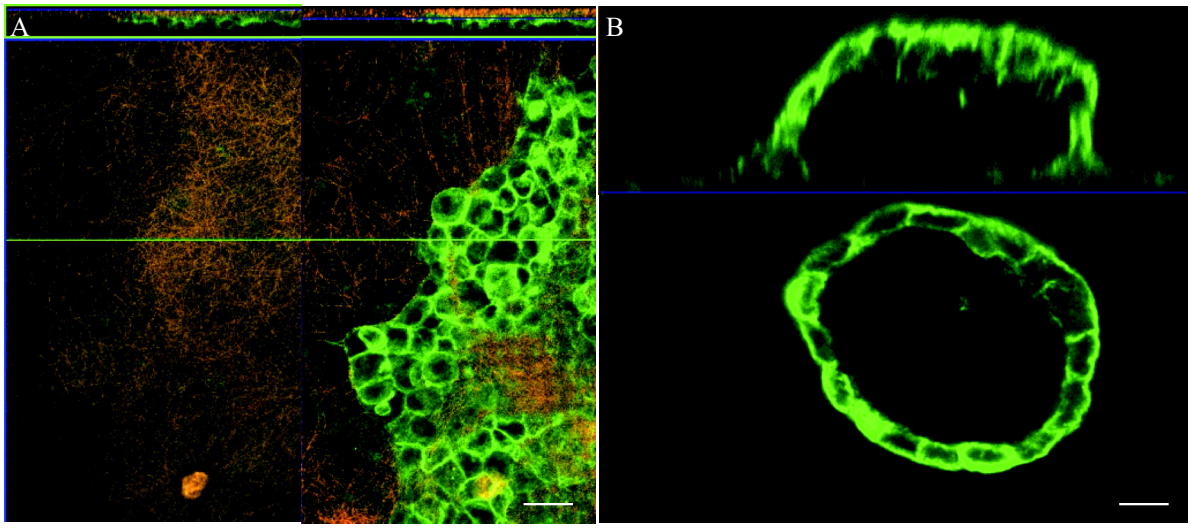

Figure 23.1: A: MDCK cells growing on a microarray in media supp.with 50 μg/ml. Collagen fibers (red) were deposited on the apical membrane (green). The dense fiber network is only allowing lumen formation near the surface and 3D cystogenisis was not observed [222]. B: As a controll cells were cultured on a non-coated microarray. Adhesion is dramatically reduced and cell-cell contacts get predominant. 3D structures with lumenal space developed over 5 to 7 days in culture. Polarity was not as distinct as on matrix surrounded cells (actin, green, is localised at the outer surface).

as observed in the case of gfr-Matrigel overlays. It can be explained by the difference in fiber density of the two gels. Collagen type I generates a dense meshwork of thick fibers that lies like a sheet on top of the cells [3] whereas a diluted gfr-Matrigel behaves as a much softer matrix [4]. The reduced spreading and the matrix overlay may play an important role in building up 3D structures instead of 2D growth of MDCK cells on the force sensor arrays.

23.2 Tubulogenesis induced by anisotropic force fields

Several groups have previously investigated the ability of MDCK cyst to build up tubules in vitro. It was shown that hepatocyte growth factor (HGF) is enhancing tubular outgrowth [23, 169, 165, 18]. There are several mechanisms involved in tubulogenesis which are influenced by HGF. First an ephitelial/mesenchymal transition occurs, and the cells form long protruding extensions. In the mesenchymal state, cell can migrate out from the cyst monolayer and form cords. After a lumenal space is generated the cords mature to tubes [119, 211, 141] (see also Introduction of this chapter). Similar effects were seen with cells growing on collagen type I coated PDMS surfaces overlaid with collagen type I or gfr-Matrigel. Cells aggregate to form islands but maintain the ability to polarize into migrating cells (see Fig. 22.8 B). Also the mitosis axis changed in some cells indicating a different cell state. The alignment of the spindle axis along the migratory direction was only seen in cell cords, whereas spindle orientation in spherical ordered cell island always turns 90°, in order to keep daughter cells

[3] the cells are collecting and condensing the fibers from the gel at their apical surface even at a collagen type I concentration as low as 50 μg/ml

[4] Collagen type IV is not a fiber forming collagen, it only produces a meshwork of short interconnected fibrilles [20]

inside the island boundary [211]. However it is not clear how surface characteristics can influence cellular behaviour. In 1994 Clark et al. investigated how different ECM proteins [5] influence HGF induced scattering of sub confluent MDCK cultures [37]. Renner et al. showed how different polymer surfaces can influence endothelial cell growth [162]. They assumed that the lower binding strength of fibronectin on hydrophilic surfaces can change cell morphology [6] by relieved fibronectin remodeling. These results may also explain why cells on collagen type I coated PDMS [7] surfaces show different polarity compared to tissue culture surfaces or filter membranes.

23.3 Integrin activation and morphological cell behavior

Surface characteristics also played a role in the detachment of confluent monolayers of MDCK cells grown on cRGD grafted to PDMS (see Fig. 22.2). Detachment of cells from surfaces normally induces anoikis (detachment-induced apoptosis) [68, 196]. But how distinguished integrin activation [8] could lead cells to detach is not clear. What is known from literature is that different protein kinase signaling pathways like FAK, ILK, PI3K, ERK MAPK are involved in the apoptosis pathway [70, 69]. Moreover small GTPases such as CDC42 and Rac1 regulate anoikis until survival of detached cells [34]. These results could be useful for the interpretation of the observed detachment on cRGD surfaces, as it is known that integrins interact closely with these two families of signal proteins. Further investigations on well-defined RGD interfaces should lead to an appropriate description of this phenomena [6].

In this chapter, biological phenomena were described strictly from a physical point of view. How far biochemical signaling can influence these processes was not investigated. It could be similar to that case of gfr-Matrigel which still contains TGF-β. This growth factor can influence cystogenesis of MDCK cells embedded in matrix derived from Matrigel [169]. Other factors from serum-supplemented media could also have an effect [9]. Future investigations analysing the influence of both biochemical signaling and mechanical stimuli on tubulugenesis in vitro will be based on new interdisciplinary approaches between physics and biology.

[5] vitronectin and fibronectin was compared

[6] cells grow in a stellate morphology on hydrophilic surfaces whereas on hydrophobic surfaces the cell monolayer was not disrupted

[7] PDMS water contact angle is 120°

[8] the cRGD was designed for interacting predominantly with $\alpha_v\beta_3$ integrins

[9] LPA influences cell contractility for instance [146]

Bibliography

[1] *Amine reactive Probes Molecular Probes.*

[2] http://golgi.ana.ed.ac.uk/kidhome.html.

[3] *NuPAGE® Technical Guide General information and protocols for using the NuPAGE® electrophoresis system.*

[4] B Alberts, A Johnson, J Lewis, M Raf, K Roberts, and P Walter. *Molecular Biology of The Cell*. Garland Science, New York, 2002.

[5] Gregory H Altman, Rebecca L Horan, Ivan Martin, Jian Farhadi, Peter R H Stark, Vladimir Volloch, John C Richmond, Gordana Vunjak-Novakovic, and David L Kaplan. Cell differentiation by mechanical stress. *FASEB J*, 16(2):270–2, Feb 2002.

[6] M Arnold, E A Cavalcanti-Adam, R Glass, J Blümmel, W Eck, M Kantlehner, H Kessler, and J P Spatz. Activation of integrin function by nanopatterned adhesive interfaces. *Chemphyschem*, 5(3):383–8, Mar 2004.

[7] A Ashkin, JM Dziedzic, and T Yamane. Optical trapping and manipulation of single cells using infrared laser beams. *Nature*, 330(6150):769–71, 1987.

[8] NQ Balaban, US Schwarz, D Riveline, P Goichberg, G Tzur, I Sabanay, D Mahalu, S Safran, A Bershadsky, L Addadi, and B Geiger. Force and focal adhesion assembly: a close relationship studied using elastic micropatterned substrates. *Nat Cell Biol*, 3(5):466–72, May 2001.

[9] C. Ballestrem, B. Hinz, B. A. Imhof, and B. Wehrle-Haller. Marching at the front and dragging behind: differential alphaVbeta3-integrin turnover regulates focal adhesion behavior. *J Cell Biol*, 155(7):1319–32, Dec 2001.

[10] G Baneyx, L Baugh, and V Vogel. Coexisting conformations of fibronectin in cell culture imaged using fluorescence resonance energy transfer. *Proc Natl Acad Sci U S A*, 98(25):14464–8, Dec 2001.

[11] G. Baneyx and V. Vogel. Self-assembly of fibronectin into fibrillar networks underneath dipalmitoyl phosphatidylcholine monolayers: role of lipid matrix and tensile forces. *Proc Natl Acad Sci U S A*, 96(22):12518–23, Oct 1999.

[12] Gretchen Baneyx, Loren Baugh, and Viola Vogel. Fibronectin extension and unfolding within cell matrix fibrils controlled by cytoskeletal tension. *Proc Natl Acad Sci U S A*, 99(8):5139–43, Apr 2002.

[13] J. B. Bard, A. Gordon, L. Sharp, and W. I. Sellers. Early nephron formation in the developing mouse kidney. *J Anat*, 199(Pt 4):385–92, Oct 2001.

[14] Loren Baugh and Viola Vogel. Structural changes of fibronectin adsorbed to model surfaces probed by fluorescence resonance energy transfer. *J Biomed Mater Res A*, 69A(3):525–34, Jun 2004.

[15] W Baumgartner, P Hinterdorfer, W Ness, A Raab, D Vestweber, H Schindler, and D Drenckhahn. Cadherin interaction probed by atomic force microscopy. *Proc Natl Acad Sci U S A*, 97(8):4005–10, Apr 2000.

[16] Michael Beil, Alexandre Micoulet, Götz von Wichert, Stephan Paschke, Paul Walther, M Bishr Omary, Paul P Van Veldhoven, Ulrike Gern, Elke Wolff-Hieber, Juliane Eggermann, Johannes Waltenberger, Guido Adler, Joachim Spatz, and Thomas Seufferlein. Sphingosylphosphorylcholine regulates keratin network architecture and visco-elastic properties of human cancer cells. *Nat Cell Biol*, 5(9):803–11, Sep 2003.

[17] Magnus Bergkvist, Jan Carlsson, and Sven Oscarsson. Surface-dependent conformations of human plasma fibronectin adsorbed to silica, mica, and hydrophobic surfaces, studied with use of Atomic Force Microscopy. *J Biomed Mater Res A*, 64(2):349–56, Feb 2003.

[18] C Birchmeier and E Gherardi. Developmental roles of HGF/SF and its receptor, the c-Met tyrosine kinase. *Trends Cell Biol*, 8(10):404–10, Oct 1998.

[19] D. E. Birk. Type V collagen: heterotypic type I/V collagen interactions in the regulation of fibril assembly. *Micron*, 32(3):223–37, Apr 2001.

[20] DE Birk, JM Fitch, JP Babiarz, KJ Doane, and TF Linsenmayer. Collagen fibrillogenesis in vitro: interaction of types I and V collagen regulates fibril diameter. *J Cell Sci*, 95 (Pt 4):649–57, Apr 1990.

[21] Ralf Blossey. Self-cleaning surfaces–virtual realities. *Nat Mater*, 2(5):301–6, May 2003.

[22] Samuel Y Boateng, Thomas J Hartman, Neil Ahluwalia, Himabindu Vidula, Tejal A Desai, and Brenda Russell. Inhibition of fibroblast proliferation in cardiac myocyte cultures by surface microtopography. *Am J Physiol Cell Physiol*, 285(1):C171–82, Jul 2003.

[23] V Brinkmann, H Foroutan, M Sachs, KM Weidner, and W Birchmeier. Hepatocyte growth factor/scatter factor induces a variety of tissue-specific morphogenic programs in epithelial cells. *J Cell Biol*, 131(6 Pt 1):1573–86, Dec 1995.

[24] G Wayne Brodland and Jim H Veldhuis. A computer model for reshaping of cells in epithelia due to in-plane deformation and annealing. *Comput Methods Biomech Biomed Engin*, 6(2):89–98, Apr 2003.

[25] R. A. Brown, G. W. Blunn, and O. S. Ejim. Preparation of orientated fibrous mats from fibronectin: composition and stability. *Biomaterials*, 15(6):457–64, May 1994.

[26] J Brunner. New photolabeling and crosslinking methods. *Annu Rev Biochem*, 62:483–514, 1993.

[27] D. A. Calderwood, S. J. Shattil, and M. H. Ginsberg. Integrins and actin filaments: reciprocal regulation of cell adhesion and signaling. *J Biol Chem*, 275(30):22607–10, Jul 2000.

[28] ABD Cassie and S Baxter. Wettability of porous surfaces. *Trans. Faraday Soc*, 40:546–551, 1944.

[29] Ada Cavalcanti-Adam. *The control of cell adhesion and adhesiondependent events by nanotemplates regulating the spatial arrangement of integrin ligands*. PhD thesis, Natural Sciences and for Mathematics of the Ruperto-Carola University of Heidelberg, Germany, 2005.

[30] Micro Chem. Nano-su-8 datasheet avaliable online @ www.microchem.com/products/pdf/su8-2-25.pdf.

[31] C. S. Chen, M. Mrksich, S. Huang, G. M. Whitesides, and D. E. Ingber. Geometric control of cell life and death. *Science*, 276(5317):1425–8, May 1997.

[32] HC Chen, PA Appeddu, H Isoda, and JL Guan. Phosphorylation of tyrosine 397 in focal adhesion kinase is required for binding phosphatidylinositol 3-kinase. *J Biol Chem*, 271(42):26329–34, Oct 1996.

[33] W Chen, A Y Fadee, M C Hsieh, D Öner, J Youngblood, and T J McCarthy. Ultrahydrophobic and ultralyophobic surfaces: Some comments and examples. *Langmuir*, 15:3395–3399, 1999.

[34] Tzu-Ling Cheng, Marc Symons, and Tzuu-Shuh Jou. Regulation of anoikis by Cdc42 and Rac1. *Exp Cell Res*, 295(2):497–511, May 2004.

[35] M. Chrzanowska-Wodnicka and K. Burridge. Rho-stimulated contractility drives the formation of stress fibers and focal adhesions. *J Cell Biol*, 133(6):1403–15, Jun 1996.

[36] E. A. Clark, W. G. King, J. S. Brugge, M. Symons, and R. O. Hynes. Integrin-mediated signals regulated by members of the rho family of GTPases. *J Cell Biol*, 142(2):573–86, Jul 1998.

[37] P Clark. Modulation of scatter factor/hepatocyte growth factor activity by cell-substratum adhesion. *J Cell Sci*, 107 (Pt 5):1265–75, May 1994.

[38] JF Colas and GC Schoenwolf. Towards a cellular and molecular understanding of neurulation. *Dev Dyn*, 221(2):117–45, Jun 2001.

[39] PM Comoglio and C Boccaccio. Scatter factors and invasive growth. *Semin Cancer Biol*, 11(2):153–65, Apr 2001.

[40] JR Cook, BE Crute, LM Patrone, J Gabriels, ME Lane, and RG Van Buskirk. Microporosity of the substratum regulates differentiation of MDCK cells in vitro. *In Vitro Cell Dev Biol*, 25(10):914–22, Oct 1989.

[41] D. Craig, A. Krammer, K. Schulten, and V. Vogel. Comparison of the early stages of forced unfolding for fibronectin type III modules. *Proc Natl Acad Sci U S A*, 98(10):5590–5, May 2001.

[42] D. R. Critchley. Cytoskeletal proteins talin and vinculin in integrin-mediated adhesion. *Biochem Soc Trans*, 32(Pt 5):831–6, Nov 2004.

[43] E Cukierman, R Pankov, DR Stevens, and KM Yamada. Taking cell-matrix adhesions to the third dimension. *Science*, 294(5547):1708–12, Nov 2001.

[44] Edna Cukierman, Roumen Pankov, and Kenneth M Yamada. Cell interactions with three-dimensional matrices. *Curr Opin Cell Biol*, 14(5):633–9, Oct 2002.

[45] Sarah M Cutler and Andrés J García. Engineering cell adhesive surfaces that direct integrin alpha5beta1 binding using a recombinant fragment of fibronectin. *Biomaterials*, 24(10):1759–70, May 2003.

[46] C.W.Extrand. Criteria for ultrahydrophobic surfaces. *Langmuir*, 20:5013–5018, 2004.

[47] J. A. Davies and J. B. Bard. The development of the kidney. *Curr Top Dev Biol*, 39:245–301, 1998.

[48] Jayanta Debnath, Senthil K Muthuswamy, and Joan S Brugge. Morphogenesis and oncogenesis of MCF-10A mammary epithelial acini grown in three-dimensional basement membrane cultures. *Methods*, 30(3):256–68, Jul 2003.

[49] P. Delvoye, P. Wiliquet, J. L. Levêque, B. V. Nusgens, and C. M. Lapière. Measurement of mechanical forces generated by skin fibroblasts embedded in a three-dimensional collagen gel. *J Invest Dermatol*, 97(5):898–902, Nov 1991.

[50] Cynthia A. Reinhart-King Micah Dembo and Daniel A. Hammer. Endothelial cell traction forces on rgd-derivatized polyacrylamide substrata. *Langmuir*, 19:1573–1579, 2003.

[51] M Dembo, T Oliver, A Ishihara, and K Jacobson. Imaging the traction stresses exerted by locomoting cells with the elastic substratum method. *Biophys J*, 70(4):2008–22, Apr 1996.

[52] W. Shannon Dillmore, Muhammad N Yousaf, and Milan Mrksich. A photochemical method for patterning the immobilization of ligands and cells to self-assembled monolayers. *Langmuir*, 20(17):7223–31, Aug 2004.

[53] Dennis E Discher, Paul Janmey, and Yu-Li Wang. Tissue cells feel and respond to the stiffness of their substrate. *Science*, 310(5751):1139–43, Nov 2005.

[54] T.J.McCarhy D.Öner. Ultrahydrophobic surfaces. effects of topography length scales on wettability. *Langmuir*, 16:7777–7782, 2000.

[55] G Dormán and GD Prestwich. Benzophenone photophores in biochemistry. *Biochemistry*, 33(19):5661–73, May 1994.

[56] GA Dunn and AF Brown. Alignment of fibroblasts on grooved surfaces described by a simple geometric transformation. *J Cell Sci*, 83:313–40, Jul 1986.

[57] A Dupuis and JM Yeomans. Modeling droplets on superhydrophobic surfaces: equilibrium states and transitions. *Langmuir*, 21(6):2624–9, Mar 2005.

[58] O. S. Ejim, G. W. Blunn, and R. A. Brown. Production of artificial-orientated mats and strands from plasma fibronectin: a morphological study. *Biomaterials*, 14(10):743–8, Aug 1993.

[59] DL Elbert and JA Hubbell. Conjugate addition reactions combined with free-radical cross-linking for the design of materials for tissue engineering. *Biomacromolecules*, 2(2):430–41, 2001.

[60] T. Elsdale and J. Bard. Collagen substrata for studies on cell behavior. *J Cell Biol*, 54(3):626–37, Sep 1972.

[61] Adam J Engler, Maureen A Griffin, Shamik Sen, Carsten G Bönnemann, H. Lee Sweeney, and Dennis E Discher. Myotubes differentiate optimally on substrates with tissue-like stiffness: pathological implications for soft or stiff microenvironments. *J Cell Biol*, 166(6):877–87, Sep 2004.

[62] H. P. Erickson. Reversible unfolding of fibronectin type III and immunoglobulin domains provides the structural basis for stretch and elasticity of titin and fibronectin. *Proc Natl Acad Sci U S A*, 91(21):10114–8, Oct 1994.

[63] VB Fainerman, EH Lucassen-Reynders, and R Miller. Description of the adsorption behaviour of proteins at water/fluid interfaces in the framework of a two-dimensional solution model. *Adv Colloid Interface Sci*, 106:237–59, Dec 2003.

[64] Lin Feng, Yanlin Song, Jin Zhai, Biqian Liu, Jian Xu, Lei Jiang, and Daoben Zhu. Creation of a superhydrophobic surface from an amphiphilic polymer. *Angew Chem Int Ed Engl*, 42(7):800–2, Feb 2003.

[65] Yuezhong Feng and Milan Mrksich. The synergy peptide PHSRN and the adhesion peptide RGD mediate cell adhesion through a common mechanism. *Biochemistry*, 43(50):15811–21, Dec 2004.

[66] B. R. Franza, K. Maruyama, J. I. Garrels, and H. E. Ruley. In vitro establishment is not a sufficient prerequisite for transformation by activated ras oncogenes. *Cell*, 44(3):409–18, Feb 1986.

[67] T. M. Freyman, I. V. Yannas, R. Yokoo, and L. J. Gibson. Fibroblast contractile force is independent of the stiffness which resists the contraction. *Exp Cell Res*, 272(2):153–62, Jan 2002.

[68] SM Frisch and H Francis. Disruption of epithelial cell-matrix interactions induces apoptosis. *J Cell Biol*, 124(4):619–26, Feb 1994.

[69] SM Frisch and RA Screaton. Anoikis mechanisms. *Curr Opin Cell Biol*, 13(5):555–62, Oct 2001.

[70] SM Frisch, K Vuori, E Ruoslahti, and PY Chan-Hui. Control of adhesion-dependent cell survival by focal adhesion kinase. *J Cell Biol*, 134(3):793–9, Aug 1996.

[71] Reiner Fürstner, Wilhelm Barthlott, Christoph Neinhuis, and Peter Walzel. Wetting and self-cleaning properties of artificial superhydrophobic surfaces. *Langmuir*, 21(3):956–61, Feb 2005.

[72] Mu Gao, David Craig, Olivier Lequin, Iain D Campbell, Viola Vogel, and Klaus Schulten. Structure and functional significance of mechanically unfolded fibronectin type III1 intermediates. *Proc Natl Acad Sci U S A*, 100(25):14784–9, Dec 2003.

[73] AJ García, MD Vega, and D Boettiger. Modulation of cell proliferation and differentiation through substrate-dependent changes in fibronectin conformation. *Mol Biol Cell*, 10(3):785–98, Mar 1999.

[74] B. Geiger and A. Bershadsky. Assembly and mechanosensory function of focal contacts. *Curr Opin Cell Biol*, 13(5):584–92, Oct 2001.

[75] J Gelles, BJ Schnapp, and MP Sheetz. Tracking kinesin-driven movements with nanometre-scale precision. *Nature*, 331(6155):450–3, Feb 1988.

[76] F. Grinnell. Fibroblast-collagen-matrix contraction: growth-factor signalling and mechanical loading. *Trends Cell Biol*, 10(9):362–5, Sep 2000.

[77] F Grinnell and CR Lamke. Reorganization of hydrated collagen lattices by human skin fibroblasts. *J Cell Sci*, 66:51–63, Mar 1984.

[78] Frederick Grinnell. Fibroblast biology in three-dimensional collagen matrices. *Trends Cell Biol*, 13(5):264–9, May 2003.

[79] Frederick Grinnell, Chin-Han Ho, Elisa Tamariz, David J Lee, and Gabriella Skuta. Dendritic fibroblasts in three-dimensional collagen matrices. *Mol Biol Cell*, 14(2):384–95, Feb 2003.

[80] C. Guidry and F. Grinnell. Contraction of hydrated collagen gels by fibroblasts: evidence for two mechanisms by which collagen fibrils are stabilized. *Coll Relat Res*, 6(6):515–29, Feb 1987.

[81] HG Hall, DA Farson, and MJ Bissell. Lumen formation by epithelial cell lines in response to collagen overlay: a morphogenetic model in culture. *Proc Natl Acad Sci U S A*, 79(15):4672–6, Aug 1982.

[82] N. L. Halliday and J. J. Tomasek. Mechanical properties of the extracellular matrix influence fibronectin fibril assembly in vitro. *Exp Cell Res*, 217(1):109–17, Mar 1995.

[83] DC Han, TL Shen, and JL Guan. Role of Grb7 targeting to focal contacts and its phosphorylation by focal adhesion kinase in regulation of cell migration. *J Biol Chem*, 275(37):28911–7, Sep 2000.

[84] Jeff Hardin and Timothy Walston. Models of morphogenesis: the mechanisms and mechanics of cell rearrangement. *Curr Opin Genet Dev*, 14(4):399–406, Aug 2004.

[85] AK Harris, P Wild, and D Stopak. Silicone rubber substrata: a new wrinkle in the study of cell locomotion. *Science*, 208(4440):177–9, Apr 1980.

[86] S. Herminghaus. Roughness-induced non-wetting. *Europhys. Lett.*, 52 (2):165–170, 2000.

[87] Ulrich Hersel, Claudia Dahmen, and Horst Kessler. RGD modified polymers: biomaterials for stimulated cell adhesion and beyond. *Biomaterials*, 24(24):4385–415, Nov 2003.

[88] S Hénon, G Lenormand, A Richert, and F Gallet. A new determination of the shear modulus of the human erythrocyte membrane using optical tweezers. *Biophys J*, 76(2):1145–51, Feb 1999.

[89] D. C. Hocking, R. K. Smith, and P. J. McKeown-Longo. A novel role for the integrin-binding III-10 module in fibronectin matrix assembly. *J Cell Biol*, 133(2):431–44, Apr 1996.

[90] MF Horster, GS Braun, and SM Huber. Embryonic renal epithelia: induction, nephrogenesis, and cell differentiation. *Physiol Rev*, 79(4):1157–91, Oct 1999.

[91] Benjamin Houseman and Milan Mrksich. Efficient Solid-Phase Synthesis of Peptide-Substituted Alkanethiols for the Preparation of Substrates That Support the Adhesion of Cells. *J Org Chem*, 63(21):7552–7555, Oct 1998.

[92] S. Huang and D. E. Ingber. The structural and mechanical complexity of cell-growth control. *Nat Cell Biol*, 1(5):E131–8, Sep 1999.

[93] Sui Huang, Gabriel Eichler, Yaneer Bar-Yam, and Donald E Ingber. Cell fates as high-dimensional attractor states of a complex gene regulatory network. *Phys Rev Lett*, 94(12):128701, Apr 2005.

[94] R. O. Hynes. Integrins: a family of cell surface receptors. *Cell*, 48(4):549–54, Feb 1987.

[95] R. O. Hynes. Integrins: versatility, modulation, and signaling in cell adhesion. *Cell*, 69(1):11–25, Apr 1992.

[96] Richard O Hynes. Integrins: bidirectional, allosteric signaling machines. *Cell*, 110(6):673–87, Sep 2002.

[97] R. V. Iozzo. Matrix proteoglycans: from molecular design to cellular function. *Annu Rev Biochem*, 67:609–52, 1998.

[98] Y Ito, M Kajihara, and Y Imanishi. Materials for enhancing cell adhesion by immobilization of cell-adhesive peptide. *J Biomed Mater Res*, 25(11):1325–37, Nov 1991.

[99] B Ivanov, W Grzesik, and FA Robey. Synthesis and use of a new bromoacetyl-derivatized heterotrifunctional amino acid for conjugation of cyclic RGD-containing peptides derived from human bone sialoprotein. *Bioconjug Chem*, 6(3):269–77, 1995.

[100] C. Marzolin J. Bico and D. Quéré. Pearl drops. *Europhys. Lett.*, 47, 2:220–226, 1999.

[101] S Jo, H Shin, and AG Mikos. Modification of oligo(poly(ethylene glycol) fumarate) macromer with a GRGD peptide for the preparation of functionalized polymer networks. *Biomacromolecules*, 2(1):255–61, 2001.

[102] R. P. Johnson and S. W. Craig. F-actin binding site masked by the intramolecular association of vinculin head and tail domains. *Nature*, 373(6511):261–4, Jan 1995.

[103] J.P.Youngblood J.T.McCarthy. Ultrahydrophobic polymer surfaces prepared by simultaneous ablation of polypropylene and sputtering of poly(tetrafluoroethylene) using radio frequency plasma. *Macromolecules*, 32:6800–6806, 1999.

[104] K. E. Kadler, D. F. Holmes, J. A. Trotter, and J. A. Chapman. Collagen fibril formation. *Biochem J*, 316 (Pt 1):1–11, May 1996.

[105] Z. Kam, E. Zamir, and B. Geiger. Probing molecular processes in live cells by quantitative multidimensional microscopy. *Trends Cell Biol*, 11(8):329–34, Aug 2001.

[106] B. Z. Katz, E. Zamir, A. Bershadsky, Z. Kam, K. M. Yamada, and B. Geiger. Physical state of the extracellular matrix regulates the structure and molecular composition of cell-matrix adhesions. *Mol Biol Cell*, 11(3):1047–60, Mar 2000.

[107] John F. W. Keana and Sui X. Cai. New reagents for photoaffinity labeling: Synthesis and photolysis of functionalized perfluorophenyl azides. *J. Org. Chem.*, 55:3640–3647, 1990.

[108] D. R. Keene, J. D. San Antonio, R. Mayne, D. J. McQuillan, G. Sarris, S. A. Santoro, and R. V. Iozzo. Decorin binds near the C terminus of type I collagen. *J Biol Chem*, 275(29):21801–4, Jul 2000.

[109] Z.Yoshimitsu A. Nakajima T.Watanabe K.Hashimoto. Effects of surface structure on the hydrophobicity and sliding behavior of water droplets. *Langmuir*, 18:5818–5822, 2002.

[110] LL Kiessling, JE Gestwicki, and LE Strong. Synthetic multivalent ligands in the exploration of cell-surface interactions. *Curr Opin Chem Biol*, 4(6):696–703, Dec 2000.

[111] M. S. Kolodney and R. B. Wysolmerski. Isometric contraction by fibroblasts and endothelial cells in tissue culture: a quantitative study. *J Cell Biol*, 117(1):73–82, Apr 1992.

[112] U Kuchinke, F Grawe, and E Knust. Control of spindle orientation in Drosophila by the Par-3-related PDZ-domain protein Bazooka. *Curr Biol*, 8(25):1357–65, 1998.

[113] Aurélie Lafuma and David Quéré. Superhydrophobic states. *Nat Mater*, 2(7):457–60, Jul 2003.

[114] G Lenormand, S Hénon, A Richert, J Siméon, and F Gallet. Elasticity of the human red blood cell skeleton. *Biorheology*, 40(1-3):247–51, 2003.

[115] W.H. Lewis and M.R. Lewis. Behavior of cells in tissue cultures. *In General Cytology (Cowdry, E.V., ed.), University of Chicago Press*, pages 384–447, 1929.

[116] Elisa Leyva, Matthew S. Platz, and and Jakob Wirz Gabriele Persy. Photochemistry of phenyl azide: The role of singlet and triplet phenylnitrene as transient intermediates. *J. Am. Chem. Soc.*, 108:3783–3790, 1986.

[117] H Lodish, A Berk, S L Zipurski, P Matsudaira, and D Baltimorand J Darnell. *Molecular Cell Biology*. W H Freeman and Company, 2000.

[118] B Lu, F Roegiers, LY Jan, and YN Jan. Adherens junctions inhibit asymmetric division in the Drosophila epithelium. *Nature*, 409(6819):522–5, Jan 2001.

[119] Barry Lubarsky and Mark A Krasnow. Tube morphogenesis: making and shaping biological tubes. *Cell*, 112(1):19–28, Jan 2003.

[120] H. J. Mardon and K. E. Grant. The role of the ninth and tenth type III domains of human fibronectin in cell adhesion. *FEBS Lett*, 340(3):197–201, Mar 1994.

[121] A Marmur. The lotus effect: Superhydrophobicity and metastability. *Langmuir*, 20:3517–3519, 2004.

[122] Karen Martin, Courtenay Hart, Jixiang Liu, Wai-Yee Leung, and Wayne F Patton. Simultaneous trichromatic fluorescence detection of proteins on Western blots using an amine-reactive dye in combination with alkaline phosphatase- and horseradish peroxidase-antibody conjugates. *Proteomics*, 3(7):1215–27, Jul 2003.

[123] R Martin. unpuplished results.

[124] R. J. Metzger and M. A. Krasnow. Genetic control of branching morphogenesis. *Science*, 284(5420):1635–9, Jun 1999.

[125] Hui Miao, Song Li, Ying-Li Hu, Suli Yuan, Yihua Zhao, Benjamin P C Chen, Wilma Puzon-McLaughlin, Takehiko Tarui, John Y-J Shyy, Yoshikazu Takada, Shunichi Usami, and Shu Chien. Differential regulation of Rho GTPases by beta1 and beta3 integrins: the role of an extracellular domain of integrin in intracellular signaling. *J Cell Sci*, 115(Pt 10):2199–206, May 2002.

[126] R Miller. *Proteins at Liquid Interfaces*. Elsevier, 1998.

[127] S. Miyamoto, B. Z. Katz, R. M. Lafrenie, and K. M. Yamada. Fibronectin and integrins in cell adhesion, signaling, and morphogenesis. *Ann N Y Acad Sci*, 857:119–29, Oct 1998.

[128] R Montesano, G Schaller, and L Orci. Induction of epithelial tubular morphogenesis in vitro by fibroblast-derived soluble factors. *Cell*, 66(4):697–711, Aug 1991.

[129] MS Mooseker and LG Tilney. Organization of an actin filament-membrane complex. Filament polarity and membrane attachment in the microvilli of intestinal epithelial cells. *J Cell Biol*, 67(3):725–43, Dec 1975.

[130] A. Morla, Z. Zhang, and E. Ruoslahti. Superfibronectin is a functionally distinct form of fibronectin. *Nature*, 367(6459):193–6, Jan 1994.

[131] M. Mrksich. Tailored substrates for studies of attached cell culture. *Cell Mol Life Sci*, 54(7):653–62, Jul 1998.

[132] M. Mrksich. A surface chemistry approach to studying cell adhesion. *Chem. Soc. Rev.*, 29:267–273, 2000.

[133] M Mrksich, CS Chen, Y Xia, LE Dike, DE Ingber, and GM Whitesides. Controlling cell attachment on contoured surfaces with self-assembled monolayers of alkanethiolates on gold. *Proc Natl Acad Sci U S A*, 93(20):10775–8, Oct 1996.

[134] M Mrksich, LE Dike, J Tien, DE Ingber, and GM Whitesides. Using microcontact printing to pattern the attachment of mammalian cells to self-assembled monolayers of alkanethiolates on transparent films of gold and silver. *Exp Cell Res*, 235(2):305–13, Sep 1997.

[135] M Mrksich and GM Whitesides. Using self-assembled monolayers to understand the interactions of man-made surfaces with proteins and cells. *Annu Rev Biophys Biomol Struct*, 25:55–78, 1996.

[136] S. Munevar, Y. Wang, and M. Dembo. Traction force microscopy of migrating normal and H-ras transformed 3T3 fibroblasts. *Biophys J*, 80(4):1744–57, Apr 2001.

[137] Celeste M Nelson, Ronald P Jean, John L Tan, Wendy F Liu, Nathan J Sniadecki, Alexander A Spector, and Christopher S Chen. Emergent patterns of growth controlled by multicellular form and mechanics. *Proc Natl Acad Sci U S A*, 102(33):11594–9, Aug 2005.

[138] H. Nogawa, K. Morita, and W. V. Cardoso. Bud formation precedes the appearance of differential cell proliferation during branching morphogenesis of mouse lung epithelium in vitro. *Dev Dyn*, 213(2):228–35, Oct 1998.

[139] Andres F Oberhauser, Carmelu Badilla-Fernandez, Mariano Carrion-Vazquez, and Julio M Fernandez. The mechanical hierarchies of fibronectin observed with single-molecule AFM. *J Mol Biol*, 319(2):433–47, May 2002.

[140] LE O'Brien, TS Jou, AL Pollack, Q Zhang, SH Hansen, P Yurchenco, and KE Mostov. Rac1 orientates epithelial apical polarity through effects on basolateral laminin assembly. *Nat Cell Biol*, 3(9):831–8, Sep 2001.

[141] Lucy Erin O'Brien, Mirjam M P Zegers, and Keith E Mostov. Opinion: Building epithelial architecture: insights from three-dimensional culture models. *Nat Rev Mol Cell Biol*, 3(7):531–7, Jul 2002.

[142] GK Ojakian and R Schwimmer. The polarized distribution of an apical cell surface glycoprotein is maintained by interactions with the cytoskeleton of Madin-Darby canine kidney cells. *J Cell Biol*, 107(6 Pt 1):2377–87, Dec 1988.

[143] GK Ojakian and R Schwimmer. Regulation of epithelial cell surface polarity reversal by beta 1 integrins. *J Cell Sci*, 107 (Pt 3):561–76, Mar 1994.

[144] GK Ojakian, R Schwimmer, and RE Herz. Polarized insertion of an intracellular glycoprotein pool into the apical membrane of MDCK cells. *Am J Physiol*, 258(3 Pt 1):C390–8, Mar 1990.

[145] Roumen Pankov and Kenneth M Yamada. Fibronectin at a glance. *J Cell Sci*, 115(Pt 20):3861–3, Oct 2002.

[146] M Parizi, EW Howard, and JJ Tomasek. Regulation of LPA-promoted myofibroblast contraction: role of Rho, myosin light chain kinase, and myosin light chain phosphatase. *Exp Cell Res*, 254(2):210–20, Feb 2000.

[147] Matthew J Paszek, Nastaran Zahir, Kandice R Johnson, Johnathon N Lakins, Gabriela I Rozenberg, Amit Gefen, Cynthia A Reinhart-King, Susan S Margulies, Micah Dembo, David Boettiger, Daniel A Hammer, and Valerie M Weaver. Tensional homeostasis and the malignant phenotype. *Cancer Cell*, 8(3):241–54, Sep 2005.

[148] N.A. Patankar. Mimicking the lotus effect: Influence of double roughness structures and slender pillars. *Langmuir*, 20:8209–8213, 2004.

[149] Neelesh A Patankar. Transition between superhydrophobic states on rough surfaces. *Langmuir*, 20(17):7097–102, Aug 2004.

[150] RJ Pelham and Y Wang. Cell locomotion and focal adhesions are regulated by substrate flexibility. *Proc Natl Acad Sci U S A*, 94(25):13661–5, Dec 1997.

[151] W. Matthew Petroll, H. Dwight Cavanagh, and James V Jester. Dynamic three-dimensional visualization of collagen matrix remodeling and cytoskeletal organization in living corneal fibroblasts. *Scanning*, 26(1):1–10, 2004.

[152] M Petronczki and JA Knoblich. DmPAR-6 directs epithelial polarity and asymmetric cell division of neuroblasts in Drosophila. *Nat Cell Biol*, 3(1):43–9, Jan 2001.

[153] DK Pettit, AS Hoffman, and TA Horbett. Correlation between corneal epithelial cell outgrowth and monoclonal antibody binding to the cell binding domain of adsorbed fibronectin. *J Biomed Mater Res*, 28(6):685–91, Jun 1994.

[154] K. A. Piez. Structure and assembly of the native collagen fibril. *Connect Tissue Res*, 10(1):25–36, 1982.

[155] K. A. Piez and B. L. Trus. A new model for packing of type-I collagen molecules in the native fibril. *Biosci Rep*, 1(10):801–10, Oct 1981.

[156] A. L. Pollack, R. B. Runyan, and K. E. Mostov. Morphogenetic mechanisms of epithelial tubulogenesis: MDCK cell polarity is transiently rearranged without loss of cell-cell contact during scatter factor/hepatocyte growth factor-induced tubulogenesis. *Dev Biol*, 204(1):64–79, Dec 1998.

[157] T.H. Pollard and W.C. Earnshaw. *Cell Biology*. Elsevier Science, 2002.

[158] Molecular Probes. *Zenon labeling protocoll for rabbit IgG avaliable online @ probes.invitrogen.com.*

[159] David Quéré. Surface chemistry: Fakir droplets. *Nat Mater*, 1(1):14–5, Sep 2002.

[160] S Reinsch and E Karsenti. Orientation of spindle axis and distribution of plasma membrane proteins during cell division in polarized MDCKII cells. *J Cell Biol*, 126(6):1509–26, Sep 1994.

[161] E. A. Reits and J. J. Neefjes. From fixed to FRAP: measuring protein mobility and activity in living cells. *Nat Cell Biol*, 3(6):E145–7, Jun 2001.

[162] L Renner, B Jørgensen, M Markowski, K Salchert, C Werner, and T Pompe. Control of fibronectin displacement on polymer substrates to influence endothelial cell behaviour. *J Mater Sci Mater Med*, 15(4):387–90, Apr 2004.

[163] D Riveline, E Zamir, NQ Balaban, US Schwarz, T Ishizaki, S Narumiya, Z Kam, B Geiger, and AD Bershadsky. Focal contacts as mechanosensors: externally applied local mechanical force induces growth of focal contacts by an mDia1-dependent and ROCK-independent mechanism. *J Cell Biol*, 153(6):1175–86, Jun 2001.

[164] S. D. Rosen and C. R. Bertozzi. The selectins and their ligands. *Curr Opin Cell Biol*, 6(5):663–73, Oct 1994.

[165] Marta Rosário and Walter Birchmeier. How to make tubes: signaling by the Met receptor tyrosine kinase. *Trends Cell Biol*, 13(6):328–35, Jun 2003.

[166] K. Rottner, A. Hall, and J. V. Small. Interplay between Rac and Rho in the control of substrate contact dynamics. *Curr Biol*, 9(12):640–8, Jun 1999.

[167] YA Rovensky, AD Bershadsky, EI Givargizov, LN Obolenskaya, and JM Vasiliev. Spreading of mouse fibroblasts on the substrate with multiple spikes. *Exp Cell Res*, 197(1):107–12, Nov 1991.

[168] E Ruoslahti. RGD and other recognition sequences for integrins. *Annu Rev Cell Dev Biol*, 12:697–715, 1996.

[169] OF Santos and SK Nigam. HGF-induced tubulogenesis and branching of epithelial cells is modulated by extracellular matrix and TGF-beta. *Dev Biol*, 160(2):293–302, Dec 1993.

[170] Yasuhiro Sawada and Michael P Sheetz. Force transduction by Triton cytoskeletons. *J Cell Biol*, 156(4):609–15, Feb 2002.

[171] P Schaffner, J Meyer, M Dard, R Wenz, B Nies, S Verrier, H Kessler, and M Kantlehner. Induced tissue integration of bone implants by coating with bone selective RGD-peptides in vitro and in vivo studies. *J Mater Sci Mater Med*, 10(12):837–9, Dec 1999.

[172] C Schmidt, F Bladt, S Goedecke, V Brinkmann, W Zschiesche, M Sharpe, E Gherardi, and C Birchmeier. Scatter factor/hepatocyte growth factor is essential for liver development. *Nature*, 373(6516):699–702, Feb 1995.

[173] C. E. Schmidt, A. F. Horwitz, D. A. Lauffenburger, and M. P. Sheetz. Integrin-cytoskeletal interactions in migrating fibroblasts are dynamic, asymmetric, and regulated. *J Cell Biol*, 123(4):977–91, Nov 1993.

[174] M. A. Schwartz, M. D. Schaller, and M. H. Ginsberg. Integrins: emerging paradigms of signal transduction. *Annu Rev Cell Dev Biol*, 11:549–99, 1995.

[175] Martin A Schwartz and Mark H Ginsberg. Networks and crosstalk: integrin signalling spreads. *Nat Cell Biol*, 4(4):E65–8, Apr 2002.

[176] US Schwarz, NQ Balaban, D Riveline, A Bershadsky, B Geiger, and SA Safran. Calculation of forces at focal adhesions from elastic substrate data: the effect of localized force and the need for regularization. *Biophys J*, 83(3):1380–94, Sep 2002.

[177] J. E. Schwarzbauer. Identification of the fibronectin sequences required for assembly of a fibrillar matrix. *J Cell Biol*, 113(6):1463–73, Jun 1991.

[178] J. E. Schwarzbauer and J. L. Sechler. Fibronectin fibrillogenesis: a paradigm for extracellular matrix assembly. *Curr Opin Cell Biol*, 11(5):622–7, Oct 1999.

[179] R Schwimmer and GK Ojakian. The alpha 2 beta 1 integrin regulates collagen-mediated MDCK epithelial membrane remodeling and tubule formation. *J Cell Sci*, 108 (Pt 6):2487–98, Jun 1995.

[180] J. L. Sechler, S. A. Corbett, M. B. Wenk, and J. E. Schwarzbauer. Modulation of cell-extracellular matrix interactions. *Ann N Y Acad Sci*, 857:143–54, Oct 1998.

[181] J. L. Sechler, H. Rao, A. M. Cumiskey, I. Vega-Colón, M. S. Smith, T. Murata, and J. E. Schwarzbauer. A novel fibronectin binding site required for fibronectin fibril growth during matrix assembly. *J Cell Biol*, 154(5):1081–8, Sep 2001.

[182] Shibuichi, Yamamoto, Onda, and Tsujii. Super Water- and Oil-Repellent Surfaces Resulting from Fractal Structure. *J Colloid Interface Sci*, 208(1):287–294, Dec 1998.

[183] N J Shirtcliffe, S Aqil, C Evans, and G McHale. The use of high aspect ratio photoresist (su-8) for super-hydrophobic pattern prototyping. *J. Micromech. Microeng.*, pages 1384–1389, 2004.

[184] Boris I Shraiman. Mechanical feedback as a possible regulator of tissue growth. *Proc Natl Acad Sci U S A*, 102(9):3318–23, Mar 2005.

[185] RR Siegel, P Harder, R Dahint, M Grunze, F Josse, M Mrksich, and GM Whitesides. On-line detection of nonspecific protein adsorption at artificial surfaces. *Anal Chem*, 69(16):3321–8, Aug 1997.

[186] AL Sieminski, RP Hebbel, and KJ Gooch. The relative magnitudes of endothelial force generation and matrix stiffness modulate capillary morphogenesis in vitro. *Exp Cell Res*, 297(2):574–84, Jul 2004.

[187] I. I. Singer, S. Scott, D. W. Kawka, D. M. Kazazis, J. Gailit, and E. Ruoslahti. Cell surface distribution of fibronectin and vitronectin receptors depends on substrate composition and extracellular matrix accumulation. *J Cell Biol*, 106(6):2171–82, Jun 1988.

[188] John L Tan, Joe Tien, Dana M Pirone, Darren S Gray, Kiran Bhadriraju, and Christopher S Chen. Cells lying on a bed of microneedles: an approach to isolate mechanical force. *Proc Natl Acad Sci U S A*, 100(4):1484–9, Feb 2003.

[189] NM Tooney, MW Mosesson, DL Amrani, JF Hainfeld, and JS Wall. Solution and surface effects on plasma fibronectin structure. *J Cell Biol*, 97(6):1686–92, Dec 1983.

[190] L Trusolino, S Cavassa, P Angelini, M Andó, A Bertotti, PM Comoglio, and C Boccaccio. HGF/scatter factor selectively promotes cell invasion by increasing integrin avidity. *FASEB J*, 14(11):1629–40, Aug 2000.

[191] AM Turner, N Dowell, SW Turner, L Kam, M Isaacson, JN Turner, HG Craighead, and W Shain. Attachment of astroglial cells to microfabricated pillar arrays of different geometries.urner. *J Biomed Mater Res*, 51(3):430–41, Sep 2000.

[192] Y Uehara, O Minowa, C Mori, K Shiota, J Kuno, T Noda, and N Kitamura. Placental defect and embryonic lethality in mice lacking hepatocyte growth factor/scatter factor. *Nature*, 373(6516):702–5, Feb 1995.

[193] KJ van Vliet, G Bao, and S Suresh. The biomechanics toolbox:experimental approaches for living cells and biomolecules. *Acta Materialia*, 51:5881–5905, 2003.

[194] Steven Vanni, B. Christoffer Lagerholm, Carol Otey, D. Lansing Taylor, and Frederick Lanni. Internet-based image analysis quantifies contractile behavior of individual fibroblasts inside model tissue. *Biophys J*, 84(4):2715–27, Apr 2003.

[195] HB Wang, M Dembo, and YL Wang. Substrate flexibility regulates growth and apoptosis of normal but not transformed cells. *Am J Physiol Cell Physiol*, 279(5):C1345–50, Nov 2000.

[196] Pengbo Wang, Anthony J Valentijn, Andrew P Gilmore, and Charles H Streuli. Early events in the anoikis program occur in the absence of caspase activation. *J Biol Chem*, 278(22):19917–25, May 2003.

[197] Bernhard Wehrle-Haller and Beat Imhof. The inner lives of focal adhesions. *Trends Cell Biol*, 12(8):382–9, Aug 2002.

[198] P. Weiss. Cellular dynamics. *Rev. Mod. Phys.*, 31:11–20, 1959.

[199] M Weliky and G Oster. The mechanical basis of cell rearrangement. I. Epithelial morphogenesis during Fundulus epiboly. *Development*, 109(2):373–86, Jun 1990.

[200] RN Wenzel. Resistance of solid surfaces to wetting by water. *Ind. Eng. Chem*, 28:988–994, 1936.

[201] EC Williams, PA Janmey, JD Ferry, and DF Mosher. Conformational states of fibronectin. Effects of pH, ionic strength, and collagen binding. *J Biol Chem*, 257(24):14973–8, Dec 1982.

[202] L. Wolpert. Positional information and the spatial pattern of cellular differentiation. *J Theor Biol*, 25(1):1–47, Oct 1969.

[203] A Woods and JR Couchman. Syndecan-4 and focal adhesion function. *Curr Opin Cell Biol*, 13(5):578–83, Oct 2001.

[204] A. Woods, R. L. Longley, S. Tumova, and J. R. Couchman. Syndecan-4 binding to the high affinity heparin-binding domain of fibronectin drives focal adhesion formation in fibroblasts. *Arch Biochem Biophys*, 374(1):66–72, Feb 2000.

[205] Michele A Wozniak, Radhika Desai, Patricia A Solski, Channing J Der, and Patricia J Keely. ROCK-generated contractility regulates breast epithelial cell differentiation in response to the physical properties of a three-dimensional collagen matrix. *J Cell Biol*, 163(3):583–95, Nov 2003.

[206] C. Wu, V. M. Keivens, T. E. O'Toole, J. A. McDonald, and M. H. Ginsberg. Integrin activation and cytoskeletal interaction are essential for the assembly of a fibronectin matrix. *Cell*, 83(5):715–24, Dec 1995.

[207] K. M. Yamada, R. Pankov, and E. Cukierman. Dimensions and dynamics in integrin function. *Braz J Med Biol Res*, 36(8):959–66, Aug 2003.

[208] Mingdi Yan, Sui Xiong Ca, Wybourne, and John F. W. Keana. Photochemical functionalization of polymer surfaces and the production of biomolecule-carrying micrometer-scale structures by deep-uv lithography using 4-substituted perfluorophenyl azides. *J. Am. Chem. SOC.*, 115:814–816, 1993.

[209] T. Young. *Philos. Trans. R. Soc.*, 95:65, 1805.

[210] Yousaf, Chan, and Mrksich. The Kinetic Order of an Interfacial Diels-Alder Reaction Depends on the Environment of the Immobilized Dienophile We are grateful for the support provided by the MRSEC (National Science Foundation, DMR-9808595) and DARPA. *Angew Chem Int Ed Engl*, 39(11):1943–1946, Jun 2000.

[211] Wei Yu, Lucy E O'Brien, Fei Wang, Henry Bourne, Keith E Mostov, and Mirjam M P Zegers. Hepatocyte growth factor switches orientation of polarity and mode of movement during morphogenesis of multicellular epithelial structures. *Mol Biol Cell*, 14(2):748–63, Feb 2003.

[212] P. D. Yurchenco, E. C. Tsilibary, A. S. Charonis, and H. Furthmayr. Laminin polymerization in vitro. Evidence for a two-step assembly with domain specificity. *J Biol Chem*, 260(12):7636–44, Jun 1985.

[213] R. Zaidel-Bar, M. Cohen, L. Addadi, and B. Geiger. Hierarchical assembly of cell-matrix adhesion complexes. *Biochem Soc Trans*, 32(Pt3):416–20, Jun 2004.

[214] Ronen Zaidel-Bar, Christoph Ballestrem, Zvi Kam, and Benjamin Geiger. Early molecular events in the assembly of matrix adhesions at the leading edge of migrating cells. *J Cell Sci*, 116(Pt 22):4605–13, Nov 2003.

[215] E. Zamir and B. Geiger. Molecular complexity and dynamics of cell-matrix adhesions. *J Cell Sci*, 114(Pt 20):3583–90, Oct 2001.

[216] E. Zamir, B. Z. Katz, S. Aota, K. M. Yamada, B. Geiger, and Z. Kam. Molecular diversity of cell-matrix adhesions. *J Cell Sci*, 112 (Pt 11):1655–69, Jun 1999.

[217] E. Zamir, M. Katz, Y. Posen, N. Erez, K. M. Yamada, B. Z. Katz, S. Lin, D. C. Lin, A. Bershadsky, Z. Kam, and B. Geiger. Dynamics and segregation of cell-matrix adhesions in cultured fibroblasts. *Nat Cell Biol*, 2(4):191–6, Apr 2000.

[218] Mirjam M P Zegers, Lucy E O'Brien, Wei Yu, Anirban Datta, and Keith E Mostov. Epithelial polarity and tubulogenesis in vitro. *Trends Cell Biol*, 13(4):169–76, Apr 2003.

[219] D Zeng, A Ferrari, J Ulmer, R Kroschewski, and J Spatz. 3d modeling of mechanical forces in the extra-cellular matrix during cystogenesis. *Biophysical Journal*, submitted.

[220] C. Zhong, M. Chrzanowska-Wodnicka, J. Brown, A. Shaub, A. M. Belkin, and K. Burridge. Rho-mediated contractility exposes a cryptic site in fibronectin and induces fibronectin matrix assembly. *J Cell Biol*, 141(2):539–51, Apr 1998.

[221] Houcine Ziani-Cherif, Kou Imachi, and Takehisa Matsuda. Preparation of aryldiazonium-, aryldiazo-, and arylazido-derivatized copolymers and their surface photografting. *Macromolecules*, 32:3438–3447, 1999.

[222] A Zuk and KS Matlin. Apical beta 1 integrin in polarized MDCK cells mediates tubulocyst formation in response to type I collagen overlay. *J Cell Sci*, 109 (Pt 7):1875–89, Jul 1996.

[223] A Zuk, KS Matlin, and ED Hay. Type I collagen gel induces Madin-Darby canine kidney cells to become fusiform in shape and lose apical-basal polarity. *J Cell Biol*, 108(3):903–19, Mar 1989.

Danksagung

Nach erkenntnisreichen drei einhalb Jahren der wissenschaftlichen Betätigung in einem interdisziplinären Forschungsgebiet, bin ich nun am letzten Abschnitt meiner Arbeit angelangt: einen gebührenden Dank auszusprechen an all diejenigen, die das hier ermöglicht haben. Auf dem Weg dorthin habe ich vieles dazugelernt, seien es neue Methoden der aktuellen Forschung, einen tieferen Einblick in die Biologie oder aber auch neue Menschen von denen manche zu Freunde wurden. Einem dieser Wegebereiter gilt meinem besonderen Dank. Denn durch Prof. Joachim Spatz bin ich in den Genuss gekommen, neue wissenschaftliche Methoden durch seine interessante Aufgabenstellung aufzugreifen und weiterzuführen. Alte Ansichtsweisen aufzugeben, um neuen Platz zu schaffen, dass ist einer der Stärken, die diesem, noch sehr jungen Arbeitsgebiet von Herrn Spatz inne wohnen.

Aside Prof. Spatz I thank my second supervisor Prof. Benjamin Geiger giving me the opportunity to work in this interdiciplinary field combining chemistry, physics and biology. He was the one giving me new impulses from biology and how to explain unexpected cell behaviour.

An dritter Stelle danke ich meiner kleinen Familie, die für die letzten Jahre unendlich viel Gedult aufbringen musste und meiner Idee des forschens nicht abgeneigt waren. Ich danke Bettina dafür, dass Sie unsere Kinder so umsorgt und erzogen hat, mit all den dazugehörigen Höhen und Tiefen. Ich danke auch meinen beiden Söhnen, León und Mateo das sie so tapfer waren und die letzte, doch sehr schwere Zeit meist ohne Ihren Papi auskommen mussten. Aber das Schwimmbad wartet schon sehnsüchtig... Zudem Danke ich Renate für Ihren unermütlichen Einsatz, auch in schwierigen Zeiten.

An vierter Stelle möchte ich meinen Eltern danken, denn ohne Sie würde ich nicht hier sitzten um diese letzte Zeilen zu verfassen. Sie haben nie den Glauben darin verloren, dass aus Ihrem Sohn mal was werden würde. Dieser Glaube hat mich immer vorangetrieben, um den steinigen Weg, zwar nicht immer gerade aus, aber dennoch zu Ende zu gehen. Um diesem grossartigen Einsatzt gerecht zu werden danke ich , indem ich Euch hiermit diese Arbeit widme!! Neben meinen Eltern möchte ich auch noch meinem Bruder danken, der mir nicht nur aus finanzieller Sicht beiseite stand.

An nächster Stelle stehen Roman Glass und Marco Arnold, die mich in den drei einhalb Jahren durch ein doch recht abwechslungsreiches Büroleben geführt haben. Sie haben aber auch dazu beigetragen, mir neue Ideen zu geben so wie ich Ihnen neue Einsichten an anderer Stelle geben konnte, danke auch hierfür. Für sein Geschick im Umgang mit IDL und den Schwierigkeiten einem Laien, wie mich darin zu schulen, danke ich Christian für die aufopferungsvollen Stunden. Zudem verdanke ich Ihm, dass ich mittlerweile zu einem echten LaTeX-Fan (man beachte bitte die genaue Schreibweise!) mutiert bin. Um der Internationalität gerecht zu werden gehe ich nun weiter in der doch mittlerweile stark angewachsenen Liste von Personen und möchte mich auch ganz herzlich bei den drei Franzosen bedanken. Jacques, den ich als langjähriger Studienkollegen schätzen gelernt habe, Alexandre als Weggefärten auf mancher Dienstreise und als rigorosen Inquisator in der Zellkultur. Und dem dritten im

Bunde, Phillipe danke ich für die gekonnte Hilfestellungen in LaTeX(!) und ImageJ. Zudem möchte ich Ada danken, mir in die grosse, weite Welt der Biologie einen Einblick gewährt zu haben. Sie war stehts hilfsbereit, und hatte so manchen biologischen Unklarheiten den gar ausgemacht. Zudem danke ich Ihr den Grossteil der hier vorliegenden Arbeit korrigiert zu haben. 'Mille grazie' Ada! Um in der Biologie zu bleiben, danke ich auch Tobias für seine fachkompetenten Ratschläge, 'frag den Tobi der weiss das schon...' und seinem Witz der Ihm, bei aller Ernsthaftigkeit der Wissenschaft doch geblieben ist. Als zwei Kollegen der ersten Stunde möchte ich noch Stefan und Wouter danken die den Pillar erst ins 'rollen' gebracht hatten. Dem gesamten bestehenden und ex-AK BIB danke ich für die, meist spontane BBQs an lauen, verregneten Mittwochabenden.... Meinen besonderen Dank gilt auch Frau Bozeck, die mit Ihrem liebevollen, oft privatem Angagement maßgeblich dazu beigetragen hat, daß die Gruppe nicht nur noch in der Wissenschaft lebt. Zudem danke ich Ihr, mich durch meine unzählige Verträge mit der Uni geschleusst zu haben und so manches notwendige Machtwort gesprochen hat (nicht nur mir gegenüber). Zu allerletzt möchte ich Richard für seine bereitwillige Tätigkeit innerhalb dieser Gruppe danken. Und wen ich jetzt noch aus unserer Gruppe vergessen habe, dem danke ich hiermit. Und für die Mitstreiter die der deutschen Sprache nicht mächtig sind, noch ein paar Worte auf Englisch. To keep all our linux machins running I had to thank Tamas. Also for some interesting discucion about maintainace of microscopes. Aldo Ferrari from the ETH Zürich, I thank for some interresting insights in advanced cell biology and also for reading my thesis and the corrections made by him, I know my english is really a pain. And last but not least I thank Baruch Zimerman from the Weizmann Institute for showing me a different part of the world. With him as a guid not only for the introduction into the secrets of cell biology but also showing me his beautiful country Israel, I felt save also during the difficult periode in his home-country. Also thanks for the delicious meals at shabats eve I had.

¡Muchas gracias a todos!

Hiermit erkläre ich an Eides statt, dass ich die vorligende Arbeit selbstständig und ohne unerlaubte Hilfsmittel angefertigt habe.

Heidelberg, den 30.5.05

Jens Ulmer